Aalto-yliopisto
Aalto-universitetet
Aalto University

Master’s Programme in Mechanical Engineering

Stiffness characteristics of hydraulic cylinder system subjected to dynamic loading

Heikki Lu

Master’s Thesis
2021

Aalto-yliopisto
Aalto-universitetet
Aalto University

Author Heikki Lu

Title of thesis Stiffness characteristics of hydraulic cylinder system subjected to dynamic loading

Programme Master's Programme in Mechanical Engineering

Major Mechanical engineering

Thesis supervisor Prof. Matti Pietola

Thesis advisors D.Sc. (tech) Jyrki Kajaste, D.Sc. (tech) Marko Jorkama

Collaborative partner Valmet Technologies Oy

Date 30.12.2021 **Number of pages** 78 **Language** English

Abstract

The purpose of this thesis is to determine the stiffness characteristics of a hydraulic cylinder system subjected to dynamic loads. The hydraulic cylinder system consists of a differential hydraulic cylinder with one-way flow control valves in both pressure lines and the configuration is used as a constant velocity actuator system in a paper machine. The hydraulic cylinder system was built and tested under sinusoidal loads with frequencies ranging from 10 to 30 Hz.

The stiffness characteristics of hydraulic cylinders are highly nonlinear and, in some cases, hard to predict accurately. The stiffnesses of hydraulic cylinders are composed of a multitude of components, and often determining the stiffnesses requires experimental testing. Examining the dynamic response of a hydraulic cylinder system inevitably leads to experimental testing due to the complexity of the system and due to the difficulty of finding details of system parameters.

In rotating machinery, such as paper machines, oscillatory loads occur according to their running speeds. The oscillatory loads often translate to the actuators the machine through structures, which limits the running speeds. Studying the dynamic response of the actuators used in such machines can enable higher running speeds for the machine, or reduce defective products, increasing productivity.

Keywords hydraulic cylinder dynamics, stiffness, vibration, valve dynamics, hydraulic resonance

Tekijä Heikki Lu

Työn nimi Hydraulisylinterijärjestelmän jäykkyysominaisuudet dynaamisilla kuormilla

Koulutusohjelma Master's Programme in Mechanical Engineering

Pääaine Konetekniikka

Vastuuopettaja/valvoja Prof. Matti Pietola

Työn ohjaaja(t) TkT Jyrki Kajaste, TkT Marko Jorkama

Yhteistyötaho Valmet Technologies Oy

Päivämäärä 29.12.2021 **Sivumäärä** 78 **Kieli** Englanti

Tiivistelmä

Tämän diplomityön tarkoituksena on määrittää hydraulisylinterijärjestelmän dynaaminen jäykkyys. Hydraulisylinterijärjestelmä koostuu differentiaalisesta hydraulisylinteristä, sekä tämän molempiin painelinjoihin kytketyistä vastusvastaventtiileistä. Sitä käytetään vakionopeuksisena toimilaitteena osana paperikonetta. Järjestelmää kuormitettiin sinimuotoisilla kuormituksilla, joiden taajuudet vaihtelivat välillä 10–30 Hz.

Hydraulisylinterien jäykkyysominaisuudet ovat epälineaarisia, ja joissain tapauksissa, hankala selvittää tarkasti. Hydraulisylinterien jäykkyys muodostuu monista komponenteista, ja usein tarkkaan määrittelyyn vaaditaan kokeellisia testejä. Dynaamisen vasteen selvittämisessä kokeelliset tutkimukset ovat välttämättömiä järjestelmän monimutkaisuuden ja usein myös tarkkojen systeemiparametrien arvojen puuttumisen johdosta.

Jaksollisia kuormia esiintyy pyörivissä koneissa, kuten paperikoneissa, ja ne määräytyvät pitkälti koneen käyntinopeuden mukaan. Jaksolliset kuormat siirtyvät rakenteiden kautta toimilaitteisiin, mikä rajoittaa käyntinopeuksia. Toimilaitteiden dynaamisen vasteen tutkiminen pyörivissä koneissa voi mahdollistaa suuremmat käyttönopeudet koneelle, tai vähentää viallisia lopputuotteita, parantaen tuottavuutta.

Avainsanat hydraulisylinterin dynamiikka, jäykkyys, värähtely, venttiilidynamiikka, hydraulinen resonanssi

Table of contents

Preface

I want to thank my thesis supervisor professor Matti Pietola for enabling this research. I also want to thank my advisors Jyrki Kajaste for guiding me through this journey and Marko Jorkama for providing such an interesting thesis topic. I want to express my gratitude to the laboratory specialist Antti Sinkkonen for sharing his expertise and providing support in the test bench design as well as the assembly process. I am grateful for the major contribution of Arttu Korhonen in assembling the test bench and conducting tests. In addition, I would like to thank the rest of the fluid power research team at Aalto University for all the great times we shared.

This research was enabled by the financial support of Valmet Technologies Oy and internal funding of the Department of Mechanical Engineering at Aalto University.

Espoo, 30.12.2021

Heikki Lu

Symbols and abbreviations

Symbols

A	[m²]	Area
A_A	[m²]	Cylinder head chamber effective piston area
A_B	[m²]	Cylinder rod chamber effective piston area
A_o	[m²]	Orifice area
A_p	[m²]	Pipe area
A_r	[m²]	Rod cross sectional area
D	[m]	Cylinder barrel inside diameter
D_1	[m]	Cylinder barrel outside diameter
C_h	[(m⁴s²/kg)]	Hydraulic capacitance
C_q	[-]	Flow coefficient
d_h	[m²]	Hydraulic diameter
d_p	[m]	Pipe diameter
E	[Pa]	Young's modulus for steel
E_h	[Pa]	Young's modulus for hose
F	[N]	Force
F_c	[N]	Coulomb force
F_L	[N]	Loading force
F_{LC}	[N]	Load cylinder force
F_s	[N]	Static friction force
F_{ss}	[N]	Steady state friction force
F_{TCH}	[N]	Test cylinder hydraulic force
$F_{TC\mu}$	[N]	Test cylinder friction force
$F_{\Delta p}$	[N]	Net hydraulic force
F_μ	[N]	Friction force
$F_{\mu 1}$	[N]	Rod seal friction force
$F_{\mu 2}$	[N]	Piston seal friction force
K_E	[Pa]	Effective bulk modulus
K_{EA}	[Pa]	Cylinder head chamber effective bulk modulus
K_{EB}	[Pa]	Cylinder rod chamber effective bulk modulus
K_f	[Pa]	Bulk modulus
K_f'	[Pa]	Nominal bulk modulus
k	[N/m]	Stiffness
k_c	[N/m]	Cylinder barrel expansion stiffness
k_{dyn}	[N/m]	Dynamic stiffness
k_h	[N/m]	Hose expansion stiffness
k_o	[N/m]	Hydraulic oil stiffness
k_p	[N/m]	Pipe expansion stiffness
k_r	[N/m]	Piston rod stiffness
k_s	[N/m]	Sealing system stiffness
k_{st}	[N/m]	Static stiffness
L_h	[kg/m⁴]	Hydraulic inductance
l	[m]	Length
l_A	[m]	Effective chamber length (A)
l_B	[m]	Effective chamber length (B)

l_r	[m]	Rod length
n	[-]	Isentropic constant
p	[Pa]	Pressure
p_A	[Pa]	Test cylinder A chamber pressure
p_B	[Pa]	Test cylinder B chamber pressure
R_h	[kg/(m^{4}s)]	Hydraulic resistance
V	[m^3]	Volume
V_0	[m^3]	Initial volume
V_A	[m^3]	Cylinder head chamber volume
V_B	[m^3]	Cylinder rod chamber volume
V_{AL}	[m^3]	Cylinder head side fluid line volume
V_{BL}	[m^3]	Cylinder rod side fluid line volume
v	[m/s]	Velocity
v_s	[m/s]	Stribeck speed
q_V	[m^3/s]	Volumetric flow rate
q_A	[m^3/s]	Head side chamber volumetric flow rate
q_B	[m^3/s]	Rod side chamber volumetric flow rate
Re	[-]	Reynolds number
U_{mean}	[m/s]	Average velocity of flow
x	[m]	Displacement
x_p	[m]	Piston position
z	[m]	Average deflection of bristles
$\dot{z}$	[m/s]	Average deflection velocity
α	[-]	Relative air content
μ	[kg/(ms)]	Dynamic viscosity
ν	[m^2/s]	Kinematic viscosity
ν_b	[-]	Poisson's ratio for steel
ρ	[kg/m^3]	Density
σ_0	[N/m]	Bristle stiffness
σ_1	[Ns/m]	Bristle damping
σ_2	[Ns/m]	Damping
Δp_r	[Pa]	Pressure loss due to pipe wall
Δp_i	[Pa]	Inertial pressure loss
ω	[rad/s]	Angular frequency

Abbreviations

FFT	Fast Fourier transform
LC	Load cylinder
TC	Test cylinder

1 Introduction

Hydraulic cylinders are linear actuators used to transfer forces and generate motion. Their stiffnesses are high, which enables transferring high forces. However, the stiffness characteristics of hydraulic cylinder systems are highly nonlinear, causing difficulties in control [1]. Namely, the most known nonlinearity in hydraulic cylinder stiffness is caused by the variance of volume in each chamber i.e., the position of the piston.

Hydraulic cylinders, as actuators exhibit dynamic functionalities. Thus, determining only the static stiffness characteristics is not enough for cylinders in dynamic applications. The stiffness characteristics calculated in static conditions differ from the stiffness when flow is allowed through the inlet ports. When the inlet ports of a hydraulic cylinder are closed, the hydraulic cylinder exhibits spring-like behavior. The stiffness is then governed by fluid temperatures, pressure levels and volumes along with the properties of the sealing systems. In some high-pressure applications, the stiffness properties of the cylinder rod and chamber must be considered as well. However, when flow is allowed through the inlet ports, the dynamic characteristics are heavily affected by all components in the hydraulic.

This thesis aims to describe the methodology for determining stiffness characteristics of hydraulic cylinder systems using relevant literature and validating them in an experimental setup. The tested hydraulic cylinder system consists of a differential hydraulic cylinder and one-way flow control valves connected to both ports of the cylinder. The one-way flow control valves are mounted so that free flow is allowed into the chambers and flow out of the chambers is throttled.

The hydraulic cylinder system is a subsystem of a paper machine, where it is used as a constant-velocity actuator in guiding the reeling process of paper. In rotating machinery like paper machines, deformations on the surfaces and displacements in the center of mass of the rotating element cause dynamic loads which are translated to the hydraulic cylinder system. Experimental examination is the only way to have a certain conclusion of the stiffness characteristics. Researching the stiffness characteristics around the working conditions of the cylinder could even lead to finding more optimal operating speeds for the paper machine.

The velocities of the cylinder vary from 1 to 3 mm/s. In its working environment, the cylinder rod is subjected to sporadic external loads with frequencies ranging from 10 to 30 Hz. The working pressures of the cylinder chambers are below 60 bar, which means that air content of the hydraulic circuit has a significant impact on the stiffness characteristics.

A testbench was built to experimentally determine the stiffness of the described hydraulic cylinder system. The cylinder system was subjected to sinusoidal loads, while extending and retracting at a constant velocity. The oscillatory loads were generated with a symmetrical servo cylinder. Testing variables were loading frequency, one-way flow control valve throttling and piston direction. The testing parameters were 10, 15, 20, 25 and 30 Hz for load frequency, 0%, 50%, 75%, and 100% for throttling, and extending and retracting for direction. The stiffness characteristics of only the hydraulic cylinder was also determined by modifying the configuration.

Chapter 2 distinguishes the defining components and parameters contributing to the stiffness of hydraulic cylinders. In this chapter, relevant literature in estimation of hydraulic cylinder system stiffnesses is reviewed.

In chapter 3, the built test setup is described in detail and the stiffness models are compiled according to chapter 2 to match the tested hydraulic cylinder system. The stiffnesses are calculated with the dimensions of the actual cylinder system and presented. In addition, the testing methods and processes are explained.

The experimental results are presented in chapter 4, and the results are evaluated in chapter 5. The relevancy and the capability of the test setup is discussed in the latter, and finally, chapter 6 summarizes the thesis.

2 Stiffness of hydraulic cylinder systems

Stiffness is the ratio of applied force to the corresponding change on translational deflection of an elastic element [2]. Stiffness of a system may vary under different environments and dynamic conditions. Stiffness measured under a static load is denoted as static stiffness, k and is described by

$$k = \frac{\Delta F}{\Delta x} \tag{1}$$

where ΔF is the static force and Δx is the corresponding deflection.

Dynamic stiffness is measured under fast periodic loads with frequencies higher than 0,5 Hz [3]. Periodic loads are often seen in supports of rotors and other rotating machinery. The motion caused by oscillating loads is noted as vibration. Fourier analysis is a common method for processing vibration measurements. Dynamic stiffness is the ratio of input force amplitude to output displacement amplitude of a system under dynamic conditions:

$$k_{dyn} = \frac{F_a}{x_\mathrm{a}} \tag{2}$$

where F_a is the amplitude of the load, and x_a is the resulting displacement response amplitude. The phase shift between the force and motion is also an important factor, which will be discussed more in chapter 3.

Hydraulic cylinders are hydromechanical systems, and their dynamic characteristics are therefore governed by hydromechanical and mechanical properties. The hydraulic cylinder system stiffness consists of hydraulic stiffness as well as mechanical stiffness. The hydraulic stiffness component is influenced by the hydraulic fluid type, temperature, volume, and flow properties. The mechanical stiffness is affected by loads, masses, elasticity, and friction. A hydraulic cylinder system is illustrated in Figure 1.

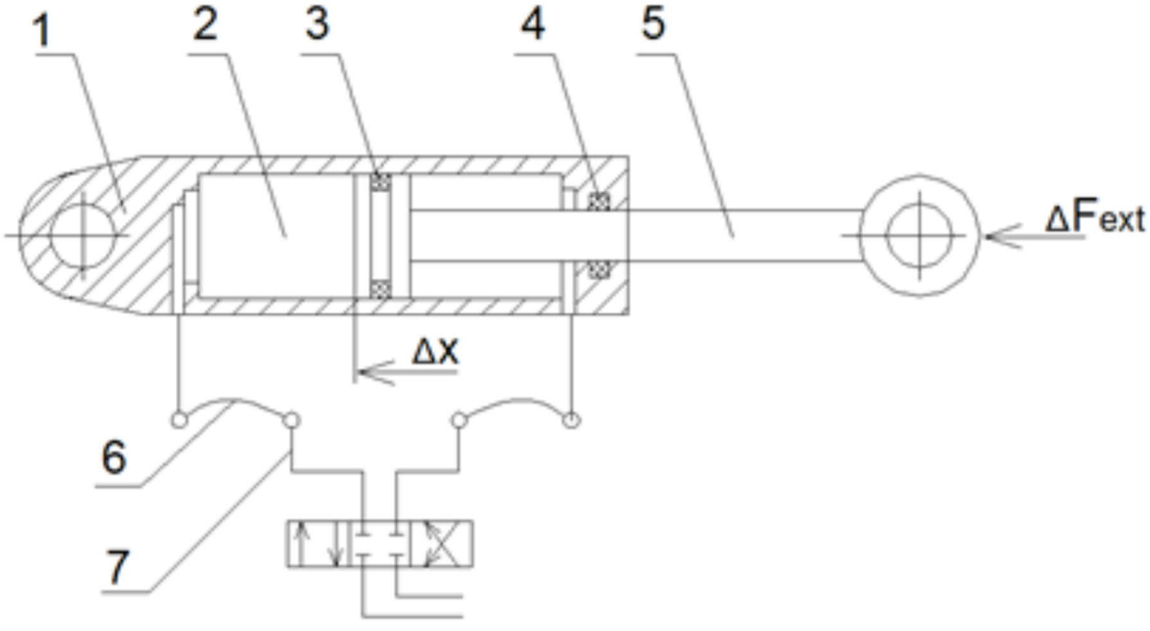

Figure 1 “A hydraulic cylinder system: 1 cylinder barrel, 2 hydraulic oil, 3 piston sealing, 4 rod sealing, 5 rod, 6 hoses, 7 metal pipes”. Source: [4]

In hydraulic cylinder systems, the cylinder rod, the cylinder chamber, seals, pipes and hoses affect the total stiffness. An extensive stiffness model of a hydraulic cylinder was presented in [4]. In the study, the net static stiffness K_{st} was derived as the sum of reciprocals of hydraulic fluid, piston rod, cylinder barrel, pipe, hose, and sealing ring stiffnesses as following:

$$\frac{1}{k_{st}} = \frac{1}{k_o} + \frac{1}{k_r} + \frac{1}{k_c} + \frac{1}{k_p} + \frac{1}{k_h} + \frac{1}{k_s} \tag{3}$$

where k_o is the stiffness of hydraulic fluid, k_r is the axial cylinder rod stiffness, k_c is the cylinder barrel expansion stiffness, k_p is the piping expansion stiffness, k_h is the expansion stiffness of hoses, and k_s is the sealing ring stiffness. Of these components, the study provides detailed mathematical models for all but sealing ring stiffnesses.

When considering the stiffness under dynamic loads, the frequency responses of the cylinder and fluid lines need to be considered. Natural resonances can cause unexpected responses of the system. Natural resonant frequencies of hydraulic cylinder systems are affected by load masses and fluid volumes.

2.1 Hydraulic stiffness

The main objectives of hydraulic fluids are power transmission, lubrication, heat transfer and corrosion protection. The most extensively used hydraulic fluids are mineral-based oils due to their suitable viscosity levels, and relatively low cost as well as satisfactory stiffness performance in many applications [5]. In a closed hydraulic circuit, the static hydraulic stiffness of cylinder systems is dominated by the fluid bulk modulus. However, when the cylinder piston is in motion, the flow changes the stiffness characteristics of the hydraulic cylinder. This section covers the influence of fluid medium and flow through orifices on hydraulic stiffness as well as the dynamic effects of transient flows.

2.1.1 Effects of bulk modulus

Hydraulic stiffness is proportional to fluid bulk modulus, K_f, which is the measure of the resistance of compressibility for a fluid. It can be also characterized as a measure of fluid stiffness [6].

$$K_f = -V\frac{\Delta p}{\Delta V} \tag{4}$$

where V is initial volume, Δp is the pressure difference and ΔV is the difference in volume before and after compression. [7]

Bulk modulus is a fluid specific characteristic, but also temperature and pressure dependent. The pressure and temperature dependency of the bulk modulus of a mineral oil is shown in Figure 2. The figure shows that increases in temperature decrease the bulk modulus and increases in pressure increase the bulk modulus.

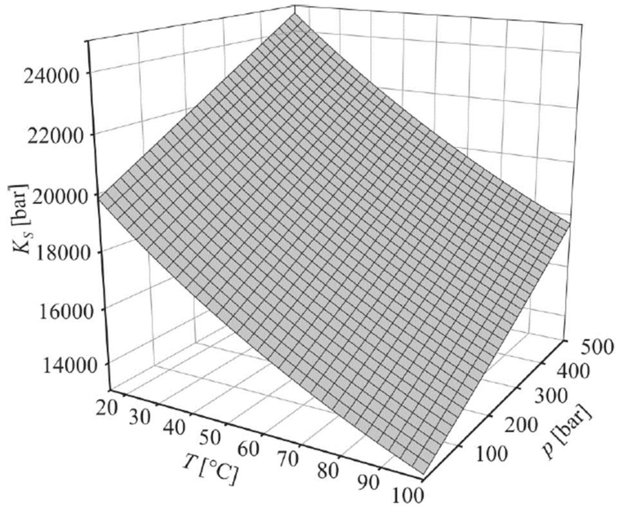

Figure 2 Bulk modulus of a mineral oil as a function of temperature and pressure. Source: [8]

For hydraulic fluids, high bulk modulus is desirable due to improved stiffness and stability. The bulk moduli of mineral-based oils range from 1,8 GPa to 2,2 GPa. However, in practical applications, including hydraulic cylinder systems, undissolved air trapped inside the hydraulic circuit decreases the effective bulk modulus of the fluid [7]–[9]. The impact of trapped air is significant in lower operating pressures (p < 60 bar), as shown in Figure 3.

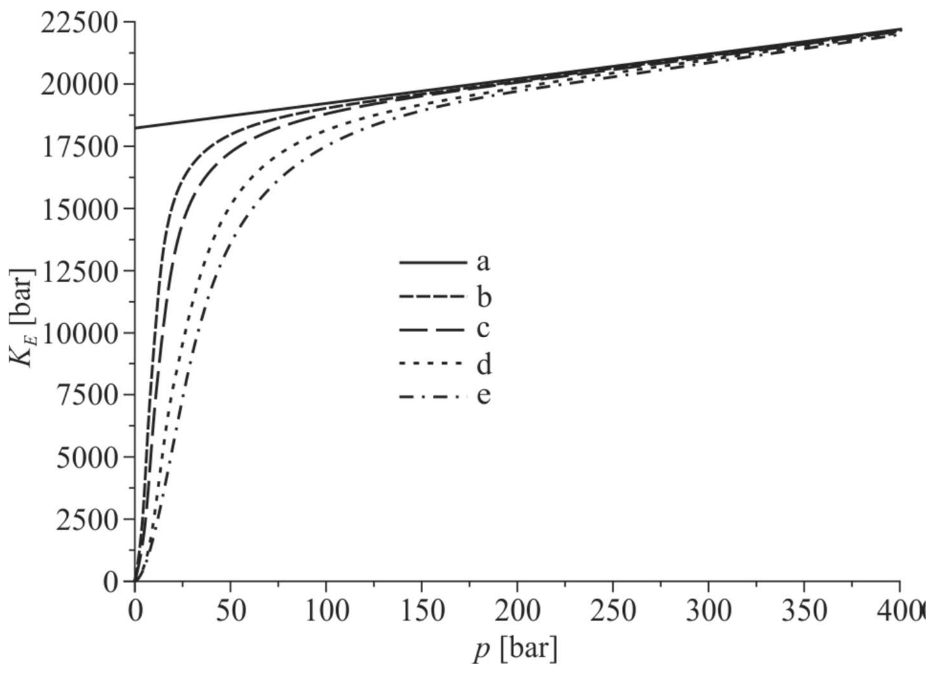

Figure 3 Effective bulk modulus at oil temperature of 30°C with different amounts of undissolved air. a) 0%; b) 0,5%; c) 1%; d) 3%; e) 5%. Source: [8]

The undissolved air content is taken into account in the effective bulk modulus, which is estimated in [10] to be

$$K_E = K_f' \frac{1 + \alpha \left(\frac{p_a}{p_a + p}\right)^{\frac{1}{n}}}{1 + \alpha\, K_f' \frac{p_a^{\frac{1}{n}}}{n(p_a + p)^{\frac{n+1}{n}}}} \tag{5}$$

where α is the volume of undissolved air in atmospheric pressure relative to the system volume, K_f' is the nominal bulk modulus of fluid in given pressure and temperature, p_a is the atmospheric pressure, p is the working pressure, and n is the isentropic coefficient (n = 1,4).

The compression of fluid in a static and closed hydraulic cylinder is illustrated in Figure 4, where a free-body diagram of a closed cylinder system is presented. In Figure 4 Δx describes the displacement of the piston caused by the static load of F_L, and $F_{\Delta p}$ is the net hydraulic force caused by the pressures acting on both sides of the piston surfaces. $F_{\mu 1}$ and $F_{\mu 2}$ are the seal friction forces for the rod and piston respectively. The seal friction forces are always opposing the loading force. The effects of friction forces on stiffness are discussed later in section 2.3.

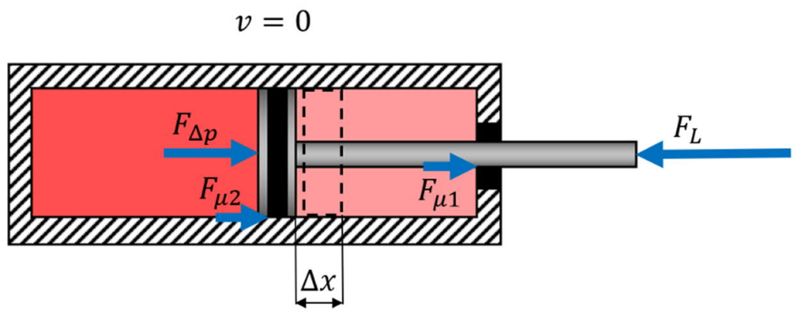

Figure 4 Free-body diagram of a hydraulic cylinder in static equilibrium.

The piston displacement Δx causes a change in volume in both chambers proportional to each respective effective piston area, and so the hydraulic fluid stiffness, K_o in a closed cylinder system can be derived as

$$k_o = K_{EA} \frac{A_A^2}{V_A + V_{AL}} + K_{EB} \frac{A_B^2}{V_B + V_{BL}} \tag{6}$$

where A_A is the head effective area, A_B is the rod end effective area, V_A is the piston position dependent head chamber volume, V_B is the piston position dependent rod chamber volume, V_{AL} is the head fluid line total volume, V_{BL} is the rod end fluid line total volume and K_{EA} and K_{EB} are the effective bulk moduli for each chamber [4]. The piston position dependent volumes V_A and V_B are more specifically defined as:

$$V_A = A_A x_p \tag{7}$$

and

$$V_B = A_B(l_s - x_p) \tag{8}$$

where x_p is piston position and l_s is stroke of the cylinder. Combining equations (5) to (11) yields an estimate of the hydraulic stiffness, k of a plugged cylinder under a static load.

Equation (6) shows that the fluid volume influences stiffness heavily. In a closed cylinder system with no fluid lines, the hydraulic stiffness is dominated by the position of the piston. The static stiffness increases asymptotically to infinity when chamber fluid volume approaches zero. The static hydraulic stiffness as a function of piston position yields a U-shaped curve as shown in Figure 5. The asymmetry of the curves is caused by the difference in effective volumes and piston areas.

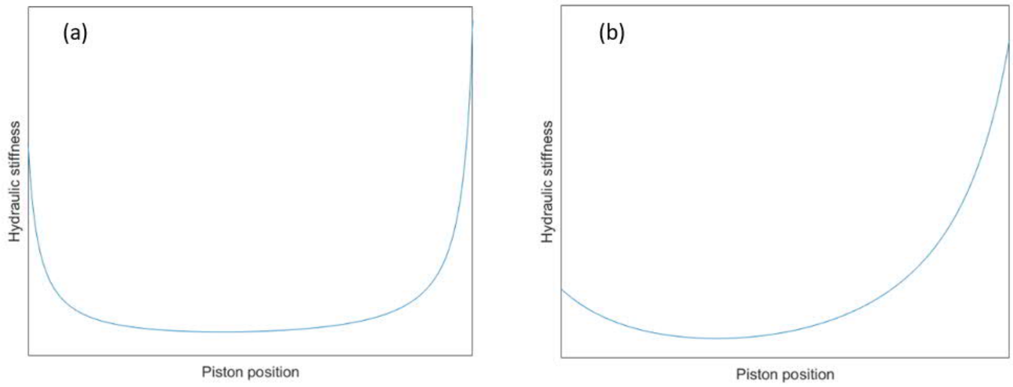

Figure 5 Static hydraulic stiffness as a function of piston position in a closed differential cylinder (a) without fluid line volumes (b) with fluid line volumes.

2.1.2 Effects of flow

The hydraulic stiffness of a closed cylinder was introduced in equation (6), which only applies to static circumstances. When a cylinder piston is in motion, flow occurs through inlet ports causing the fluid volumes to change. In addition, the flow rate changes in relation to the pressure difference caused by external forces. How flow rate changes due with pressure changes in a system, also known as hydraulic inductance, is determined by orifice flow areas, conduit lengths and fluid density. If we recap the definition of stiffness of a system as the proportion of an external force to the resulting displacement, it is evident that the hydraulic inductance affects the system stiffness in dynamic conditions.

A static pressure difference in an open circuit cylinder induces fluid flow. Fluid inside the cylinder chambers flows through the cylinder ports. The free-body diagram of a hydraulic cylinder extending with a constant velocity of v is presented in Figure 6. $F_{\Delta p}$ is the net

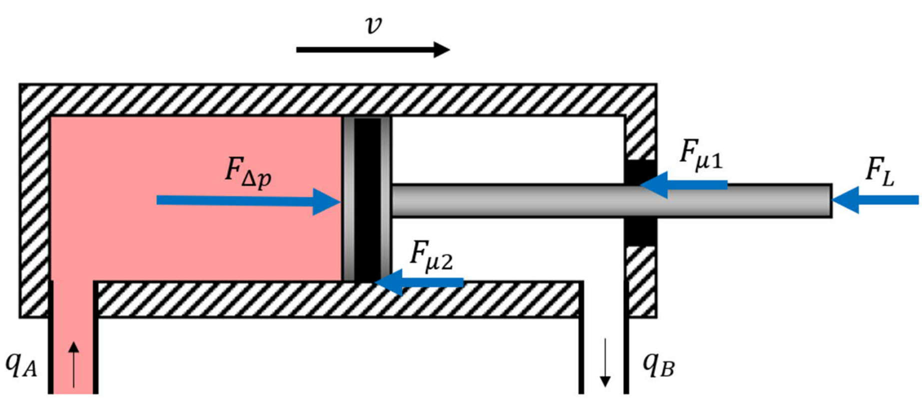

Figure 6 Free-body diagram of a hydraulic cylinder with constant flow and velocity.

hydraulic force, F_L is the loading force, $F_{\mu 1}$ and $F_{\mu 2}$ are the rod and piston seal friction respectively, q_A and q_B represent the volumetric flow of the head chamber and rod end chamber respectively.

The steady-state volumetric flow, q_V through an orifice is:

$$q_V = C_q A_o \sqrt{\frac{2\Delta p}{\rho}} \tag{9}$$

where C_q is the flow coefficient, A_o is the cross-sectional area of the orifice, Δp is the pressure differential caused by the load and ρ is the fluid density. The flow coefficient is dependent of the Reynolds number of the flow and the roundness of the orifice edges. The theoretical value for the flow coefficient of a sharp-edged orifice is $C_q = 0{,}611$. [1], [11]

The flow coefficient C_q varies with lower flow rates. Reynolds number Re gives a quantified measure of the flow and is determined in orifices as:

$$Re = \frac{U_{mean} d_h}{\nu} \tag{10}$$

where U_{mean} is the average velocity of flow through orifice, d_h is the hydraulic diameter, which is the orifice diameter for a circular orifice, and ν is the kinematic viscosity of the fluid [12]. The relation of Reynolds number and flow coefficient for different dimensions of orifices is presented in Figure 7.

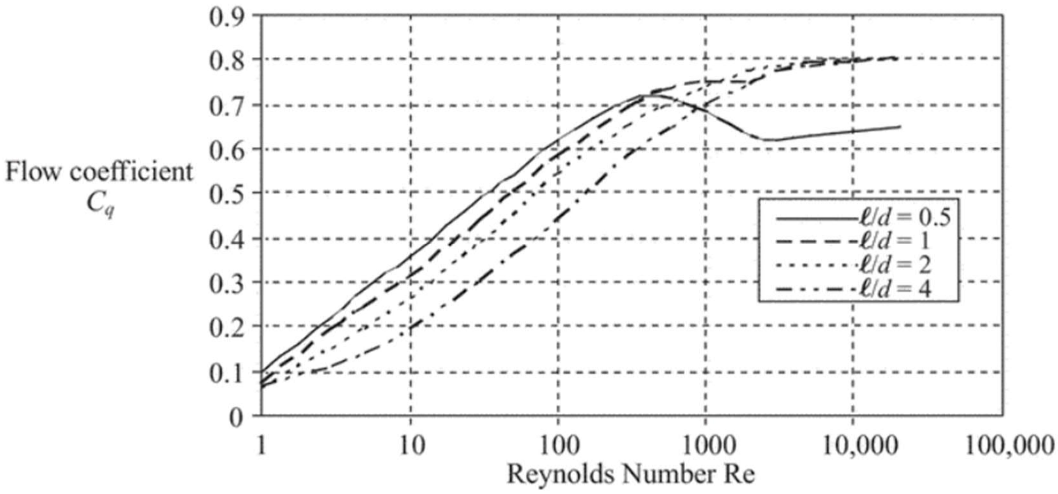

Figure 7 The variation of flow coefficient in relation to Reynolds number Source: [12]

2.1.3 Pipeline dynamics and hydraulic resonance

Dynamic response of pipelines is dominated by the piping dimensions and fluid density, bulk modulus, and viscosity. Density governs the inertial effects, and along with bulk modulus, it determines the wave propagation speed in the fluid. Viscosity and pipe dimensions determine the friction losses in the pipe.

For laminar flow, pressure loss due to friction between a pipe wall and fluid is approximated by:

$$\Delta p_r = \frac{128\mu l}{\pi d_p^4} q_V \tag{11}$$

where, μ is dynamic viscosity and d_p is the pipe diameter [12]. Often, when considering laminar flow through pipes, the pressure loss is specified by the electrical circuit analogy, where pressure is analogous to voltage and flow is analogous to electrical current. The hydraulic resistance, R_h is then:

$$R_h = \frac{128\nu\rho l}{\pi d_p^4} \tag{12}$$

where μ is replaced with $\nu\rho$ to be able to use the kinematic viscosity, ν.

The inertial effects of the fluid in a pipe are captured by

$$\Delta p_i = \frac{l\rho}{A_p}\frac{dq_V}{dt} \tag{13}$$

The same electric circuit analogy applies to fluid mass inertia, or hydraulic inductance L_h. Inductance describes the effects of pressure difference on the changes of flow rates and is characterized by:

$$L_h = \frac{l\rho}{A_p} \tag{14}$$

where l is pipe length, ρ is fluid density and A_p is pipe cross-sectional area.

The amount of compression of a fluid is the change of volumetric flow:

$$\Delta q_V = q_{Vin} - q_{Vout} = \frac{V_p}{K_f}\frac{dp}{dt} \tag{15}$$

where V_p is pipe volume and K_f is fluid bulk modulus.

Following the same analogy, compressibility of fluid, or hydraulic capacitance C_h, is the ratio of volume and bulk modulus:

$$C_h = \frac{V_p}{K_f} \tag{16}$$

Pressure pulsations and oscillations in fluid power applications can be addressed with hydraulic resonators such as Helmholtz resonators, shown in Figure 8. A Helmholtz resonator consists of a cavity and a tube. The working principle of a hydraulic resonator is based on either absorbing the pressure pulsation or attenuating it with a reflection through resonance. [13] Resonators can be used to attenuate or amplify pressure amplitudes at specific frequency ranges. However, sizing and tuning the resonators often requires experimental testing [14].

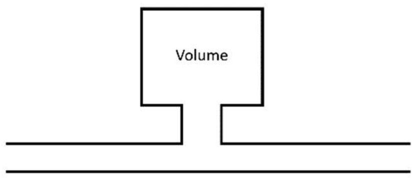

Figure 8 Helmholtz resonator

In fluid power systems, resonators are often used to address high frequency ranges. For example, pressure accumulators are feasible to target frequencies between 50 and 300 Hz. Typically, the problem with resonators operating at lower frequencies is that the dimensions of the resonator tend to be impractically large. [13]

In hydraulic cylinder systems, attenuating the pressure oscillation caused by an external load would decrease the stiffness of the cylinder. Amplifying the pressure oscillation with a reflective resonator such as T-pipe, shown in Figure 9, can increase the dynamic stiffness of a cylinder through resonance. T-pipes function, however, at a very narrow frequency range. Also, the added oil volume of resonators reduces the stiffness of a hydraulic cylinder system significantly in all but the specific frequency range.

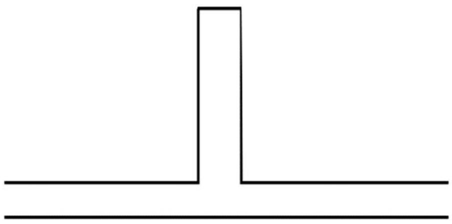

Figure 9 T-pipe resonator

Antiresonances occur in fluid line systems, where one end is plugged. The pressure wave travels through the pipe and is reflected from the plugged end. The length of the T-line is varied, so that resonance is reached. A plugged fluid line attenuates pressures, if the fluid line length is half or an even multiple of half the wavelength, as:

$$l_f = \frac{n\lambda}{2} = \frac{na}{2f};\ n = 1, 2, 4, 6, \ldots \tag{17}$$

where l_f is pipe length, λ is wavelength, a is wave propagation velocity and f is frequency.

The amplification of the pressure oscillation is reached when the T-line is in resonance, i.e., when the T-line length is an odd multiple of the wavelength:

$$l_f = \frac{n\lambda}{4} = \frac{na}{4f};\ n = 1, 3, 5, \ldots \tag{18}$$

Substituting a practical wave propagation velocity value for mineral oil, a = 1300 m/s and frequency, f = 20 Hz, yields l_f = 16,25 m. So, to amplify the pressure pulsation at 20 Hz (and ultimately to increase the stiffness of a cylinder system) the pipe length would have to be 16,25 m.

A lumped model approach can be applied to hydraulic components with significant inductances and capacitances. The hydraulic resonant frequency can be estimated as:

$$f_n = \frac{1}{2\pi\sqrt{L_h C_h}} \tag{19}$$

which can be combined with equations (14) and (16) for considerably large pipelines.

In practice, the inductances and capacitance are distributed throughout the volume and length of the components. Any dynamic hydraulic system should be designed so that the operating conditions – loads and structural vibrations – do not cause undesired vibrations in hydraulic fluid.

2.1.4 Pressure transients and wave propagation

Transients in hydraulics are sudden pressure surges or waves occurring after an instantaneous change in fluid flow [15]. Common causes for pressure transients are valve movement, opening or closing fluid lines, or pump failures [16], [17]. Pressure transients are widely studied in pipeline systems especially in water distributing networks [17]–[19]. If not addressed properly in the design of pipeline systems, possible pressure transients may cause damage to the components and ultimately failure. A numerical analysis of transient flow through orifices was conducted in [20].

Transient responses in fluid power systems are also studied in [21] and in [22]. Ideally, transients propagate at the speed of sound in the fluid medium, which is:

$$a = \sqrt{\frac{K_E}{\rho}} \tag{20}$$

where K_E is the effective bulk modulus and ρ is the fluid density. As the speed of sound in a fluid is affected by bulk modulus; pressure levels, air content, temperature, and volume affect it. Additionally, transient responses are dependent on the area of fluid flow. Therefore, the orifices and pipe diameters affect the overall transient response of the system [21]. The speed of sound in mineral oils in their typical working pressures and temperatures are around 1500 m/s but due to the high variability of bulk modulus, a practical value of 1300 m/s is often used in hydraulic system design [23]. Even experimental measurements show lower pressure wave propagation velocities than is expected [24].

In a hydraulic system with pipes with closed ends, transient pressure waves reflect from the end due to the compression of the fluid, hydraulic capacitance. The frequency response of pressure transients in hydraulic systems mostly depend on the lengths of the piping.

2.1.5 One-way flow control valves

In hydraulic systems, the rate of movement of hydraulic actuators depends on the flow rate. Therefore, controlling fluid flow is crucial in managing velocities of hydraulic systems. Flow control valves are widely used to regulate flow in hydraulic systems. [25] Many different types of flow control valves are available and suitable valve types need to be considered to fit the application. In this thesis, only the characteristics and operation of one-way flow control valves is covered, since they are included in the hydraulic system being tested.

One-way flow control valves, shown in Figure 10, are utilized to adjust the flow in one direction. The valves consist of two fluid lines: one equipped with an adjustable orifice and a flow bypass line equipped with a check valve. The adjustable orifice enables control over flow from 1 to 2, and the check valve line allows free flow from 2 to 1. The bypass line is typically preventing cavitation after the valve.

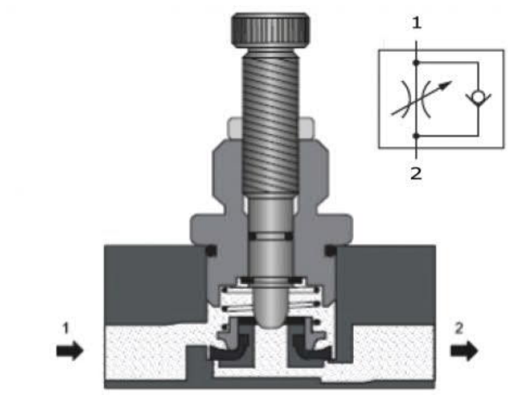

Figure 10 One-way flow control valve section and symbol. Source: [26]

Check valves are typically equipped with a poppet and a spring. The poppet geometry and shape may vary from ball shapes, cone shapes to plate shapes. The spring forces the poppet to shut. When a certain pressure difference is reached, the valve opens allowing flow through. The pressure difference needed to overcome the force of the spring is called cracking pressure. High cracking pressures lead to higher pressure losses. An ideal check valve prevents flow reversal entirely, but the inertia, friction, and possible damping effects of the poppet cause the valve to close slightly after the flow reversal [27].

One-way flow control valves can be used in hydraulic cylinder systems to adjust the velocity of a cylinder piston. The adjustable orifice restricts flow to one direction and the embedded check valve allows more flow to pass through to the other direction. By connecting proper flow control valves to both cylinder ports, cavitation in fluid lines and cylinder chambers is prevented. The restriction of flow increases the stiffness of the cylinder system.

The effects of flow in hydraulic stiffness were presented in the previous section. The flow through an orifice was introduced in equation (9). As flow is proportionate to the area of the orifice, the flow through one-way flow control valves is discontinuous. The effective flow area of the valve increases when cracking pressure is reached.

2.2 Mechanical stiffness

Hydraulic cylinder systems typically consist of steel components and joints, which have significantly higher stiffnesses than hydraulic fluids. Therefore, the contribution of mechanical stiffness components to the static net stiffness of hydraulic cylinder systems are often low, but not negligible. This section covers the stiffnesses of cylinder rods, expansion stiffnesses of pipes, hoses, and cylinder chambers, along with sealing system stiffnesses.

The cylinder rod is a solid steel rod, and its axial stiffness K_r can be calculated simply as:

$$k_r = \frac{EA_r}{l_r} \tag{21}$$

where E is the Young's modulus for steel, A_r is the cross-sectional area of the rod and l_r is the rod length.

The expansion stiffness of the cylinder barrel is different for the head and rod chambers. Both head and rod chamber expansion stiffnesses, k_{cA} and k_{cB} respectively, are derived in [4] to be

$$k_{cA} = \frac{E_b A_A}{2l_A} \frac{1}{\lambda_c + \nu_b} \tag{22}$$

and

$$k_{cB} = \frac{E_b A_B}{2l_B} \frac{1}{\lambda_c + \nu_b} \tag{23}$$

where E_b is the Young's modulus of cylinder barrel, A is the corresponding effective piston area, l is the corresponding effective chamber length, λ_c is the expansion coefficient of cylinder barrel and ν_b is the Poisson ratio of cylinder barrel. The expansion coefficient for a cylindrical structure is

$$\lambda_c = \frac{D_1^2 + D^2}{D_1^2 - D^2} \tag{24}$$

where D_1 is the outer diameter and D is the inner diameter.

The expansion stiffness of metal pipes is presented in [4] to be

$$k_p = \frac{2E_p \mathrm{A}^2}{\pi D_p^2 l_p (\lambda_p + \nu_p)} \tag{25}$$

where E_p is the young's modulus of pipe, A is the corresponding effective piston area, l_p is the pipe length, λ_p is the expansion coefficient of pipe, presented in equation (24), ν_p is the Poisson ratio of pipe. The expansion stiffness for hoses can also be calculated with equation (25) by substituting the pipe parameters with the corresponding hose parameters. Then, the expansion stiffness for hoses is:

$$k_h = \frac{2E_h A^2}{\pi D_h^2 l_h (\lambda_h + \nu_h)} \tag{26}$$

where E_h is the Young's modulus of the hose. However, hydraulic hoses are multilayered; typically composing of an inner rubber layer, a steel winding or braiding, covered by an anticorrosive rubber layer. The thicknesses and the number of layers and even the steel braiding patterns vary. Therefore, the elasticity modulus E_h of a hydraulic hose is nonlinear and hard to determine accurately. An estimate of the elasticity modulus was presented to be 17,8 GPa by [4] based on experimental data. It should be noted that the value was extracted by only one measurement conducted at a pressure of 160 bar, and no details about the braiding types were presented. Thus, the resulting elasticity modulus can only be used to achieve a rough estimate for hose stiffnesses in general.

2.3 Effects of friction

Friction is a force reacting tangentially between two contacting surfaces. It is governed by various parameters such as contact geometry and topology, surface materials, displacement and relative velocity of the contacting bodies, and presence of lubrication [28]. This has led to difficulties in developing accurate friction models and left uncertainties in friction modelling [29]. In hydraulic cylinders, the sealing parts; rod and piston sealing systems are the main source of friction.

2.3.1 Simplified friction models

Classical and simplified approaches to friction modelling are shown in Figure 11. Coulomb friction model (a), also known as dry friction, only considers the normal force affecting the surfaces. Stiction (b) includes the Coulomb friction as well as the static friction. Stribeck friction (c) is a more advanced classical friction model, which considers Coulomb friction, stiction, the Stribeck effect and viscous friction. The Stribeck effect describes the friction force right after entering the sliding regime, where the increase in absolute velocity decreases the friction force. Viscous friction denotes the linear incline of friction force after the Stribeck effect regime. However, aforementioned models cannot predict the precise behavior of friction forces due dynamic friction phenomena, such as hysteresis, friction lag and stick-slip motion. [29]

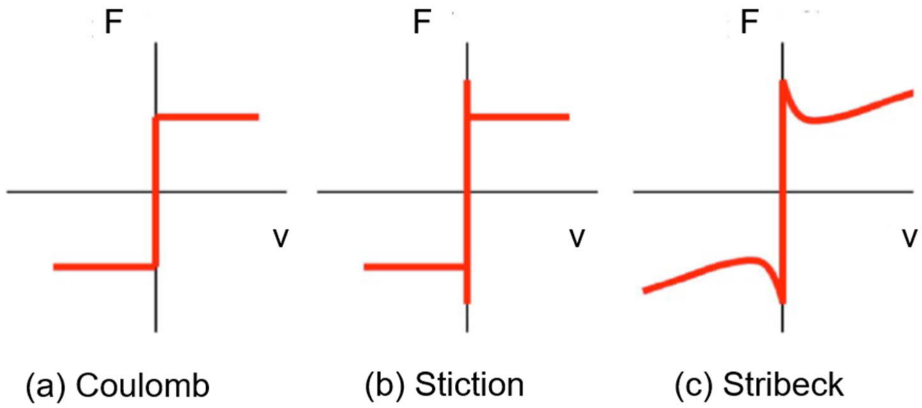

Figure 11 Friction force versus relative velocity of surfaces for: (a) Coulomb friction (b) stiction and (c) Stribeck friction models. Source: modified from [30]

2.3.2 LuGre friction model

A widely used dynamic friction model for hydraulic cylinders is the LuGre model. It offers a good trade-off between complexity and accuracy in modelling friction characteristics

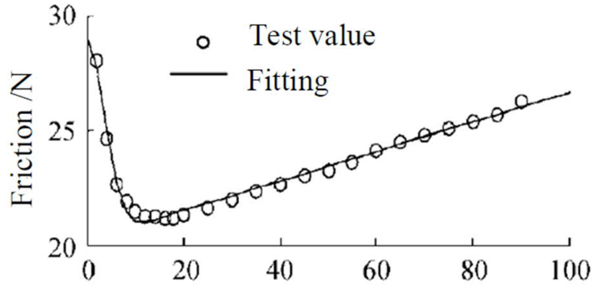

Figure 12 LuGre curve fitting comparison to tested values. Source: [31]

[31]. An illustration of the accuracy of the LuGre model is presented in Figure 12. The model covers most static and dynamic phenomena present in friction.

In the LuGre model, a simplification of the contacting surfaces is done by observing the friction surfaces as elastic bristles, where the bristles are modeled as spring-damper systems as shown in Figure 13. The bristles represent the microscopic peaks and valleys of the contacting surfaces originating from the roughness of the surfaces.

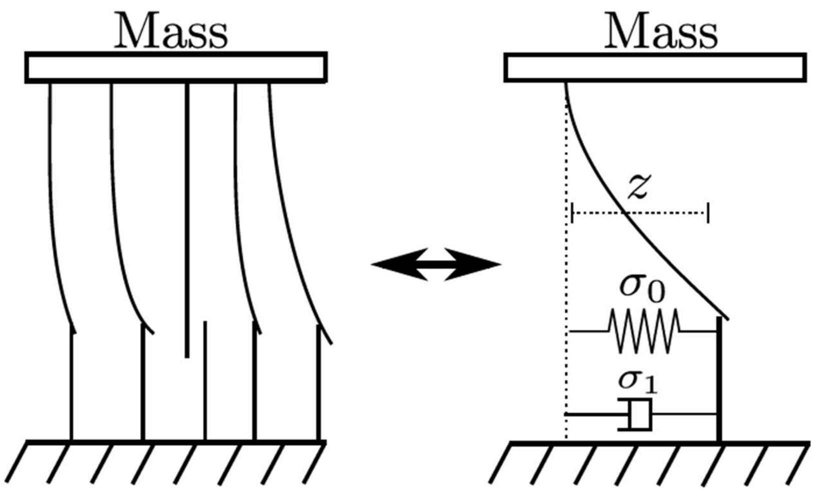

Figure 13 LuGre bristle modeling. Source: modified from [32]

The LuGre model is described by the following equations

$$\dot{z} = v - \sigma_0 \frac{|v|}{g(v)} z \tag{27}$$

$$F = \sigma_0 z + \sigma_1 \dot{z} + f(v) \tag{28}$$

where v is the relative velocity between the contacting surfaces, z is the average deflection of the bristles, F is the friction force, σ_0 is the bristle stiffness, σ_1 is the bristle damping, $f(v)$ is the viscous friction, also known as damping term, and $g(v)$ is a velocity dependent function which captures the Coulomb friction and the Stribeck effect. The viscous friction term $f(v)$ is often denoted as a linear damping component:

$$f(v) = \sigma_2 v \tag{29}$$

where σ_2 is damping. The Coulomb friction and Stribeck effect function, $g(v)$ is often approximated by

$$g(v) = F_c + (F_s - F_c) e^{-\left|\frac{v}{v_s}\right|^{\alpha}} \tag{30}$$

where F_c is the Coulomb friction force, F_s is the static friction force, v_s is Stribeck speed, which expresses how rapidly $g(v)$ approaches the Coulomb friction and α is a geometry dependent coefficient. [33]

The functions $f(v)$ and $g(v)$ can be acquired by experimentally examining the steady-state friction with constant velocities. The steady state friction force F_{ss} for constant velocities is determined by [33]:

$$F_{ss} = g(v)sgn(v) + f(v) \tag{31}$$

Then, determining the bristle average spring and damping coefficients, σ_0 and σ_1 respectively, yields the complete friction model. The spring and damping coefficients are material parameters and can be found in literature.

2.3.3 Friction in hydraulic cylinder sealing systems

Dynamic sealing systems, also known as reciprocating seals are used in hydraulics to prevent the leakage of hydraulic fluid and to keep contaminants out [34]. In hydraulic cylinder sealing solutions, there is always a tradeoff between isolating properties, lifecycle, and efficiency. For example, good isolation properties require a higher level of seal squeeze, but as a result the lubrication decreases, which causes the seal to wear faster. Meanwhile, the volumetric efficiency increases but the mechanical efficiency decreases due to increased friction force. A large number of research on sealing systems has been the result of the growing demand for more efficient systems [35].

In hydraulic cylinders, friction occurs between the contact surfaces of the sealing elements and guiding elements. It should be noted that piston and rod sealing systems often contain multiple sealing and guiding elements, often with different materials and profiles, as illustrated in Figure 14. The variance in material parameters and the cross-sectional profiles makes it difficult to predict friction forces in hydraulic cylinders. Thus, accurate analysis of friction requires experimental examination.

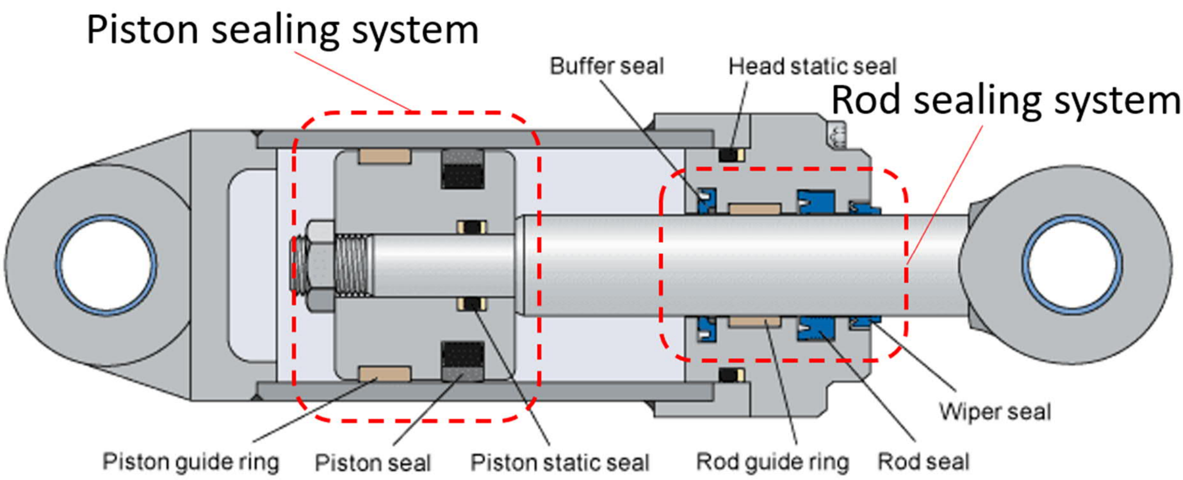

Figure 14 Illustration of a piston sealing system and a rod sealing system. Source: modified from [36]

O-rings arguably inhibit the simplest profile of reciprocating seals. A general guide for factors effecting friction in O-rings is provided by a major hydraulics manufacturer in

Table 1. The table highlights the high number of variables affecting seal friction. The most important parameters are the amount of squeeze and the metal surface finishes of rod and chamber.

Table 1 Factors affecting friction in O-rings in order of significance. Source: modified from [37]

To increase friction	Factor	To reduce friction
Increase	Squeeze	Decrease
Increase	Metal surface finish (RMS)	Decrease
Increase	Seal material hardness	Decrease
Decrease	Relative motion speed	Increase
Increase	Cross section of seal	Decrease
Decrease	Hydraulic pressure	Increase
Decrease	Temperature	Increase
Decrease	Groove width	Increase
Increase	Diameter of rod or bore	Decrease
Decrease	O-ring surface finish	Increase

The stiffness effects on the cylinder rod of reciprocating seals disappear when the piston is in motion, therefore they have trivial contribution to the overall stiffnesses of hydraulic cylinders in dynamic conditions. Under dynamic loads, the contribution of seal friction is more associated with the velocity term, damping. When the piston is in motion, the seals are in sliding regime, meaning that the friction force is determined by the relative velocity of the two surfaces.

In static and quasi-static loading, the maximum force acting on the seals is the stiction force. The effects of friction can be estimated in static conditions by determining the deflection of the seal with the breakaway force.

However, the deflections are typically miniscule and the magnitudes of friction forces in hydraulic cylinders are often significantly smaller than the working forces. Combining equations (28) and (29) from the previous chapter yields the friction force according to the LuGre model as:

$$F = \sigma_0 z + \sigma_1 \dot{z} + \sigma_2 v \tag{32}$$

where only the $\sigma_0 z$ term accounts for stiffness. Said term also only contributes to the total stiffness when velocity is close to the zero-crossing point. In dynamic conditions, only the damping terms are seen.

3 Description of test configuration

In this section the testing setup and calculation methods are presented. The aim of this thesis is to determine the dynamic stiffness characteristics of a cylinder system illustrated in Figure 15. The system consists of a 40/25-220 differential cylinder paired with one-way flow control valves. Working pressures are 20,5 bar and 42 bar for the head end and rod end respectively. The working pressures cause a downward net force of about 640 N.

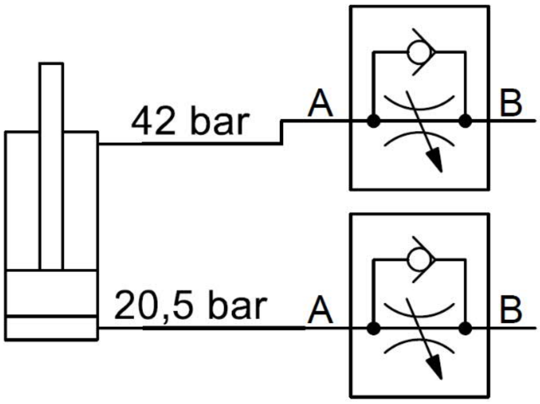

Figure 15 Hydraulic diagram of the hydraulic cylinder system.

The test bench is presented in Figure 16. It consists of a symmetrical load cylinder, on top, and the differential test cylinder, below, mounted to a vertical frame. In between the cylinders a load cell is measuring the load forces. The load cylinder is driven to cause force excitations to the test cylinder. Control is implemented with a direct operated proportional valve paired with the load cylinder. The control system and data acquisition are run with an industrial PC.

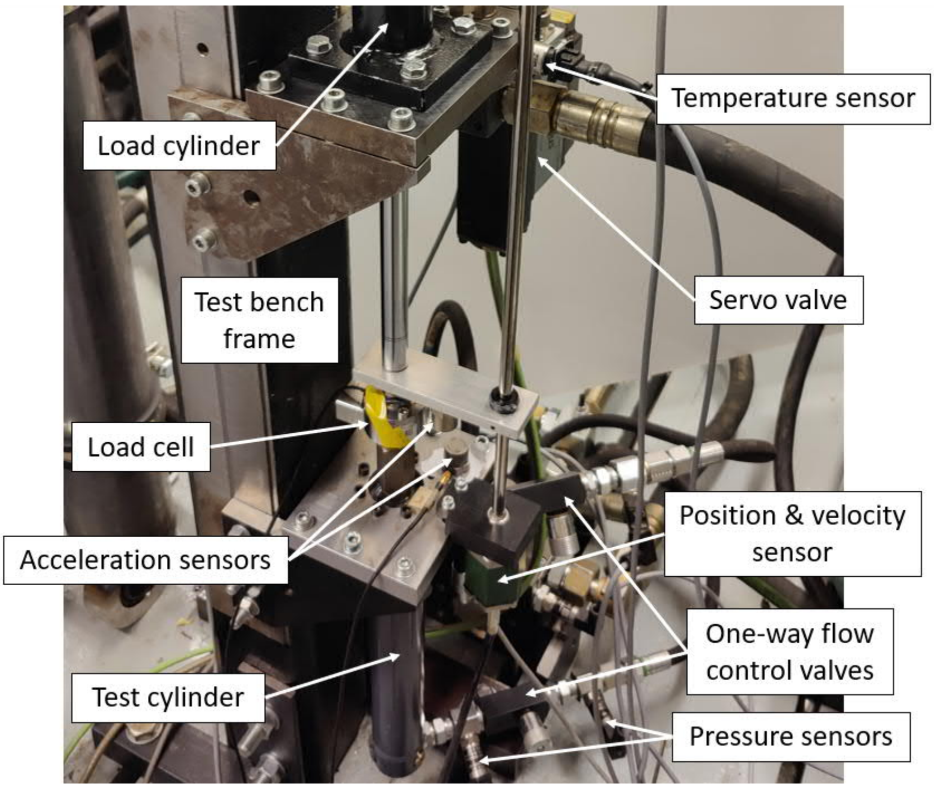

Figure 16 Test bench setup.

Two types of tests were conducted with the test bench: static stiffness tests and dynamic stiffness tests. For the static stiffness tests, flow through the test cylinder chamber was entirely blocked. The static stiffness was determined by measuring the force and the corresponding deflection of that force. In the dynamic tests, the stiffnesses were determined in the frequency domain through force and velocity measurements.

The dynamic stiffness tests were designed for both extending and retracting motions. The load cylinder was set to extend or retract the test cylinder with a constant velocity of 2-3 mm/s. A sinusoidal force disturbance was added to the constant-velocity motion to cause excitations. The displacement and force amplitudes were measured, and the dynamic stiffnesses in different piston positions were resolved.

The testing parameters for the dynamic loads were amplitude, frequency, flow control valve opening, and direction. The amplitude was manually defined to values which would not exceed the limits of the ±5 kN load cell used to measure the force. The tests were conducted with excitation amplitudes based on proportional valve spool opening of the load cylinder. The testing frequencies were 10, 15, 20, 25, and 30 Hz. The flow control valves were adjusted in three throttling positions: fully open, 50% closed, and 75% closed. Dynamic tests were also conducted with the one-way flow control valves fully closed. This required the testing to be conducted in set positions. The last test parameter, direction, was adjusted manually by applying an offset to the proportional valve opening, causing motion in either direction. The offsets were adjusted to each test configuration separately since the dynamics of the system changed significantly when varying the other parameters.

3.1 Hydraulic components

The detailed test bench hydraulic diagram is shown below in Figure 17.

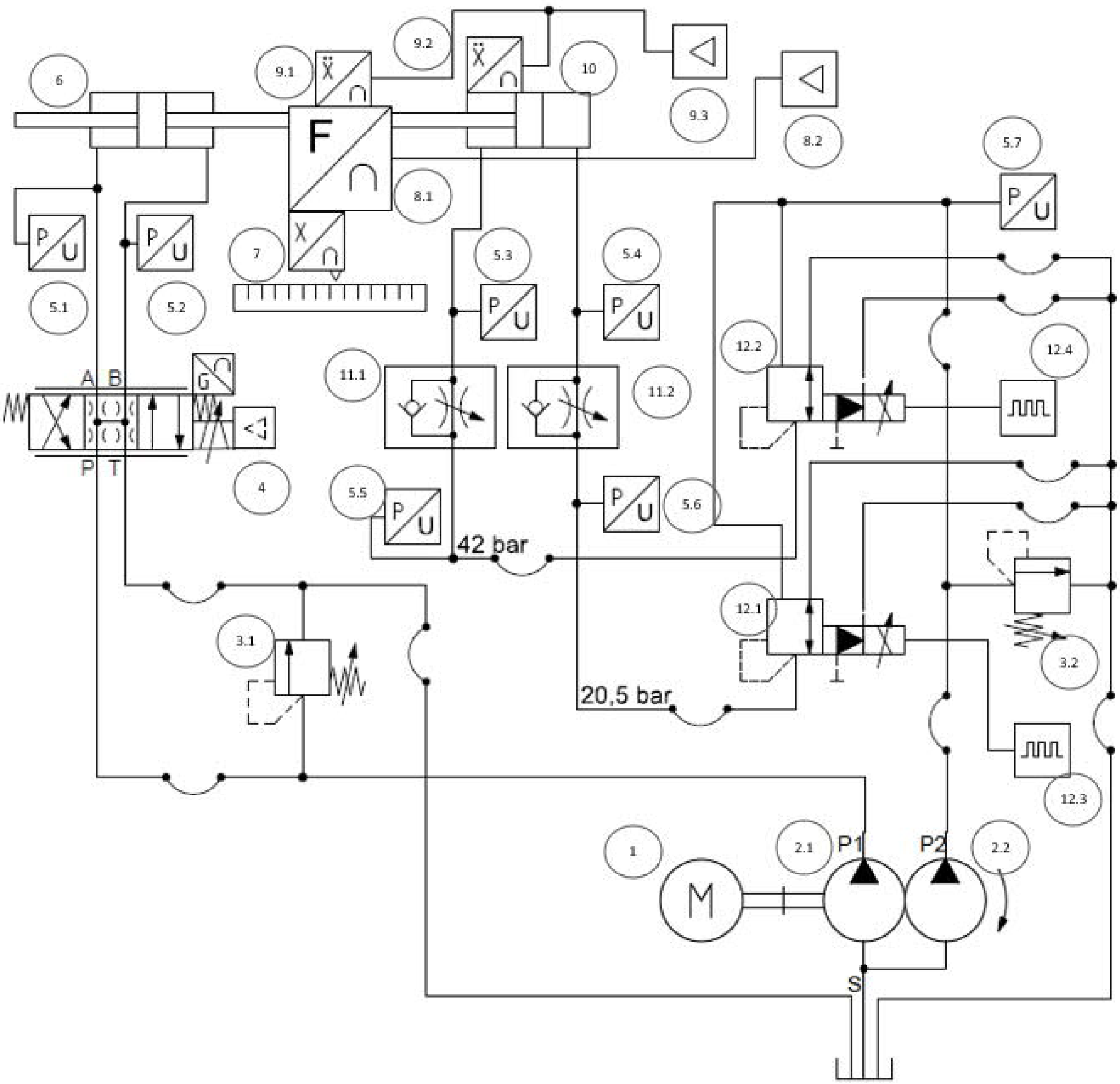

Figure 17 Test setup hydraulic diagram.

The hydraulic system is powered by a 22-kW electric motor coupled with two gear pumps to pressurize the circuits. The electric motor and pumps are shown in Figure 18. The first pump powers up the load cylinder circuit and the second one powers up the test cylinder circuit. The pressure in both test cylinder and load cylinder circuits are adjusted with pressure relief valves (PRVs).

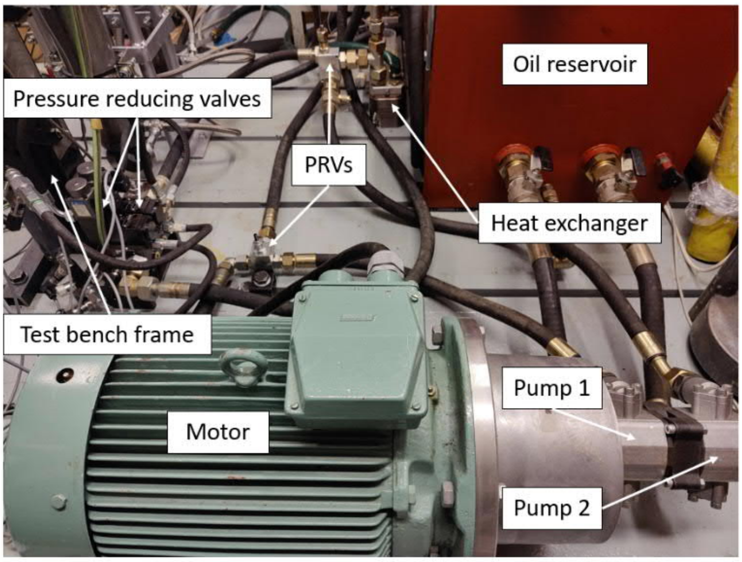

Figure 18 The electric motor and gear pumps.

The load cylinder is a symmetrical cylinder with a stroke of 250 mm and piston diameter of 40 mm. The rod, coming through both ends, has a diameter of 20 mm. The sealing elements were chosen to be as frictionless as possible. Both piston and rod sealing systems consist of PTFE seal rings alloyed with bronze, coupled with O-rings. The load cylinder is actuated by a Parker DFplus direct operated proportional valve. The proportional valve inhibits a high frequency response due to voice coil actuation.

The pressure levels for the 40/25-220 test cylinder are adjusted coarsely with a PRV and more accurately with proportional pressure reducing valves for each cylinder chamber. Between the proportional pressure reducing valves and the cylinder chambers are the one-way flow control valves. Pressures are measured on both sides of the one-way flow control valves to be able to detect the opening of the check valves and to record the pressure losses over the valves. Also, pressure is measured between the PRV and the proportional pressure reducing valves, to record the pressure variance caused by loading the system.

The test cylinder hydraulic diagram is represented in Figure 19. The hoses and pipes are also labeled in the diagram with “H” and “P” respectively, and their dimensions are presented in Table 2.

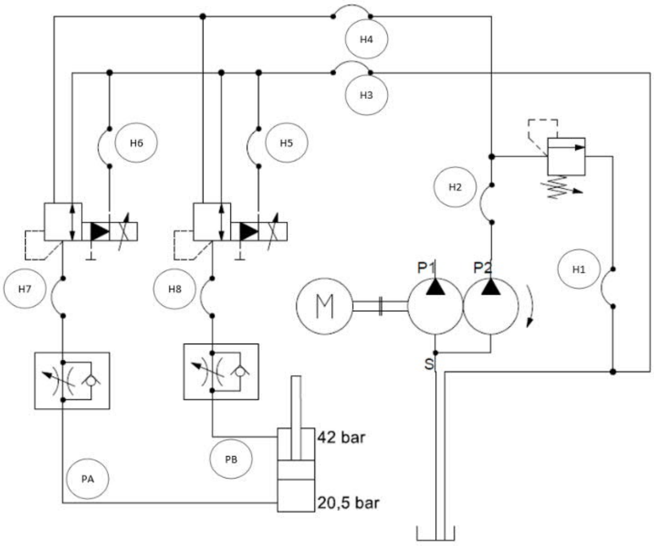

Figure 19 Test cylinder hydraulic diagram.

Table 2 Dimensions of test cylinder circuit hoses and pipes. Labels referring to Figure 19.

Component	Length [m]	Inner diameter [mm]	Outer diameter [mm]
H1	0,6	25	30
H2	1,2	25	30
H3	1,0	25	30
H4	0,8	25	30
H5	0,4	9,5	12
H6	0,4	9,5	12
H7	0,6	9,5	12
H8	0,8	9,5	12
PA	0,1	9,5	N/A
PB	0,1	9,5	N/A

When determining the stiffness under dynamic loads, the expansion stiffness of at least hoses H7, H8 (as well as their additional fluid volume) need to be addressed. The pipelines PA and PB consist of several hydraulic fittings, meaning that the outer diameters are not uniform throughout their lengths. Therefore, the expansion stiffness of said pipelines can be considered as arbitrarily large. Thus, only the added fluid volumes of the pipes (PA and PB) is considered when calculating the stiffness of the system.

The one-way flow control valve, mounted on both test cylinder ports, is shown in Figure 20. The valve consists of a needle for throttling and a spring-poppet to enable free flow in one direction. The effective orifice areas of free flow and needle valve when the needle is fully open are 0,64 cm² and 0,22 cm² respectively.

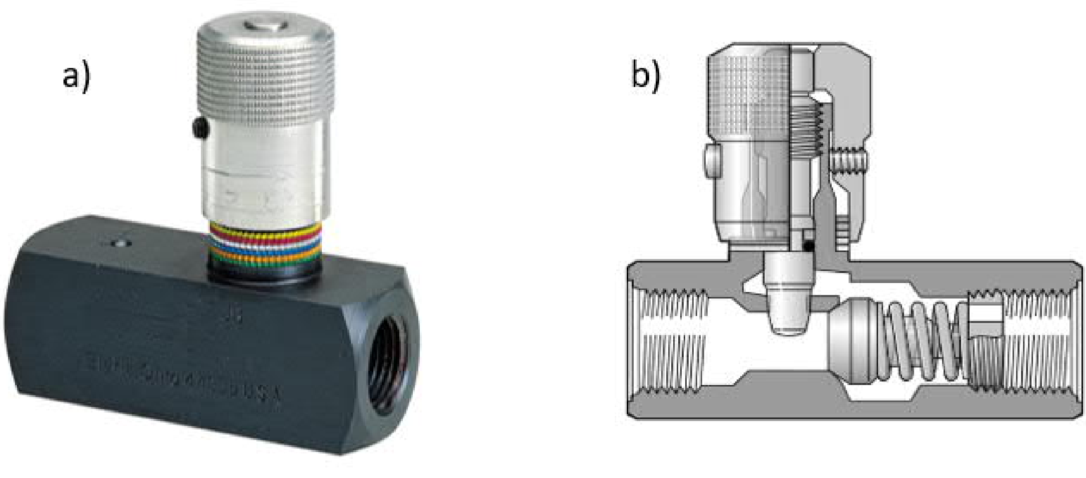

Figure 20 Parker F series one-way flow control valve a) overview b) partial section view. Source: [38]

The one-way flow control valves are connected to Parker VMY series pilot operated proportional reducing valves, shown in Figure 21. The valves are utilized to set the working pressures in the test cylinder as 20,5 bar and 42 bar for A and B chambers respectively.

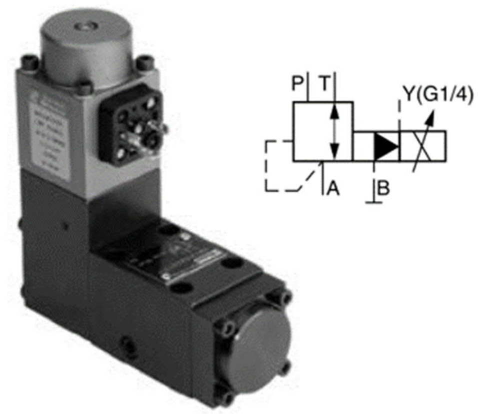

Figure 21 Parker VMY pilot operated proportional reducing valve overview and symbol. Source: [39]

The full list of hydraulic components is presented in Table 3. The item numbers refer to the full hydraulic diagram shown in Figure 17.

Table 3 Hydraulic components bill of materials. Numbering referring to Figure 17.

Item no.	**Item description**	**Type**	**Manufacturer**
2.1	Gear pump	-	-
2.2	Gear pump	-	-
3.1	Pressure-relief valve (load cylinder)	-	-
3.2	Pressure-relief valve (test cylinder)	-	-
4	Direct operated proportional valve (DFplus)	D1FPE50MA9NB00	Parker
6	Load cylinder	40/20-250 (symmetrical)	Ravaltsu Oy
10	Test cylinder	40/25-220 (differential)	-
11.1	One-way flow control valve	F600	Parker
11.2	One-way flow control valve	F600	Parker
12.1	Proportional reducing valve	VMY-100K06NV1P	Parker
12.2	Proportional reducing valve	VMY-100K06NV1P	Parker

3.2 Electrical components

Data acquisition and test run logic were executed with a C6920 Beckhoff Industrial PC, presented in Figure 22. The system was programmed and run in TwinCAT 3 - the automation software provided by Beckhoff.

Figure 22 Beckhoff C6820 Industrial PC. Source: [40]

The absolute position of the cylinder ends was tracked with a GYSE-A analog linear magnetostrictive sensor, shown in Figure 23. The contactless sensor measures the displacement of the circular magnet over the sensor rod. The magnet was attached to a flat bar which was mounted in between the load cylinder and the load cell (described in more detail in section 3.3).

Figure 23 GYSE-A magnetostrictive linear sensor. Source: [41]

The relative piston velocity was determined with two Brüel & Kjær accelerometers with frequency range of 0,1 Hz to 4800 Hz. One accelerometer was attached to the frame and another was mounted on the flat bar, where the magnet for the GYSE sensor was located. Both accelerometers were coupled with a charge amplifier with built-in integrator to acquire the velocity amplitudes.

Figure 24 B&K accelerometer. Source: [42]

The force measurements were conducted with an HBM U2B load cell, shown in Figure 25. The load cell measuring range was ±5 kN, and it was placed between the load and test cylinders. The measurement method is based on a strain gauge inside the frame of the load cell. The nominal deformation with a 5 kN force is provided by the manufacturer as 0,047 mm. Therefore, its stiffness can be approximated as: 106 MN/m. This will be considered in further stiffness calculations.

Figure 25 HBM U2B load cell. Source: [43]

Electrical components used in the test bench (excluding the control and data acquisition components) are listed in Table 4.

Table 4 Electrical components bill of materials. Numbering referring to Figure 17.

Item no.	Item description	Type	Manufacturer
1	Electric motor 22 kW, 1480 r/min	HXUR 368G2 B3	Oy Strömberg Ab
5.1	Pressure sensor 250 bar	HDA 4700	HYDAC
5.2	Pressure sensor 250 bar	HDA 4700	HYDAC
5.3	Pressure sensor 100 bar	NAT 8252 100.0A	Trafag
5.4	Pressure sensor 40 bar	NAT 8252 40.0A	Trafag
5.5	Pressure sensor 100 bar	NAT 8252 100.0A	Trafag
5.6	Pressure sensor 40 bar	NAT 8252 40.0A	Trafag
5.7	Pressure sensor 100 bar	NAT 8252 100.0A	Trafag
7	Position & velocity sensor	A-500-M-N-CNCD10VA999	GYSE
8.1	Load cell ±5 kN	U2B	HBM
8.2	Strain gauge amplifier	DPM-603A	Kyowa
9.1	Accelerometer (rod)	4381	Brüel & Kjær
9.2	Accelerometer (frame)	4381	Brüel & Kjær
9.3	Charge amplifier	Nexus 2692-A	Brüel & Kjær
12.3	PWM module for proportional reducing valve (12.1)	PWDXXA-40X	Parker
12.4	PWM module for proportional reducing valve (12.2)	PWDXXA-40X	Parker

Other accessories include Beckhoff terminals and the industrial PC for data acquisition and control. The Beckhoff system configuration used to implement data acquisition and control of the test bench is shown in Figure 26.

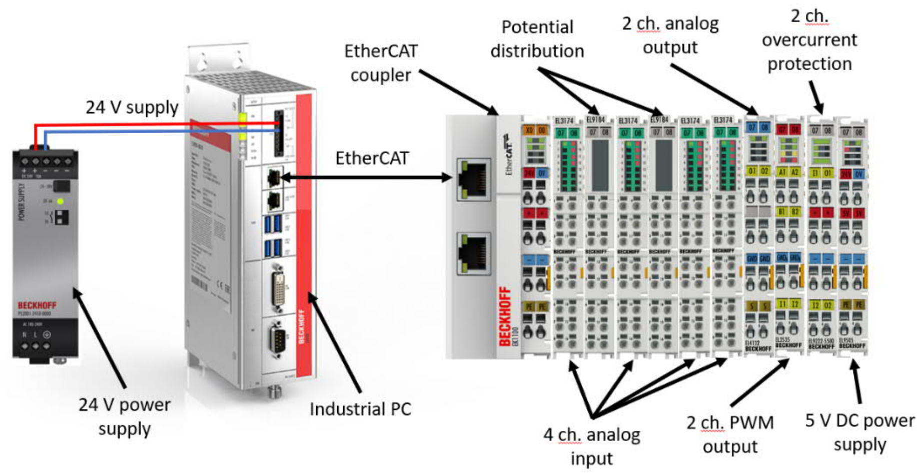

Figure 26 Control and data aqcuisition system configuration.

The Beckhoff accessories used are listed in Table 5. Type details and descriptions are included.

Table 5 Beckhoff control system bill of materials

Item no.	Qty.	Item description	Type
1	1	Power supply 24 V, 10 A	PS2001-2410-0000
2	1	Industrial PC	C6920-0050
3	1	EtherCAT coupler	EK1100
4	4	4-channel analog input terminal	EL3174
5	2	Potential distribution terminal	EL9184
6	1	2-channel analog output terminal	EL4132
7	1	2-channel PWM output terminal	EL2535-0002
8	1	2-channel overcurrent protection terminal	EL9222-5500
9	1	5 V DC power supply terminal	EL9505

3.3 Determining the stiffness of the test cylinder

In chapter 2, static stiffness was introduced as the ratio of applied force proportional to the corresponding displacement. Determining the stiffness of a hydraulic cylinder system requires measurements throughout the stroke of the cylinder. This section covers the stiffness calculations with the presented models, as well as the measurement and testing processes.

Force and displacement are required to determine the stiffness of a hydraulic cylinder. The configuration of the most crucial measurements is shown in Figure 27. The figure highlights the placement of the sensors and thus the measuring points of the force, velocity, and position, which are all used to determine the stiffness in different setups. The displacements caused by static loads were determined with the GYSE-A position sensor and the displacements caused by dynamic loads were recorded with the accelerometers.

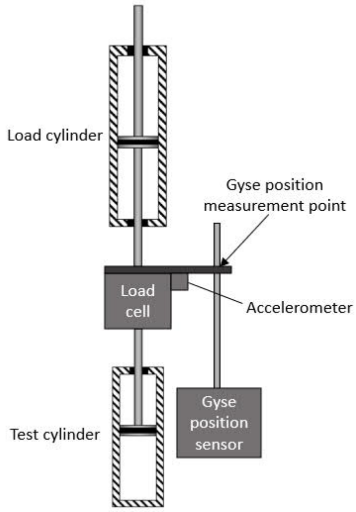

Figure 27 Illustration of force, velocity and position measurements in the test bench.

The free-body diagrams of the cylinders are shown in Figure 28. Forces are measured by an inner strain gauge in the load cell, meaning forces elongating the load cell are positive and forces compressing the load cell are negative.

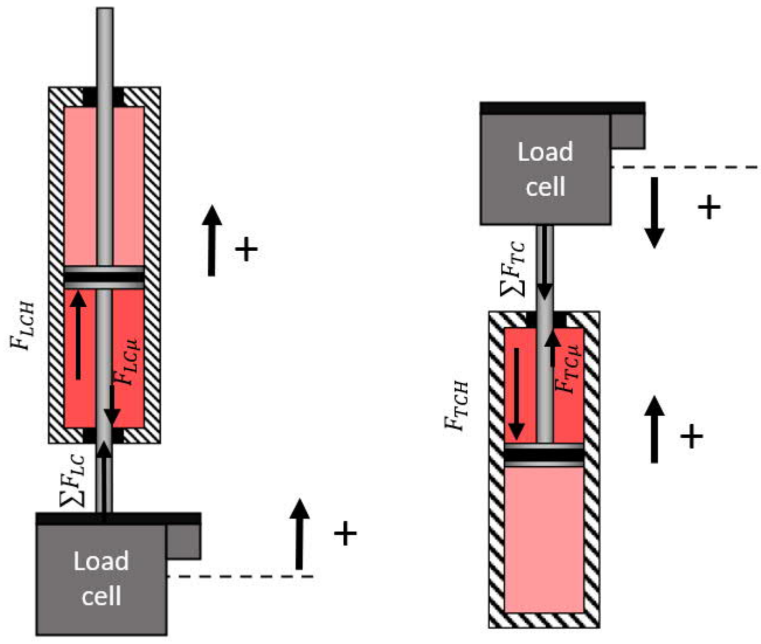

Figure 28 Free-body diagrams of the cylinders in the test bench with an upward loading force.

Based on this, the load cell force, F_L, is:

$$F_L = \Sigma F_{LC} = \Sigma F_{TC} \tag{33}$$

where ΣF_{LC} is total load cylinder force, and ΣF_{TC} is total test cylinder force. ΣF_{LC} consists of the load cylinder hydraulic force, F_{LCH} and load cylinder friction force $F_{LC\mu}$, as can be seen in Figure 28, but it is also the actual loading force acting on the test cylinder rod recorded by the load cell, F_L. Since the test cylinder positive force direction is upwards (and the load cell bottom half positive force direction is downwards), the load cell force is:

$$F_L = F_{TCH} - F_{TC\mu} \tag{34}$$

where F_{TCH} and $F_{TC\mu}$ are the total test cylinder hydraulic force and total test cylinder total seal friction force respectively. The pressures in both chambers of both cylinders are measured, so the hydraulic forces can be determined. The hydraulic force of a cylinder is:

$$F_{TCH} = p_A A_A - p_B A_B \tag{35}$$

where p_A and p_B are the pressures in the cylinder chambers and A_A and A_B are the effective areas of the piston for each chamber. As F_L and F_{TCH} are measured in the system, the friction force of the test cylinder can be estimated as:

$$F_{TC\mu} = F_L - p_A A_A - p_B A_B \tag{36}$$

Friction is always directed towards the opposite direction of motion.

3.3.1 Stiffness model for static tests

The static stiffness model for the cylinder system was compiled according to equation (3). In the test bench, piston position is measured from the end of the load cylinder. Therefore, the stiffness of the load cell needs to be considered as an addition. Corresponding system parameters were assigned according to the test bench, and the theoretical static stiffness was calculated as a function of piston position. The static stiffness of the test cylinder is then

$$k = \left(\frac{1}{k_o} + \frac{1}{k_r} + \frac{1}{k_c} + \frac{1}{k_L}\right)^{-1} \tag{37}$$

where k_L is the stiffness of the load cell, which was calculated earlier as 106 MN/m. MATLAB was used to calculate and plot the stiffness curve. The resulting test cylinder static stiffness is plotted as a function of piston position in Figure 29. A bulk modulus value of 1600 MPa was used to calculate and plot the stiffness.

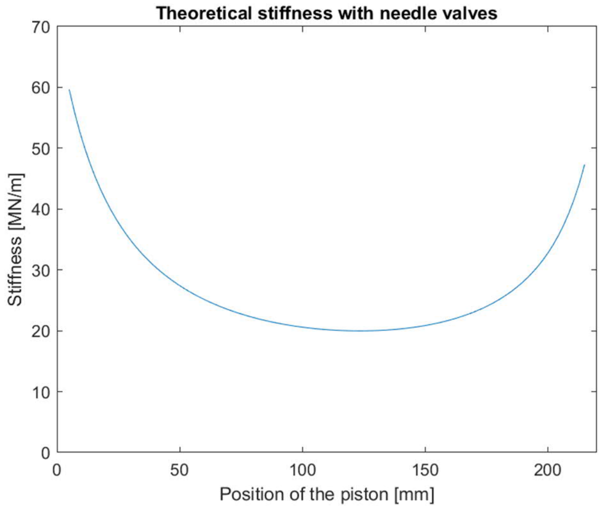

Figure 29 Theoretical test cylinder static stiffness as a function of piston position.

3.3.2 Static stiffness measurement process

To determine the static stiffness of the test cylinder, the configuration was modified. The one-way flow control valves were replaced with needle valves to disable flow through the cylinder chambers as shown in Figure 30. Measurements without flow in the cylinder chambers would disclose estimates of the bulk modulus and air contents in the cylinder. To measure the static stiffness throughout the whole stroke, several piston positions need to be included.

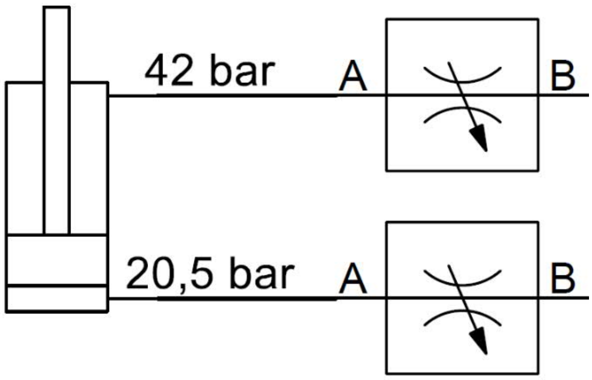

Figure 30 Test cylinder configuration for testing only the cylinder stiffness characteristics.

The static stiffness of the hydraulic cylinder was determined experimentally with the modified configuration in Figure 30. The testing process, shown in Figure 31, occurred as following: the desired starting position was sought with a P control loop (1), then the throttle valves were closed manually (this can be seen in the force data smoothening, as the pump no longer causes pressure oscillations in the chambers) (2), and a static load of 4 kN was ramped up by a 2 second ramp (3) and was applied on the test cylinder for 3 seconds, which resulted in a displacement of the piston (4). After the static loading ended (5), the throttle valves were opened (6), and process was repeated for the next piston position.

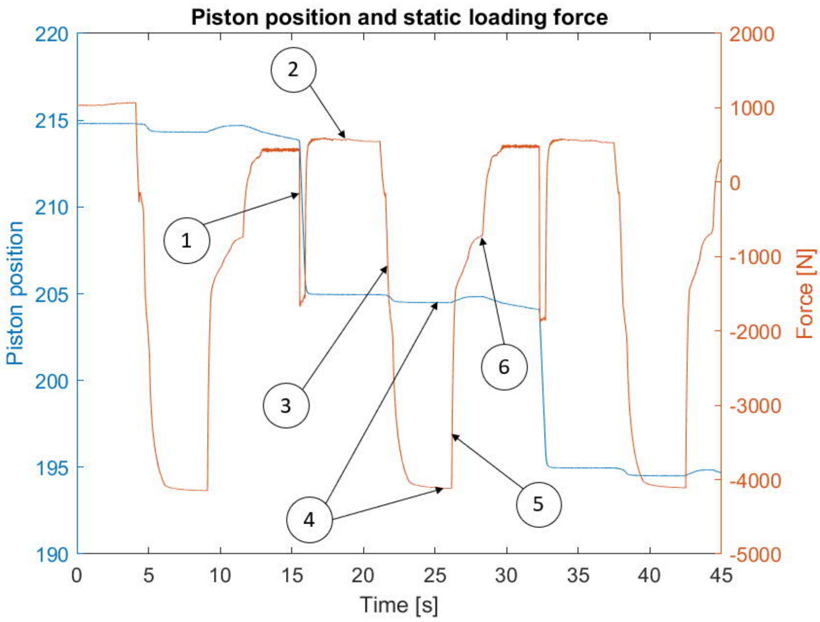

Figure 31 Static loading testing process.

The interval between piston test positions was 10 mm, and the start and end positions were 5 mm from each end of the stroke. In all, 22 measurements were taken within a test run. The loading direction and the starting points were varied between test runs. In each test run the starting point was either at piston position 5 mm or 215 mm. In a single test run, loads were only applied in one direction which resulted in four separate runs:

1) starting position 5 mm, load up;
2) starting position 5 mm, load down;
3) starting position 215 mm, load up; and finally,
4) starting position 215 mm, load down.

The axial force was extracted with the HBM U2B load cell paired with the Kyowa strain gauge amplifier and the piston position from the GYSE-A position sensor. Then the stiffness was simply calculated by dividing the changes in axial forces with the corresponding deflections.

3.3.3 Stiffness model for dynamic test setup

In the main testing setup, presented earlier in Figure 15, the hose expansion stiffness and additional volume of the fluid lines were considered when calculating the theoretical stiffness. Stiffness is then:

$$k = \left(\frac{1}{k_o} + \frac{1}{k_r} + \frac{1}{k_c} + \frac{1}{k_L} + \frac{1}{k_h}\right)^{-1} \tag{38}$$

The resulting stiffness curve is plotted in Figure 32. This will act as the baseline for the dynamic tests. The stiffness is calculated with an air compensated bulk modulus value of 1300 MPa.

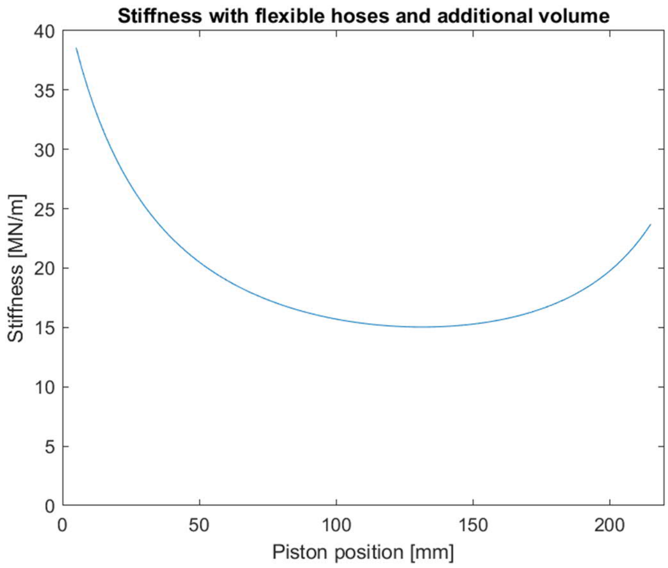

Figure 32 Theoretical stiffness of test cylinder with flexible hoses and additional volume as a function of piston position between 5 to 215 mm.

The characteristics of flow is crucial in modelling the cylinder system. The dynamic response of orifices can be applied as:

$$p_1 - p_2 = \frac{\rho}{\sqrt{\frac{C_q A_o \pi}{2}}}\left(\frac{dq}{dt}\right) + \frac{\rho q^2}{2\left(C_q A_o\right)^2} \tag{39}$$

where p_1 is the pressure between the valve and the head chamber, and p_2 is the pressure on the other side of the valve, as shown in Figure 33.

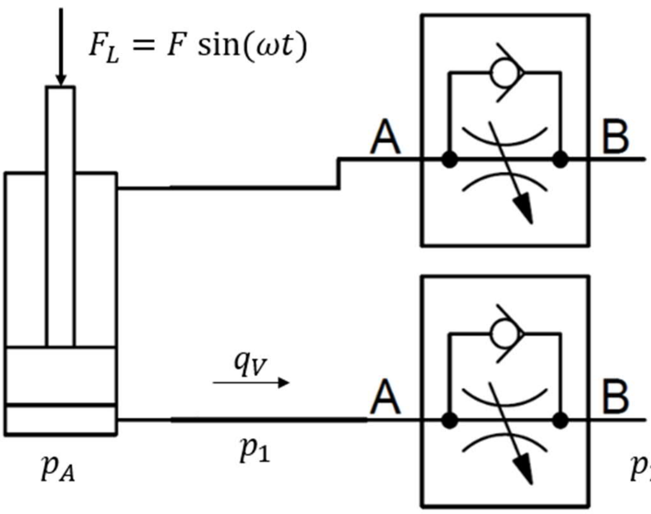

Figure 33 Dynamic loading configuration and variables.

The pressure in the head chamber is determined by the chamber hydraulic force as:

$$p_A = \frac{F_{LA}}{A_A} \tag{40}$$

where F_{LA} is the hydraulic force of the head chamber and A_A is the head chamber piston effective area. Assuming the flow resistance of the cylinder port to be negligible, we can express $p_A = p_1$, so:

$$p_1 = \frac{F_{LA}}{A_A} \tag{41}$$

The flow is induced by an external force acting on the cylinder rod, which translates to the fluid via the effective piston area. Therefore, the volumetric flow, q_V is proportionate to the speed of the piston as

$$q_V + \Delta q_V = A_A v \tag{42}$$

where Δq_V is the amount of compression, which was defined in equation (15). Rearranging equation (42) and applying equation (15) yields:

$$q_V = A_A v - \frac{V_A}{K_f}\frac{dp_1}{dt} \tag{43}$$

Applying equation (41) gives:

$$q_V = A_A v - \frac{V_A}{K_f A_A}\frac{dF\sin(\omega t)}{dt} \tag{44}$$

where F is the force amplitude.

$$q_V = A_A v - \frac{V_A}{K_f A_A}\omega F cos(\omega t) \tag{45}$$

and $\omega = 2\pi f$, in which f is loading frequency. As the throttle (orifice flow area) is varied, the flow required to reach the cracking pressure of the check valve varies as well. Additionally, the effective piston area is different for the test cylinder chambers.

The maximum flow rates in the dynamic tests without the check valves opening are reached with 10 Hz loading and no throttle. The base velocity is 3 mm/s at maximum and the velocity amplitude of the piston is no more than 20 mm/s until the check valve in the head side opens (this is presented later in the results section). Calculating the Reynolds number, the system can inhibit in the dynamic tests yields a Reynolds number of 100,8, when U_{mean} is estimated only by the relation of the piston head area A_A to the orifice area A_o as:

$$U_{mean} = \frac{A_A}{A_o} v \tag{46}$$

in which v is the piston velocity. This simplification disregards the compressibility in the system and in practice, the average velocity of flow would be smaller, which would result in a smaller Reynolds number. Comparing the calculated Re to Figure 7, we can see that the flow coefficient is around its theoretical value $C_q = 0{,}611$, but as the flow oscillates due to the sinusoidal load, the Reynolds number changes as well. The flow coefficient therefore changes between 0 to 0,611 during the loading. As equation (39), which captures the dynamic response of orifices, is heavily affected by the flow coefficient, it is extremely difficult to estimate flow rates (and compression due to orifices) in an oscillating cylinder system without flow measurements since the flow may change between laminar and turbulent in the system. However, flow (and the lack of flow) can be seen in the measurement data through comparing pressure levels throughout the system.

3.3.4 Measuring hydraulic cylinder dynamic stiffness separately

In the first part of the dynamic tests, the cylinder was once again isolated from the rest of the system with needle valves as shown earlier in Figure 30. The testing process, illustrated in Figure 34, in this stage was very similar to the static tests. The piston was set to the desired position with a P control loop (1), then the needle valves were closed (2), and a load was applied, only, the loading was dynamic (3). Then the needle valves were opened (4) and the process was repeated. The testing position intervals were the same as in the static tests: 10 mm. Starting positions of the test runs were 5 mm from the head end. Tests were conducted with dynamic load frequencies of 10, 20 and 30 Hz.

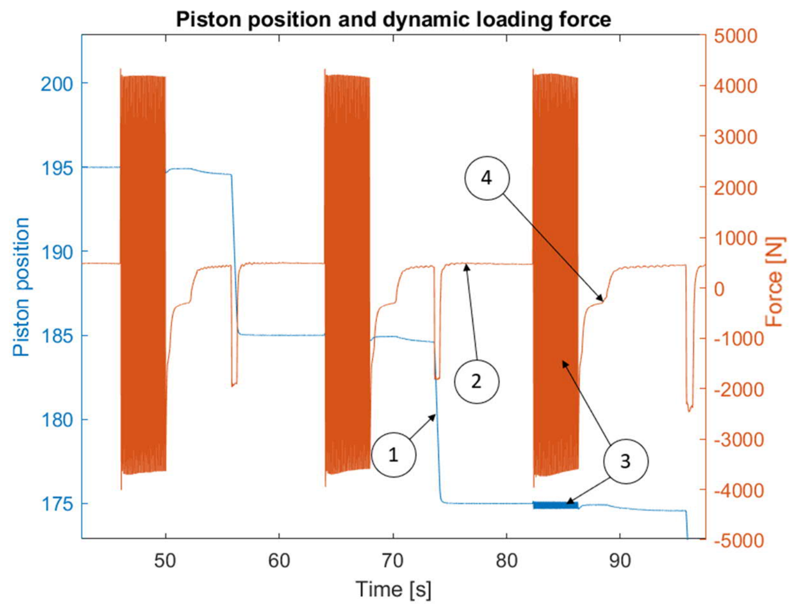

Figure 34 Dynamic test run process.

The dynamic load was applied for four seconds, and three seconds of velocity and force data was extracted from each testing position to determine the stiffnesses. The loading amplitudes resulted from open-loop control over the loading cylinder. A sinusoidal command signal was given as input to the load cylinder proportional valve. The amplitude of the signal was set to correspond 8% opening of the valve spool at all frequencies. Due to the dynamics of the proportional valve, 20 and 30 Hz signals needed to be amplified to reach the corresponding 8% opening amplitude.

The measurement data were acquired from the acceleration sensors and load cell. The velocity data was readily available from the charge amplifier of the accelerometers, and it was integrated further in the data processing stage to acquire the position amplitude of the piston rod end. Two accelerometers were used: one was mounted to a flat iron bar between the load cylinder and load cell, as shown earlier in Figure 27, and another on the test bench frame, as seen in Figure 16. The velocity data were subtracted from each other to cancel out the vibrations on the test bench frame, resulting in only the piston velocity relative to the test cylinder mounting.

In the dynamic tests, frequency domain analyses were conducted. The velocity and force data were examined in the frequency domain to calculate the stiffnesses specifically in the loading frequency. Fast Fourier transform (FFT) was applied to both velocity and force datasets in a MATLAB script. The amplitudes at the loading frequency were extracted from the Fourier transforms of the datasets to filter out noise and disturbances from the data. The Fourier transform of velocity was then integrated to get the displacement amplitude. Then the amplitudes at loading frequencies of the piston displacement and axial force (shown in Figure 37) were used to calculate the stiffness of the cylinder.

3.3.5 Measuring the whole hydraulic cylinder system dynamic stiffness

After the isolated cylinder tests were conducted, the needle valves were replaced by the original one-way flow control valves of the system. The testing variables were loading frequency, throttle level, and direction. Tests were carried out with the different testing parameters with piston in motion. However, the boundary condition of fully throttling the valves forced to conduct tests with the piston in static position.

To measure the dynamic stiffness throughout the stroke of the hydraulic cylinder, an offset was applied to the dynamic load so that test cylinder piston was on average either retracting or extending at a velocity of 2 to 3 mm/s, which is close to the system's initial working state. The piston motion is illustrated in Figure 35. The loading force amplitude was implemented by setting the proportional valve spool opening amplitude of 8 %. As the test runs were conducted from 5 to 215 mm of the stroke, each dynamic loading test run lasted from 70 to 105 seconds.

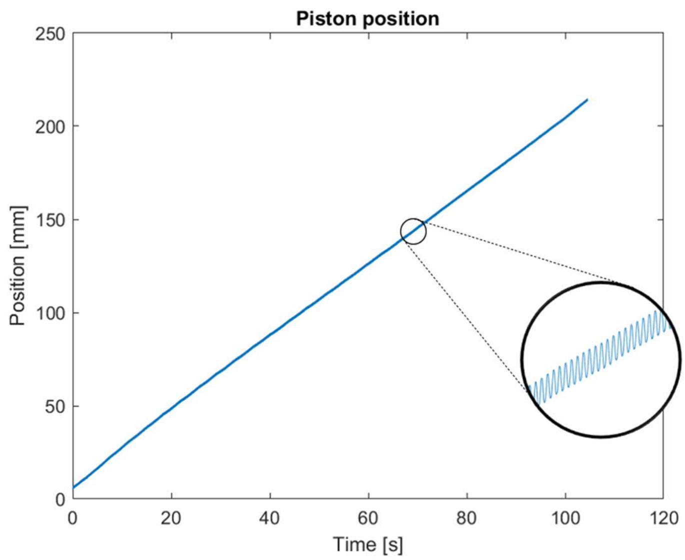

Figure 35 Piston position data of a full dynamic test run. Piston rod extending.

Each test run dataset was exported from TwinCAT environment to MATLAB. In a MATLAB script, the data was split into smaller, 5 second datasets, as illustrated in Figure 36. The interval between the 5 second datasets was 2,5 seconds, meaning overlap between the datasets. The overlap allowed more frequent calculations of the stiffnesses throughout the stroke. The interval of 5 seconds ensured that enough data was recorded on each dataset to achieve good results. Long time intervals for the datasets would flatten out the stiffness data and the nonlinear traits would not be recorded properly.

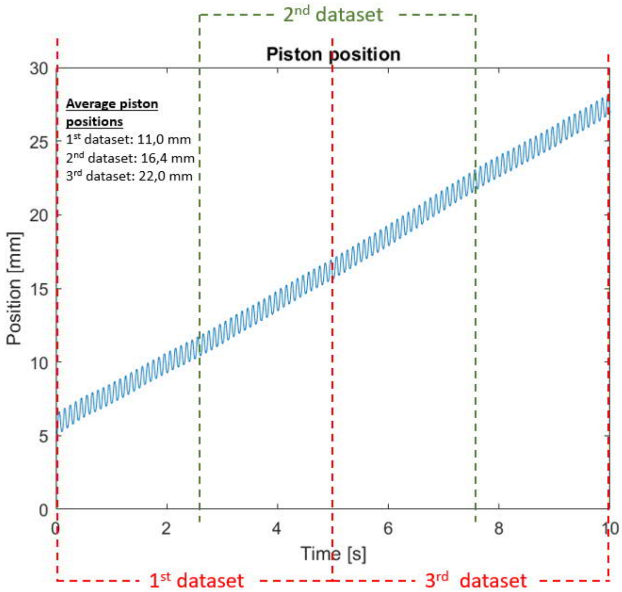

Figure 36 Dataset split into intervals. Position data from Gyse-A sensor.

Like in the dynamic loading tests with the needle valves, the forces and velocities were acquired with the load cell and accelerometers. The loading amplitudes were also adjusted similarly by amplifying the open-loop sinusoidal command signal to correspond 8% spool opening. In each of those datasets, the average displacement amplitude and average force amplitude were resolved by computing their Fourier transforms. The Fourier transform of the velocity data was, again, integrated to acquire the position. Then the amplitudes corresponding to the loading frequency were used to calculate the stiffness in the average position of the piston. Examples of the Fourier transform amplitude peaks are presented in Figure 37.

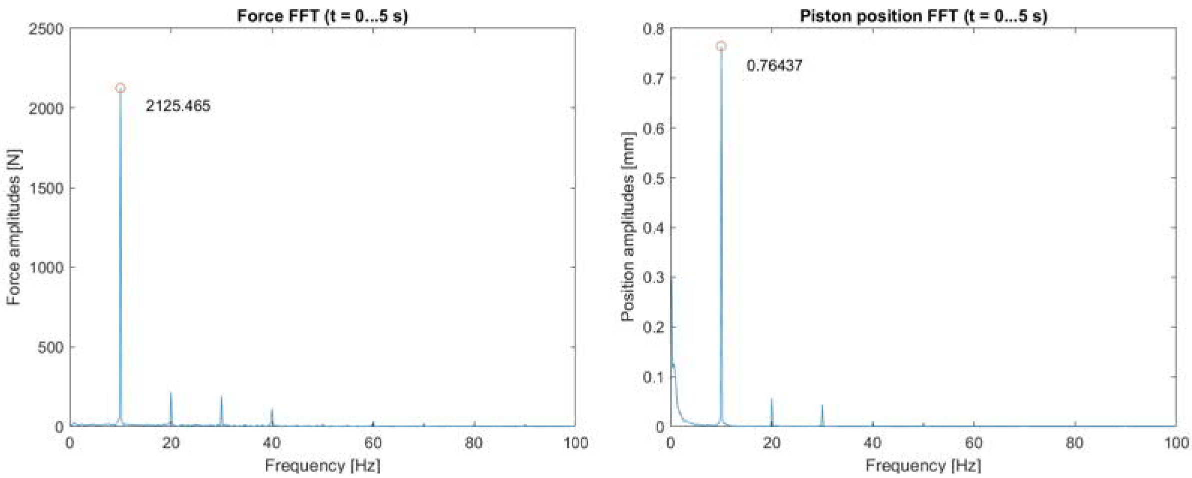

Figure 37 Fourier transform of first dataset axial force and piston position.

Full throttling of the one-way flow control valves disables flow out of the chambers. Therefore, the piston base velocity must be zero in the boundary condition of full throttle. Test runs with the one-way flow control valves fully throttled were conducted identically with the dynamic loading with the needle valves (in section 3.3.4); the desired position was reached with the P control loop with valves open, then the valves were closed, and the dynamic loading occurred. The valves were then opened, and the new piston position was set, and testing procedure repeated. The piston position intervals and the starting positions were again, 10 mm and 5 mm respectively.

The opening of the check valves was monitored by measuring the pressures on both sides of the one-way flow control valve as shown in Figure 38. The pressure difference between A and B was calculated (A - B). If the measured pressure difference drops below -0,4 bar the check valve opens.

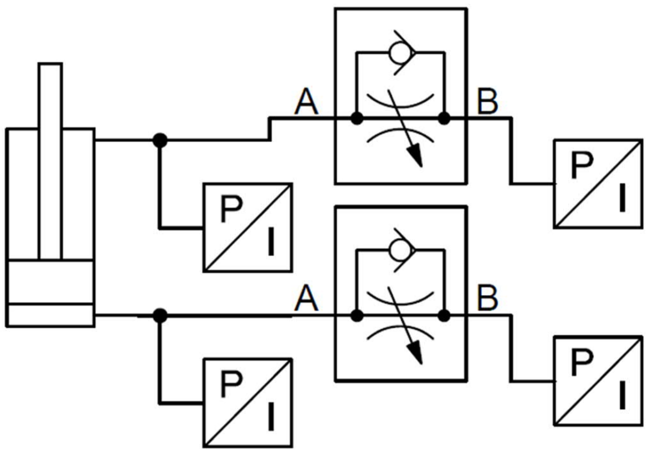

Figure 38 Pressure measurements to determine the opening of the check valves.

Phase shift between force and velocity, which is easily extracted from the FFT data, contains information of the response of the system. Calculating the Fourier transforms yields a complex number. In this application, the imaginary part represents damping and the real part stiffness. Therefore, the phase shift between the two yields an estimate of the spring-damper behavior. More specifically, the phase shift between force and velocity describes if the system is dominated by the stiffness characteristics or the damping characteristics.

A sinusoidal force acting on a freely moving mass, causes a sinusoidal velocity with a shifted phase. If the inertial effects of the mass are neglected and the mass is not deformed by the force, the phase shift of the force and resulting velocity is 90°. As the velocity is sinusoidal, the resulting displacement will also be sinusoidal, and the phase shift relative to velocity will be 90°. Thus, the phase shift of force and displacement will be 180°.

Therefore, phase shifts between the measured forces and velocities of each run yields information of the traits of the cylinder system; if the phase shift is 90°, the system behaves like a spring system, and if the phase shift is 0°, it behaves like a damper system. In practice, the phase shift is expected to be between 0° and 90°, making it a damped spring system.

4 Results

The conducted measurements covered both static and dynamic stiffness tests. To determine the baseline static stiffness of only the hydraulic cylinder, static loads were applied. For this measurement, the one-way flow control valves were replaced with throttle valves to cut flow through the cylinder ports entirely. These static stiffness measurements served as a baseline for the maximum stiffness of the hydraulic cylinder. Then, the test cylinder system stiffness was investigated under dynamic loads in three different piston conditions: static, extending and retracting. The throttle of the one-way flow control valves was varied along with the frequency of the load. Restricting the flow increases the stiffness and therefore the cylinder system inhibited the highest stiffnesses when the valves were closed. This chapter covers all the experimental data and results.

4.1 Static stiffness measurements

The displacements, caused by the static loads, were measured with the absolute position sensor. The forces acting on the test cylinder rod end were captured with the load cell between the load cylinder and the test cylinder. The four separate runs to determine the static stiffnesses were:

1) direction up, load up
2) direction up, load down
3) direction down, load up
4) direction down, load down

Stiffnesses were calculated and plotted over the piston position as follows. In the graphs, “up” is analogous with the direction to which the cylinder extends and “down” to which it retracts. The resulting stiffness curves were smoothened with the MATLAB smooth function.

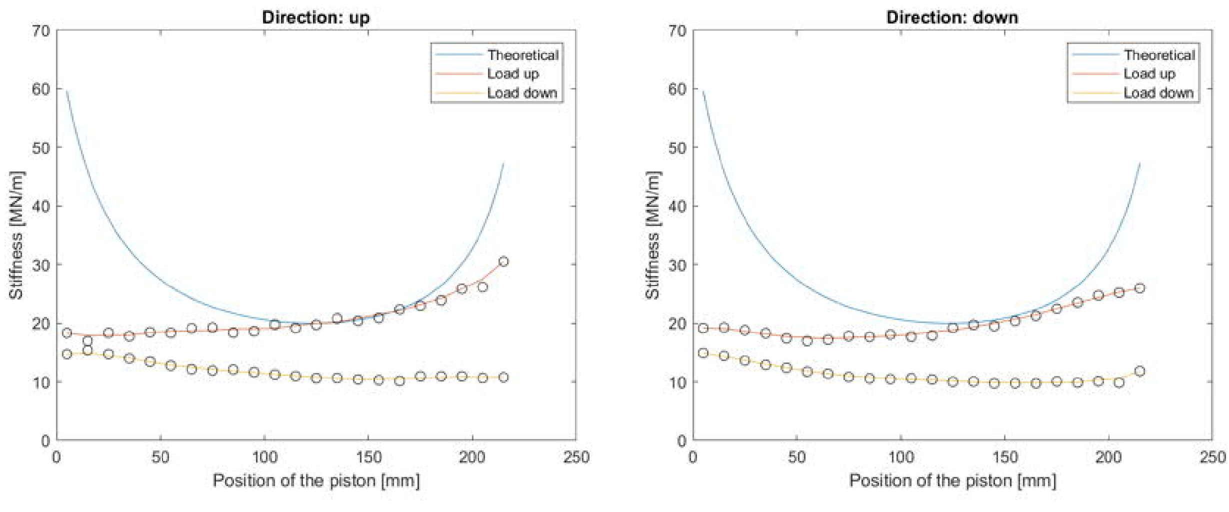

Figure 39 Measured stiffnesses with static loading.

There are some discrepancies with the measured and predicted stiffnesses in the ends and when the load is downwards. The measured data itself does not vary between the piston direction.

In the first graph in Figure 39, the loading force upwards was 3,4 kN and 4,6 kN downwards. On the second graph on the right, the loading force upwards and downwards were 3,5 kN and 5,1 kN respectively. The loading forces were set as 4 kN, with 2 a second ramp-up to the maximum value, but the working pressure difference in the test cylinder causes a downward force, offsetting the force values while the piston is static. Static loading forces are displayed in Figure 40. It also displays that the load cylinder sealing system leaves the load cell pinned when the direction is up. The load cell force stays elevated after the desired position is reached.

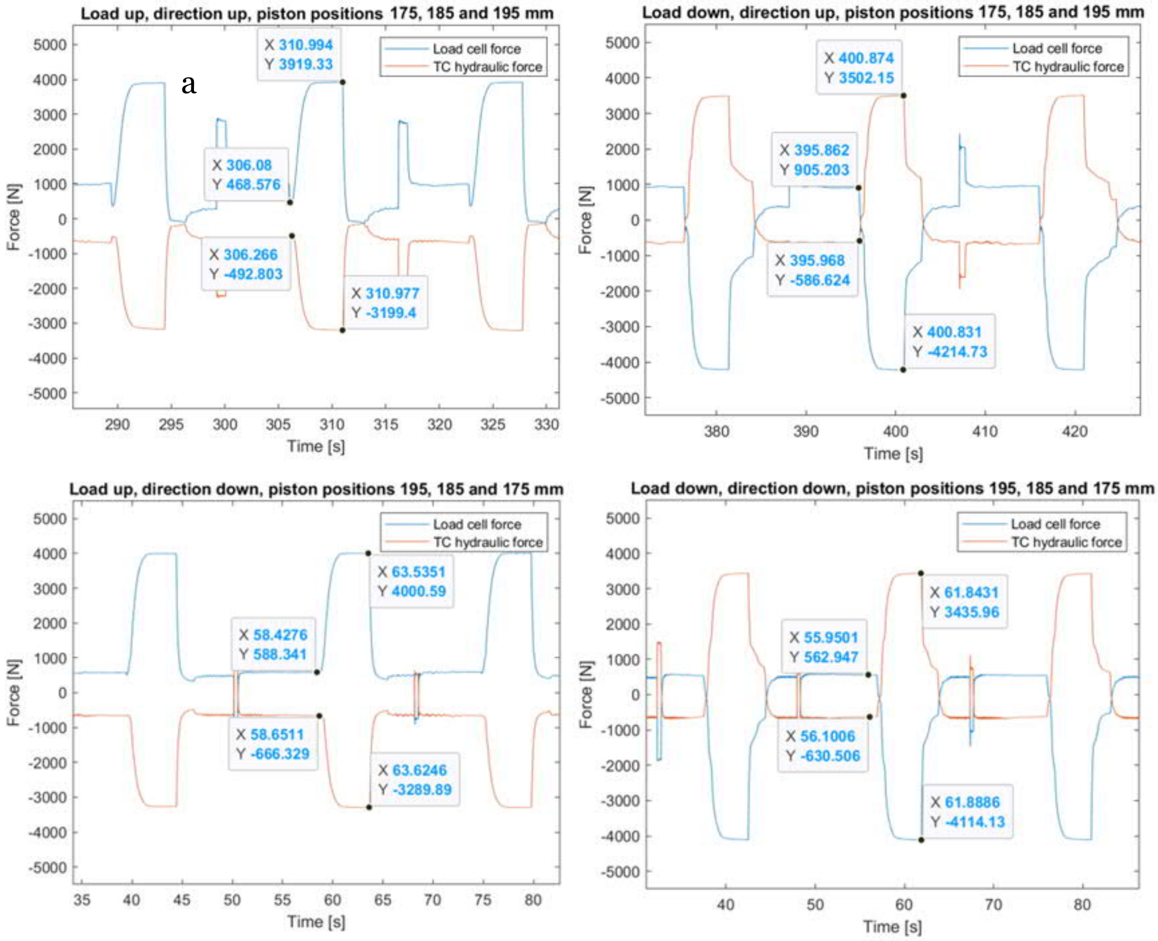

Figure 40 Static loading forces from load cell and test cylinder hydraulic forces.

Test cylinder chamber pressures at the same piston positions are shown in Figure 41. All the highlighted pressure values are at piston position 185 mm. The pressure level in the head chamber drops down to 12 bar, while the pressure in the rod chamber climbs up to 62 bar, when loading is upwards. The increase in pressure in the chambers opposing the loading force is approximately at a constant of 20 bar. However, the decline in the chamber in which the pressure drops due to the loading force, varies with the loading direction. The decreases and increases in pressure levels are significant. The bulk modulus varies according to the pressure levels, and the variance is significant if the system has any undissolved air.

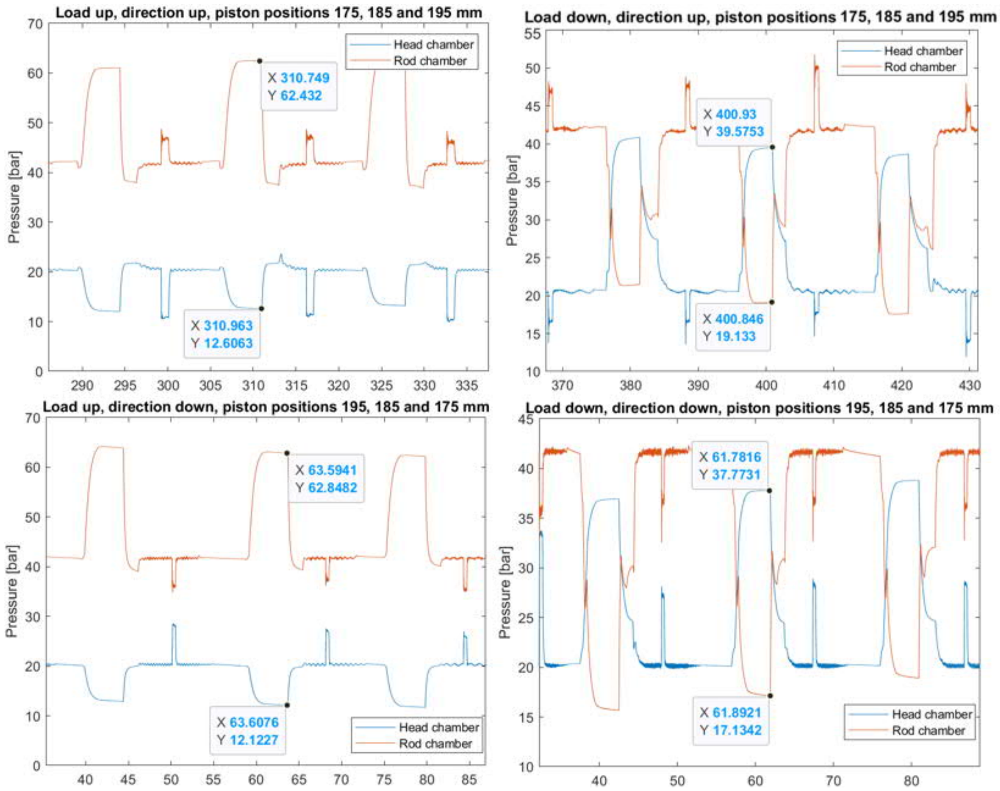

Figure 41 Test cylinder head and rod chamber pressures during static loading.

The resulting piston displacements with constant load force steps throughout the test cylinder stroke are presented in Figure 42. The resulting displacements were between:

1) 0,31...0,48 mm (load down, direction up),
2) 0,31...0,47 mm (load down, direction down),
3) 0,11...0,20 mm (load up, direction up),
4) 0,13...0,21 mm (load up, direction down).

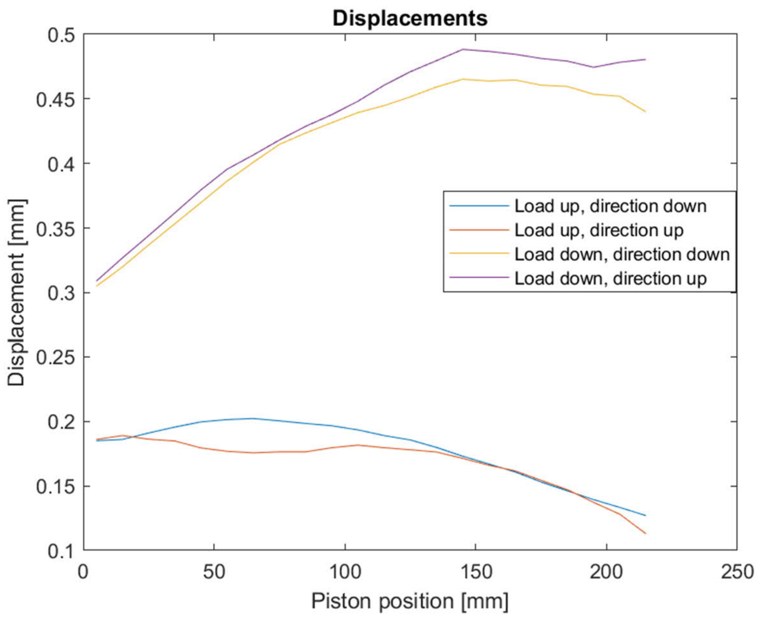

Figure 42 Displacements caused by static loads. Data processed with MATLAB smooth function.

Absolute values of all four static test runs are presented in Figure 43. Hysteretic behavior can be seen in the force data when the load was applied downwards. The piston is driven from end to end with a relatively high speed with the P controller before the test run begins. Also, the same piston speeds occur between the loadings, when adjusting the piston to the new loading position. This might contribute to elevated pressure levels in the test cylinder and cause hysteresis.

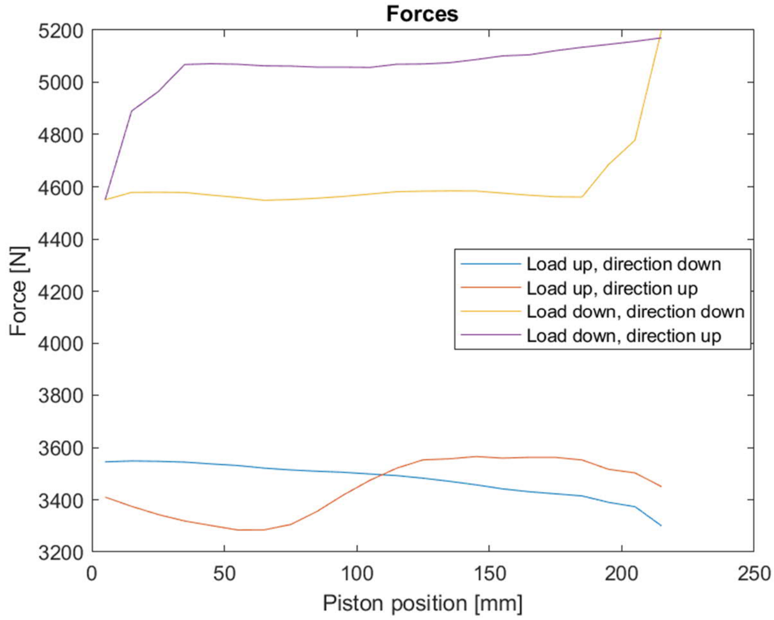

Figure 43 Static forces measured with load cell. Data processed with MATLAB smooth function.

The measurements, however, show no significant difference between the direction and stiffness. The displacements ultimately determine the stiffness since the loading method and configuration is not changed between the test runs. The loading cylinder is a symmetrical cylinder, and its pressure levels were kept constant.

The fact that the perceived stiffness was lower when the loading direction was downwards could be explained by undissolved air in the system. The downward force decreases the pressure from 42 bar down to 17 to 19 bar in the rod chamber, which could cause dissolved air to emerge from the hydraulic fluid, which would cause the stiffness to decrease further. Additional air volume in either chamber would significantly decrease the effective bulk modulus as discussed in section 2.1.2.

4.2 Dynamic loading tests

Dynamic loads were applied to the cylinder system in the two different configurations of the cylinder ports, 1) with needle valves which is discussed in section 3.3.4; and 2) with one-way flow control valves which is also discussed in section 3.3.5 Needle valves were used to acquire the isolated hydraulic cylinder stiffness characteristics under dynamic loads. The one-way flow control valves were reinstalled to determine the stiffnesses of the initial hydraulic cylinder system.

4.2.1 Dynamic loading tests cylinder stiffness

The first dynamic loading tests were conducted with the needle valves preventing flow through the cylinder ports during loading. Tests were done with loading frequencies of 10, 20, and 30 Hz. The resulting stiffness curves are presented in Figure 44.

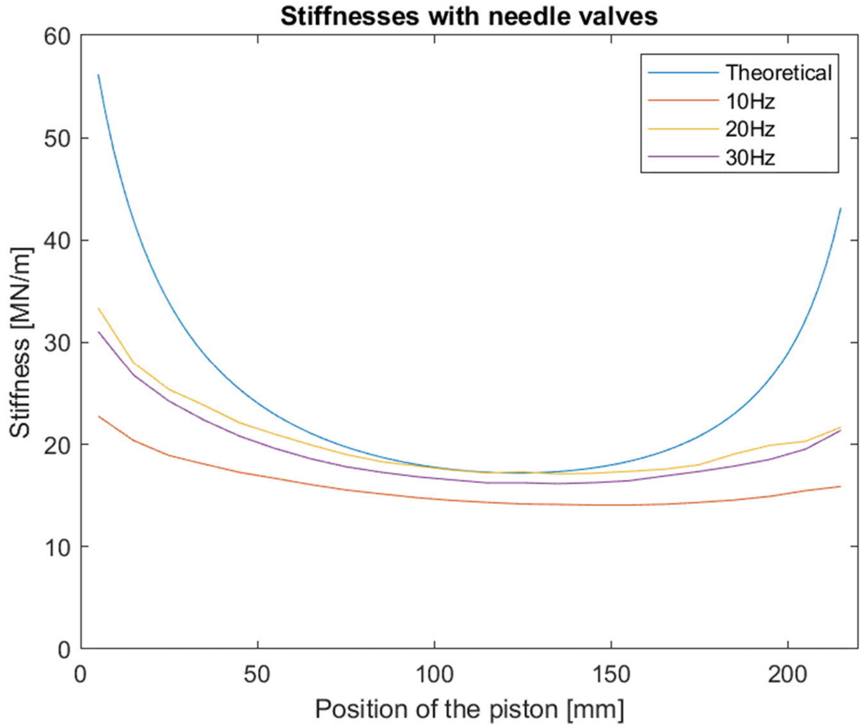

Figure 44 Measured dynamic stiffnesses of the test cylinder without flow.

The velocities, test cylinder hydraulic forces and load cell forces for different loading frequencies are shown in Figure 45. The test cylinder hydraulic forces were calculated by measuring the pressure difference over its chambers. Even though the loading cylinder proportional valve command signal was corrected so that the spool would reach 8% opening with all frequencies, the loading force amplitudes still varied substantially: 3,9 kN for 10 Hz, 2,2 kN for 20 Hz and 1,2 kN for 30 Hz. However, the velocity amplitude remains fairly constant.

The force data from the load cell is slightly delayed compared to the test cylinder hydraulic force data. This is highlighted by plotting the test cylinder hydraulic force as negative in Figure 45. The load is generated in the load cylinder, which is attached to the test cylinder. So, in principle, the test cylinder hydraulic force phase ought to be delayed, and not the other way around, as it unfolds in the data. This may mean for example that the pressure sensors in the test cylinder inhibit better response times than the load cell and the strain gauge amplifier.

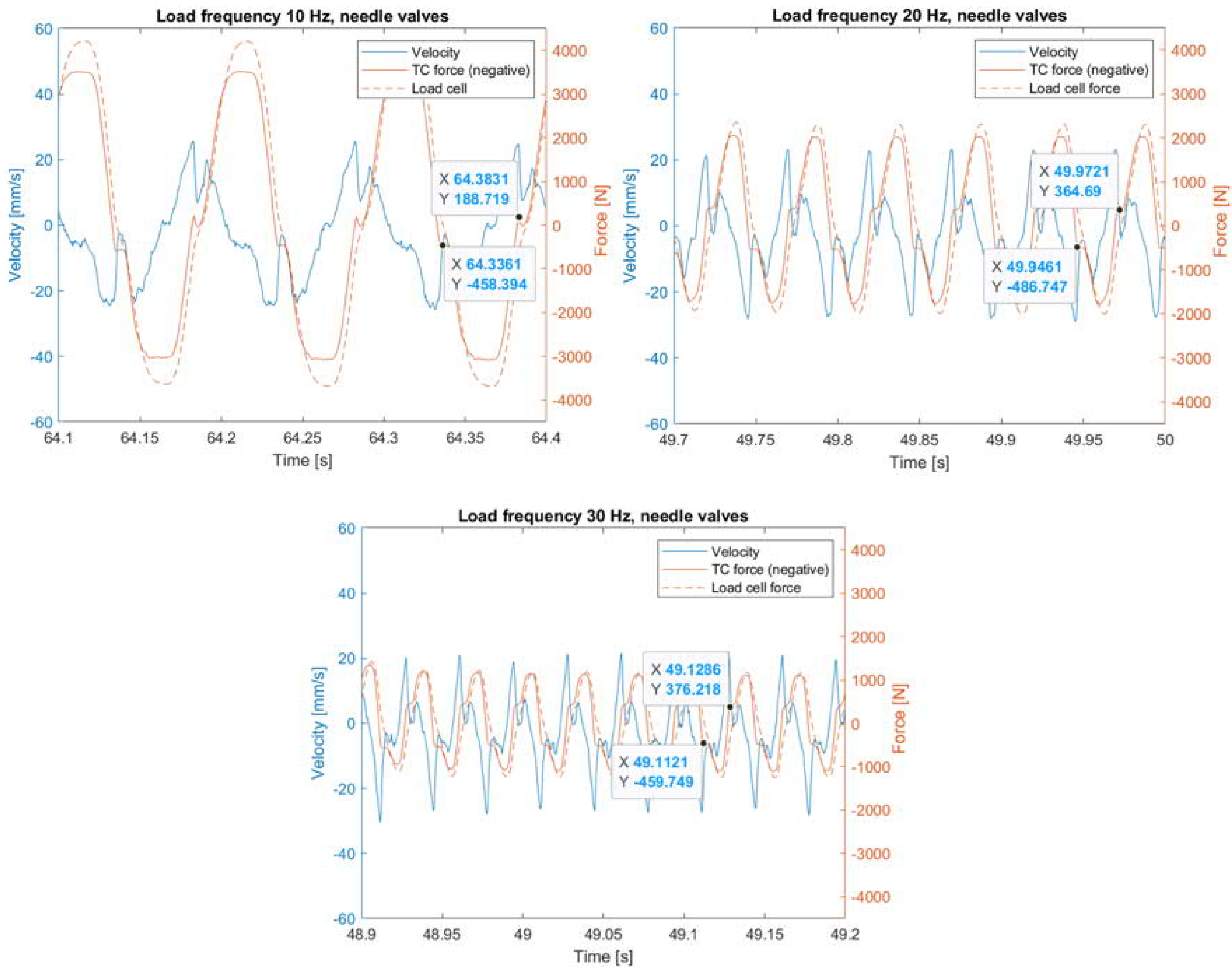

Figure 45 Velocity and force data derived from accelerometers, pressure sensors and load cell. Piston position is 185 mm in all graphs.

The load cell force amplitudes are also higher than the hydraulic force due to the hydraulic force neglecting sealing element friction. The decrease in force amplitude implies that the pressure rise in the load cylinder chambers is insufficient to keep the loading at a constant magnitude. This may be due to too high flow resistance in between the proportional valve and load cylinder.

The velocity in Figure 45 drops suddenly soon after going past the force zero-crossing point. This is likely due to the behavior of the seals in the cylinder. When sliding on the surface of a rigid body, an elastic sealing element deforms in the direction of the friction force (which is opposite to the direction of velocity). After reaching the sliding regime, the deflection stays constant. When the loading force changes direction, the seal deflects in the other direction, likely causing the nonlinearity seen in the velocity data. This is demonstrated in Figure 46 which shows the previously discoursed LuGre bristle model. The nonlinearity also shows in the hydraulic force data of the test cylinder, but the response time of the load cell is not sufficient to capture the nonlinearity properly.

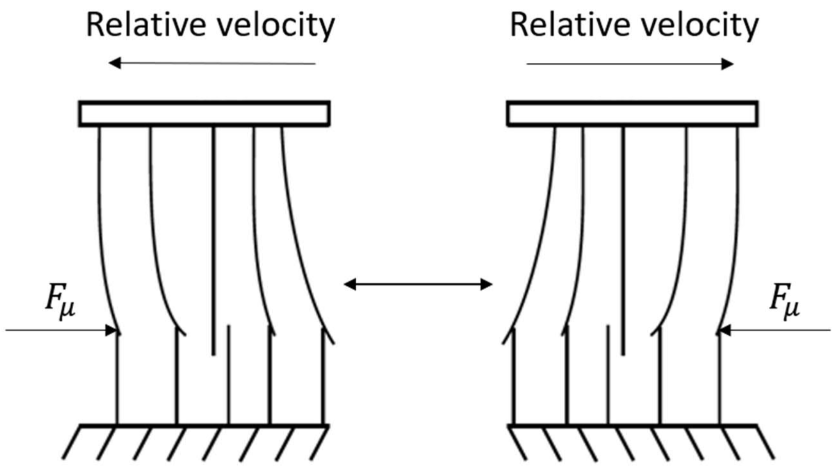

Figure 46 Bristle modelling of an elastic component sliding against a rigid surface. Source: modified from [32]

The starting point of the nonlinearity shifts further away from the zero-crossing point with higher frequencies when the piston is going upwards, but not when going downwards. This is highlighted in the graphs in Figure 45: the beginning of the nonlinear behavior in the hydraulic force is seen in different values. The values being 188,7 N at 10 Hz; 364,7 N at 20 Hz; and 376,2 at 30 Hz.

4.2.2 Dynamic stiffness measurements of entire hydraulic cylinder system

The whole cylinder system stiffness was measured with the one-way flow control valves as described in section 3.3.5. The stiffness plots are divided by the direction of motion. This section covers the upwards and downwards motion tests in respective order.

The dynamic loading tests with the test cylinder in upwards motion yielded stiffness curves are shown in Figure 47. The testing variables were one-way flow control valve throttle level, frequency, and direction.

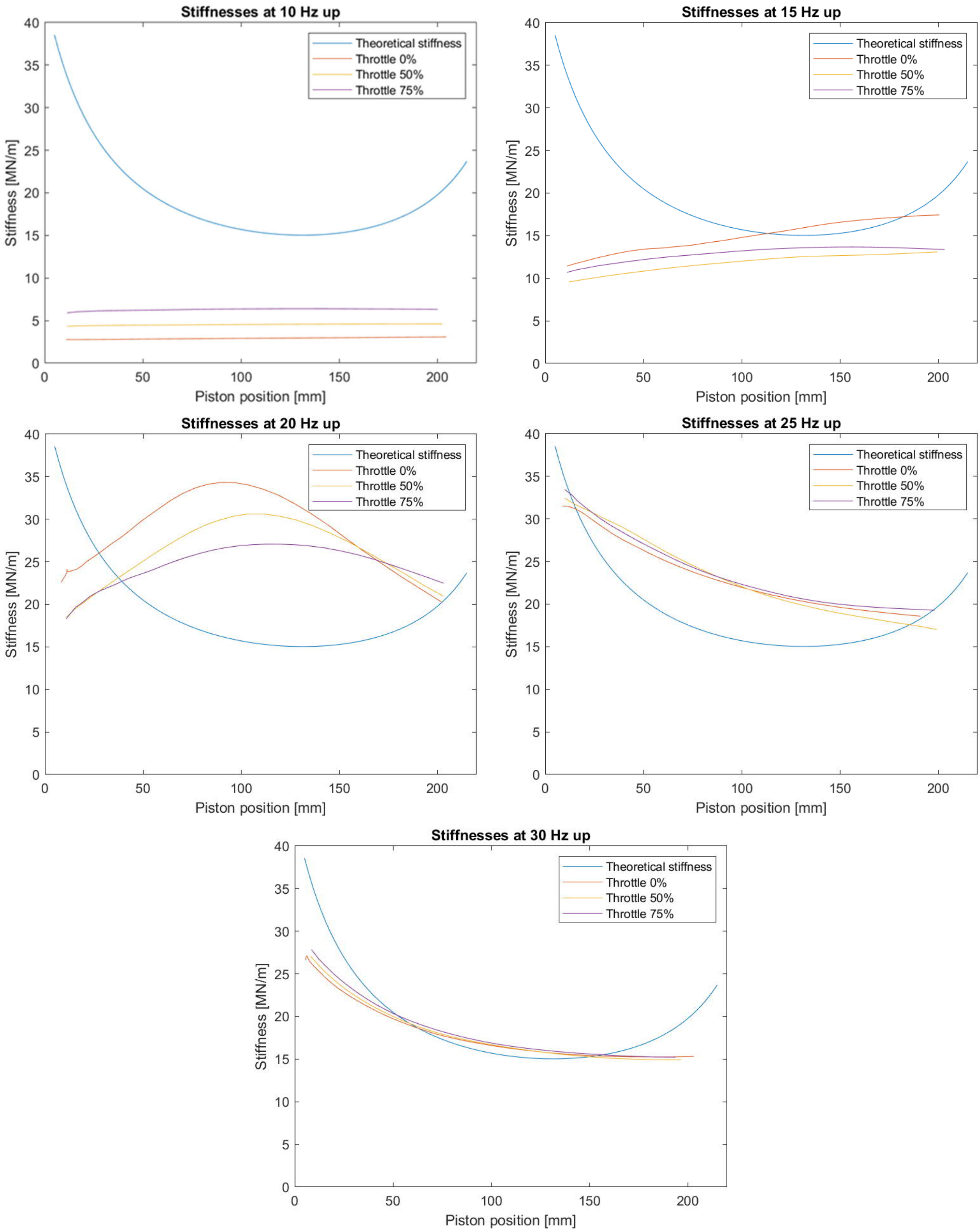

Figure 47 Measured cylinder stiffnesses of dynamic test runs upwards.

The impacts of throttling on the resulting stiffness reduce with higher loading frequencies. When the loading frequency is 25 and 30 Hz, throttling contributes very little to the stiffness. This means that flow through the one-way flow control valves reduces to nonexistent. When flow is minimized, the effect of other components decreases, and the cylinder stiffness characteristics appear more like the cylinder with plugged fluid lines.

Stiffness peaks are seen in 20 Hz loading frequency. The throttling decreases the stiffness peak values, which points that the cause is related to the whole system, involving other components outside the cylinder and one-way flow control valve subsystem.

Figure 48 shows that the phases of the hydraulic forces in the chambers are out of phase when the piston is close to the ends. In all but 20 Hz loading frequencies, the test cylinder chamber pressures (and the corresponding hydraulic forces) are in the opposite phases throughout the test runs, which is what is expected, since the pressure in one chamber should rise in one chamber at the same time as the other should decrease.

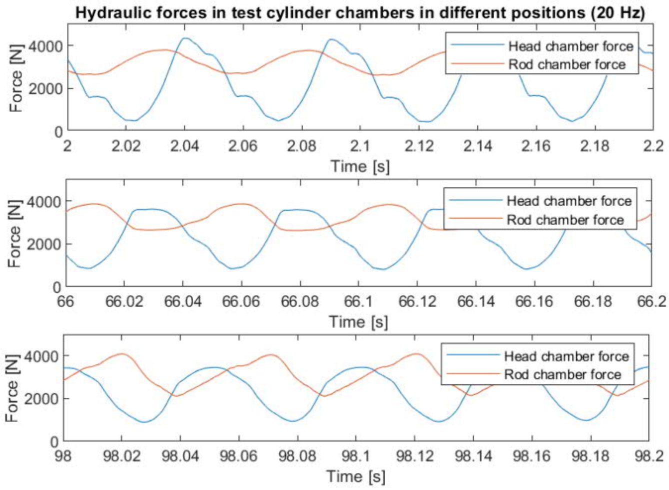

Figure 48 Hydraulic forces in cylinder chambers at 20 Hz loading frequency and no throttling at piston position: a) ~7 mm; b) ~92 mm; and c) ~204 mm.

Figure 49 presents the hydraulic forces in around the same piston positions as in Figure 48, with 10 Hz loading frequency, for reference. In Figure 49, the chamber hydraulic forces are in opposite phase. The pressures being in opposite phases causes antiresonance, which limits the displacement amplitude. This is considered in the theoretical stiffness calculations.

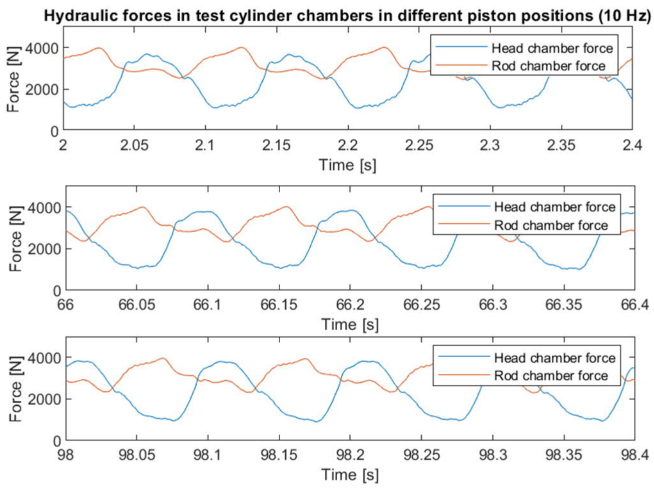

Figure 49 Hydraulic forces in cylinder chambers at 10 Hz loading frequency and no throttling at piston position: a) ~5 mm; b) ~64 mm; c) ~172 mm.

The phase shifts between the measured forces and velocities with the cylinder extending are presented in Figure 50. Phase shift of zero degrees implies that the system behaves like a damper and phase shift of -90 degrees means that the cylinder system behaves like a spring. Positive phase shift indicates that the inertia of the system (piston rod and fluid inertia) dominates the motion.

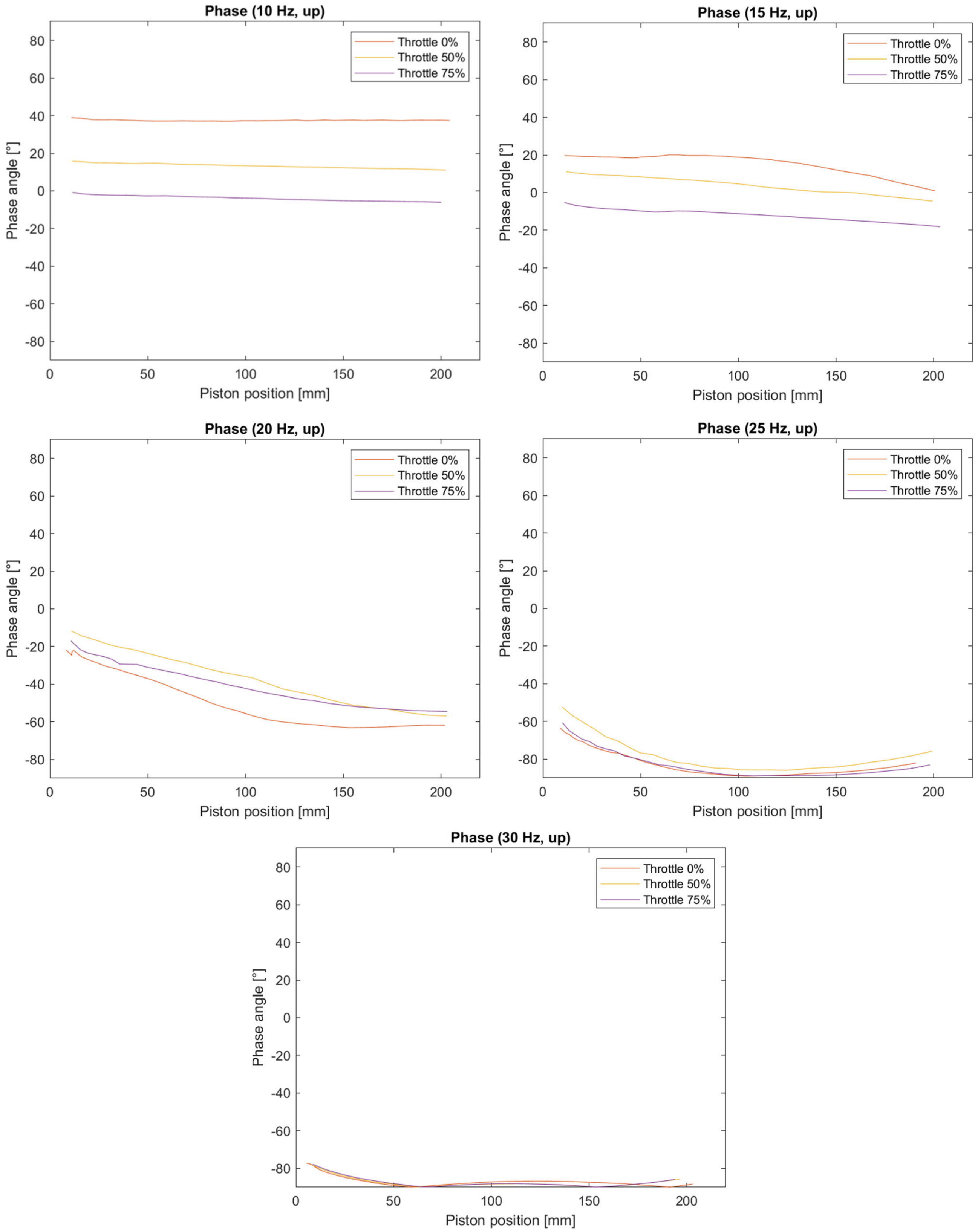

Figure 50 Phase shift between load cell force and velocity from accelerometers.

Displacements and forces used to calculate the stiffness are presented in Figure 51. All graph values are mean values of each FFT datasets. A decline in the force amplitudes can be seen at higher frequencies.

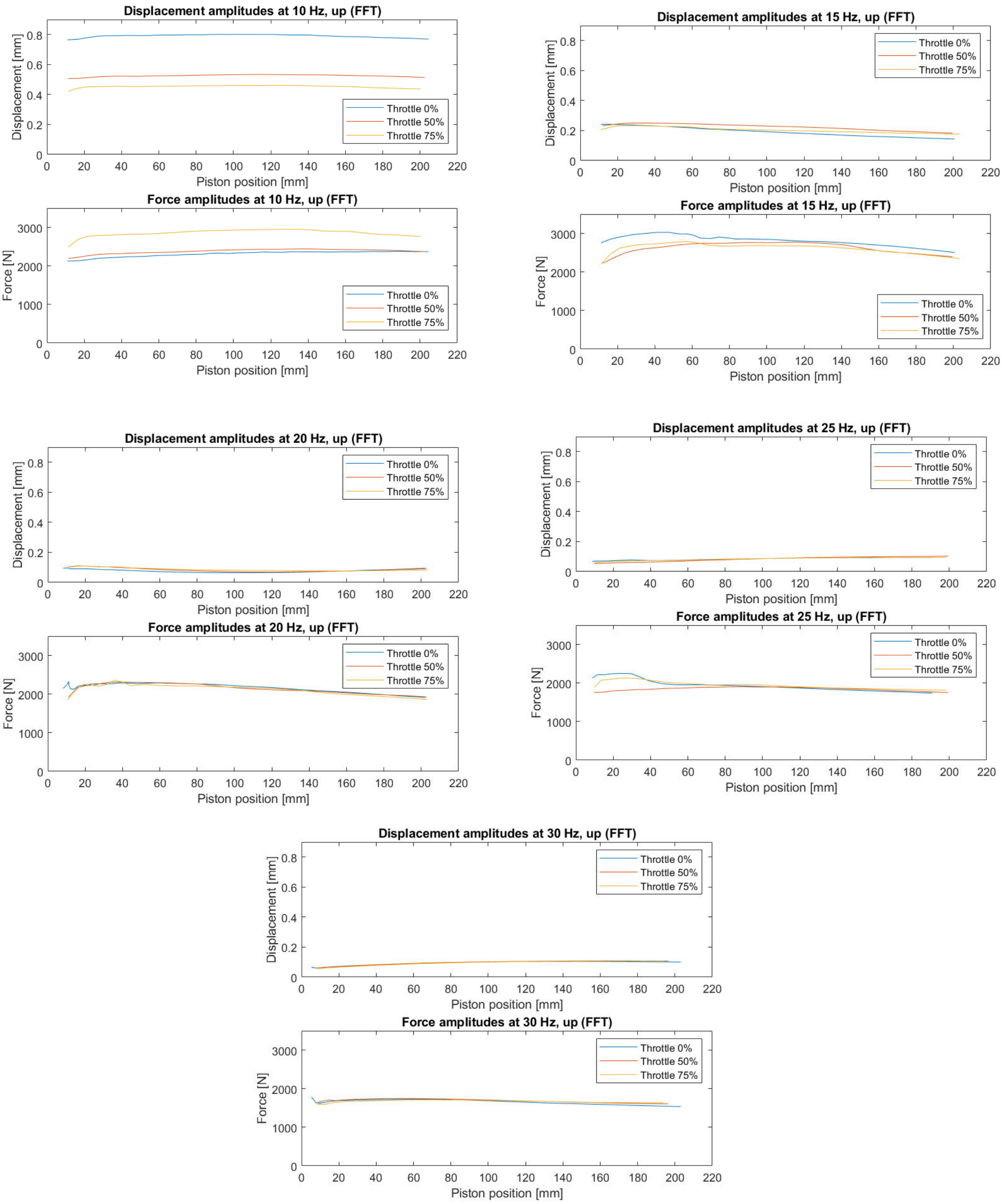

Figure 51 FFT data of displacements and forces throughout the test runs.

Stiffnesses with the cumulative piston motion downwards is presented in Figure 52. Similarities can be seen between runs with the piston going upwards and downwards. The same stiffness peaks at 20 Hz are seen here as well. Since the system is rather direction-independent stiffness-wise, further results and comparison will be presented in only one direction.

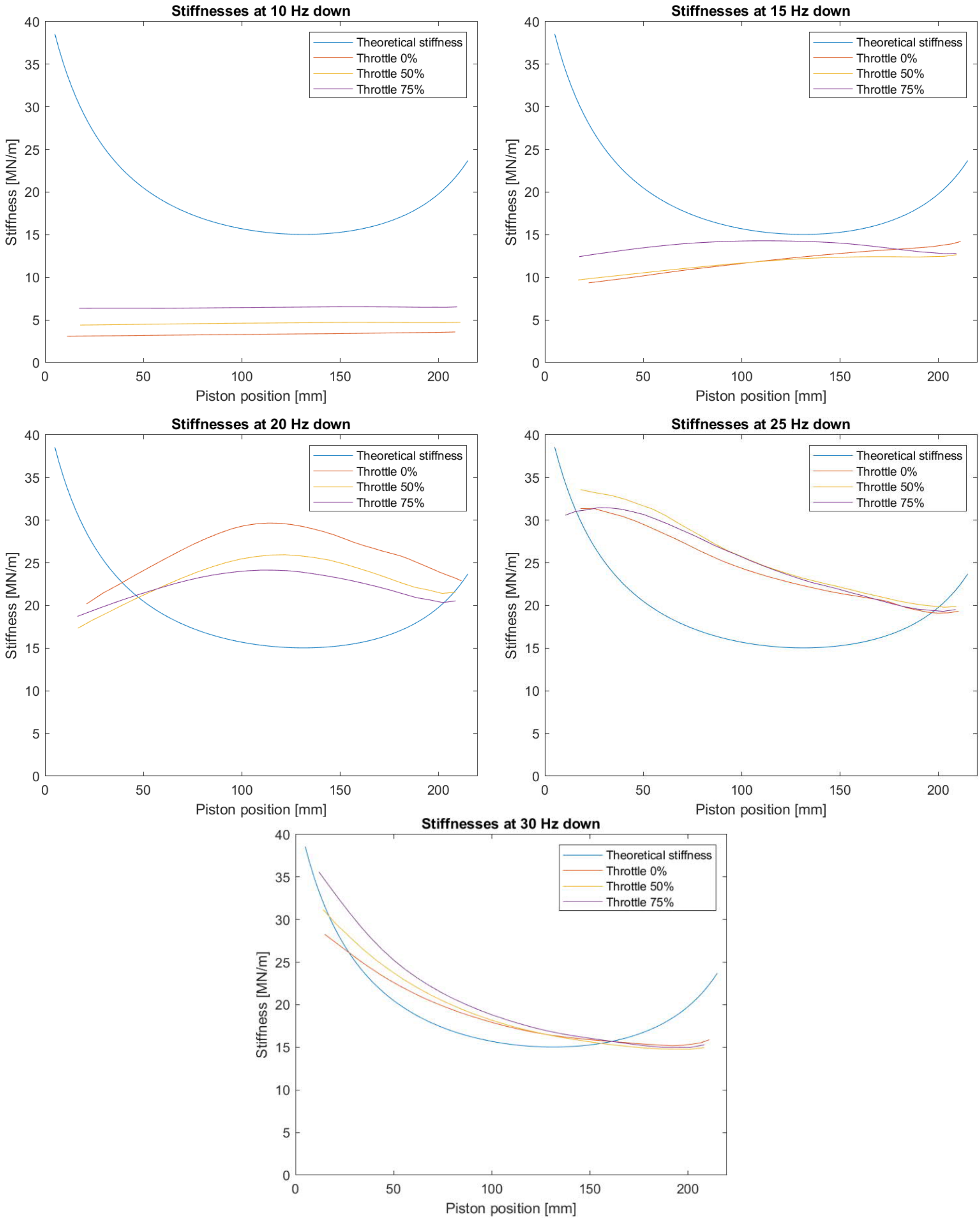

Figure 52 Stiffnesses under dynamic loads with piston motion downwards.

Phase shifts between the force and velocity measurements with the cylinder retracting are shown in Figure 53.

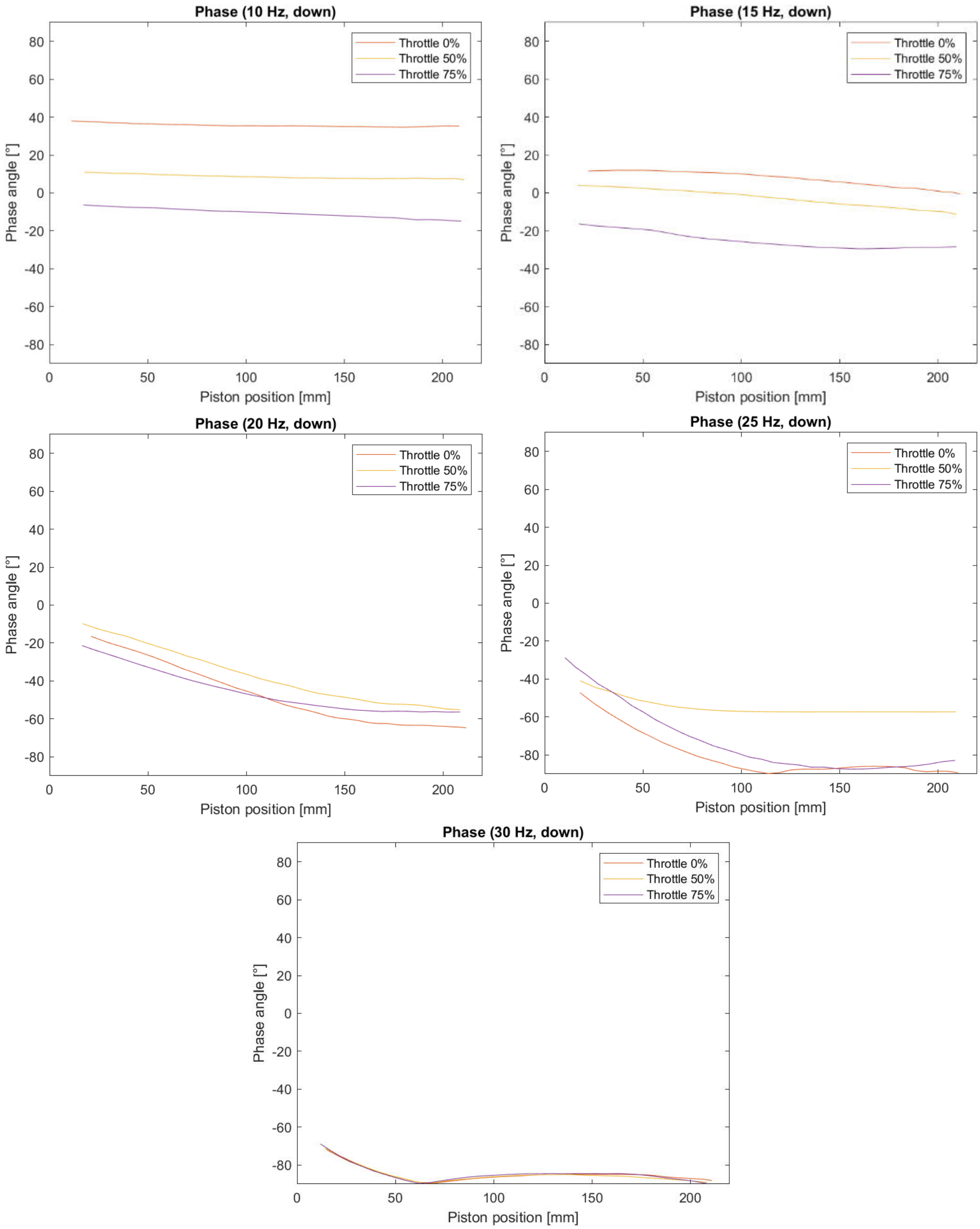

Figure 53 Phase shifts between measured force and velocity. Piston direction downwards.

The displacement amplitudes and force amplitudes extracted with FFT is shown in Figure 54.

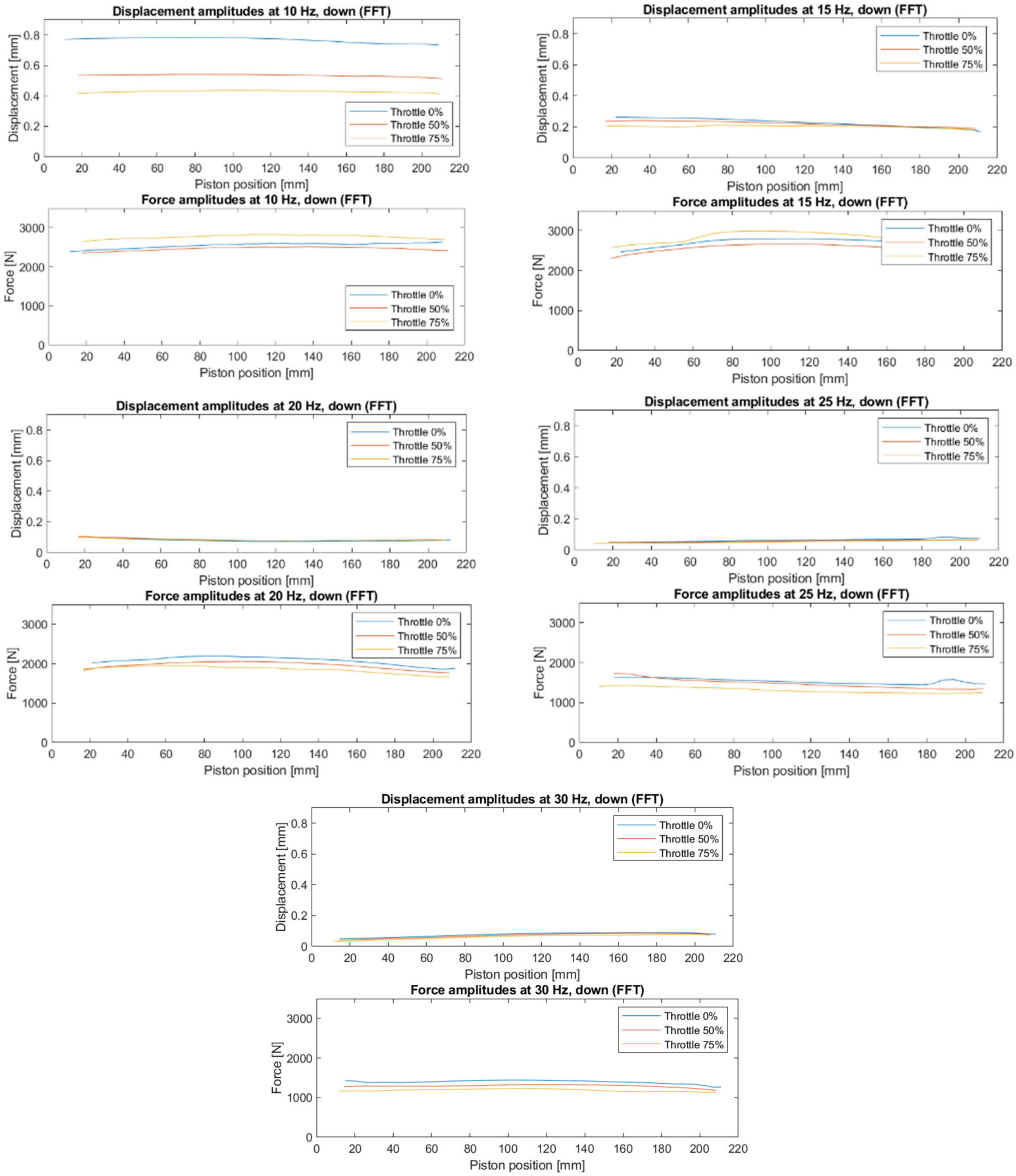

Figure 54 Measured displacement and force amplitudes. Piston in downward motion.

Velocity data from the accelerometers and the force data from the load cell is shown in graphs in Figure 55. Amplitudes of both velocity and force are reduced when the loading frequency increases. The difference in phase shift can be seen from the graphs as well. With 10 Hz loading, the velocity phase is lagging in relation to the force, and with 30 Hz loading, the force is behind in phase.

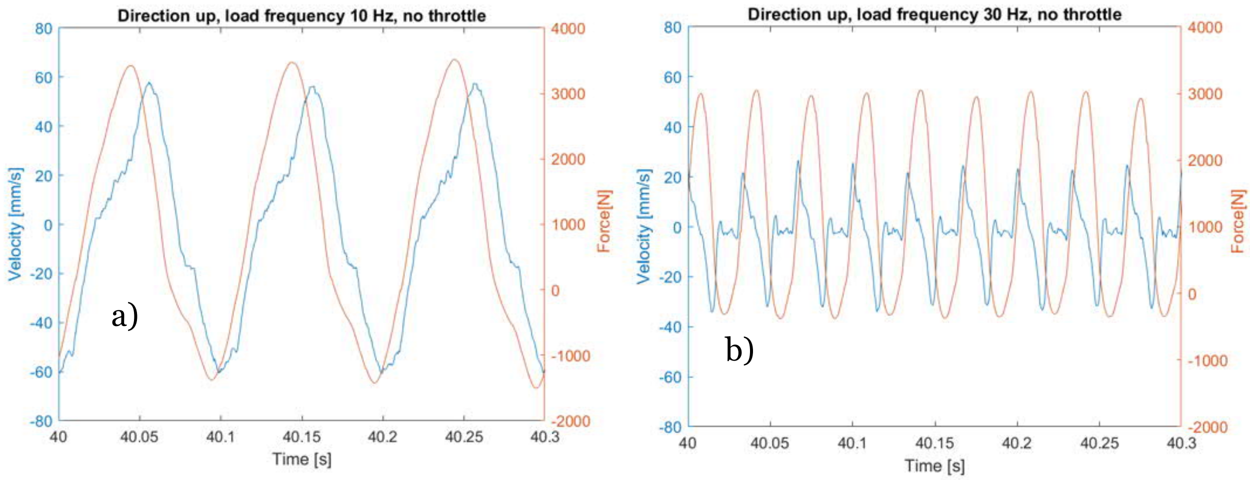

Figure 55 Velocity and force data. Direction up, loading frequencies: a) 10 Hz and b) 30 Hz.

The pressure difference over the one-way flow control valves was measured to monitor the opening of the check valves. In Figure 56, the pressure differences in both fluid lines are presented. The testing parameters are the same as in Figure 55 above. The pressure difference over head side one-way flow control valve drops below -0,4 bar in the 10 Hz loading frequency test (t = 40,05 s; 40,15 s and 40,25 s), which can be seen as sudden increases in velocity in Figure 55 a) in the same corresponding times. The same phenomenon occurs in the 30 Hz loading frequency. Without throttle, rod side check valves seem to stay shut.

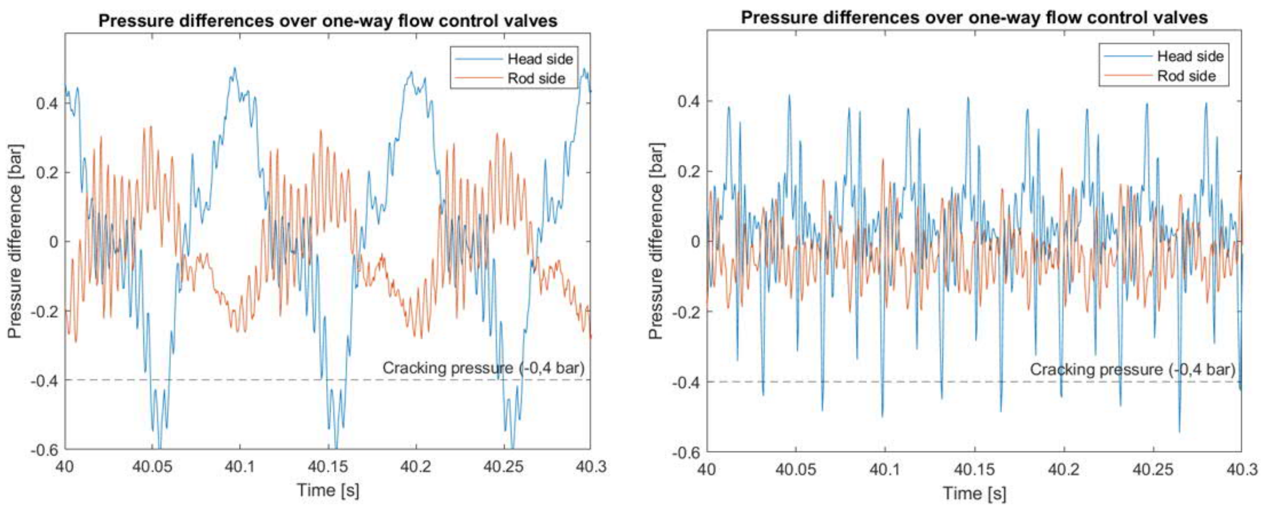

Figure 56 Pressure differences over one-way control valves. Testing parameters corresponds to graphs in Figure 55.

Similar graphs with higher throttling are presented below. The velocity and force data are shown in Figure 57.

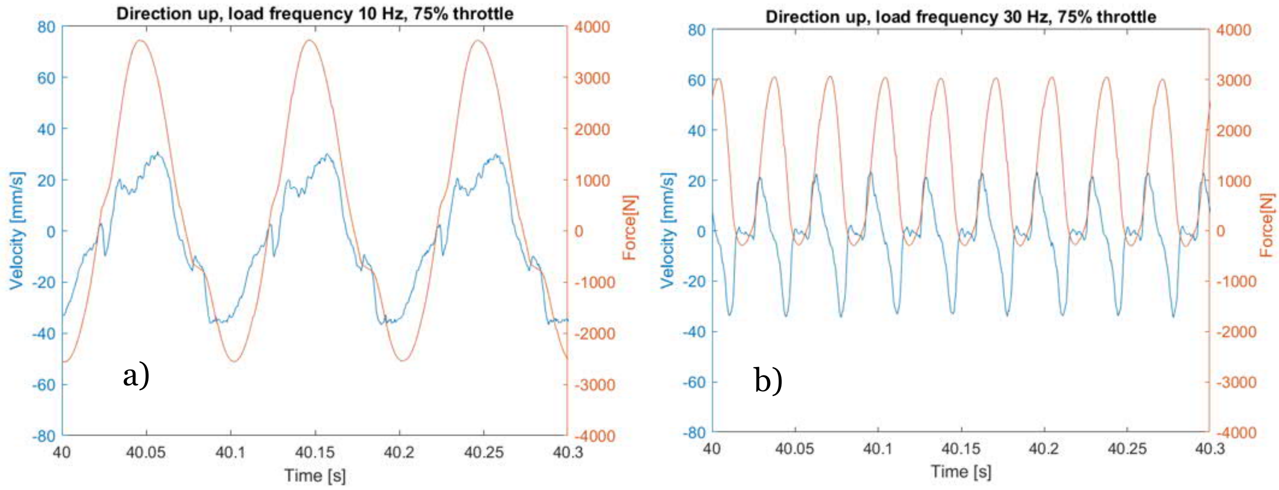

Figure 57 Velocity and force data. Throttle 75%, loading frequency a) 10 Hz and b) 30 Hz.

Figure 58 shows the pressure differences over both one-way flow control valves. In Figure 58 a), the opening of the check valve is evident and clear. When the pressure difference reaches the cracking pressure, the pressure difference saturates to the cracking pressure with some oscillation. At 30 Hz loading frequency, the pressure difference data is not that clear. The head side one-way flow control valve opens, but whether the rod side valve opens, is difficult to determine because the pressure is only briefly in the cracking pressure range.

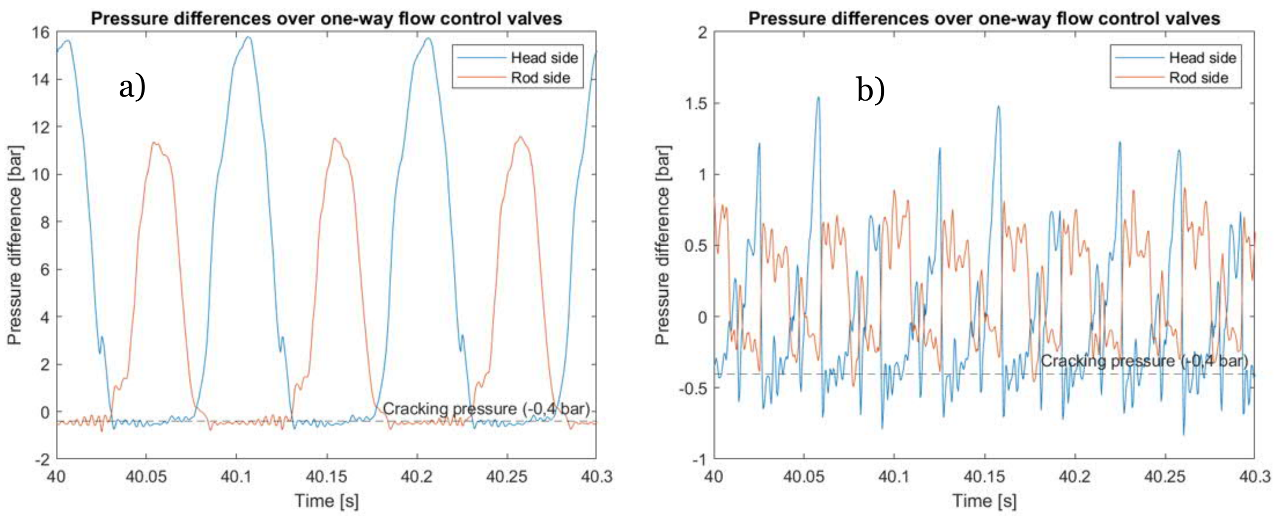

Figure 58 Pressure difference over one-way flow control valves. Testing parameters corresponds to graphs in Figure 57.

Figure 59 shows the sealing system slip (which was discussed in the dynamic tests with needle valves in section 3.3.4) and the check valve opening times. The head side check valve opens at the same time as the rod side check valve closes. After the next force zero-crossing point, the head valve closes and shortly after that, the rod valve opens. When the motion is turning downwards, the seal slip cannot be seen separately. It is likely, that it occurs at the same time as the check valves open.

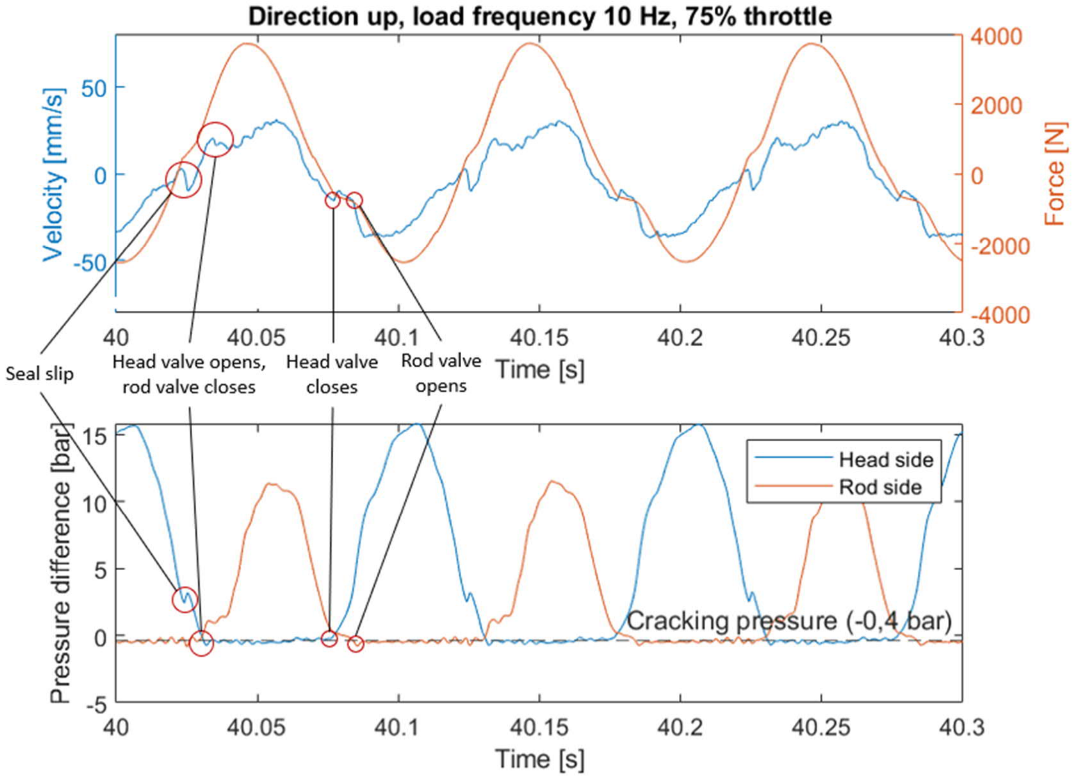

Figure 59 Velocity, force, and pressure differences over one-way flow control valves. Data from Figure 57 and Figure 58.

Figure 60 shows that the response time of the check valve is small: the pressure difference overshoots very little below the cracking pressure. Then the pressure difference oscillates around the cracking pressure due to pressure oscillations caused by the pump.

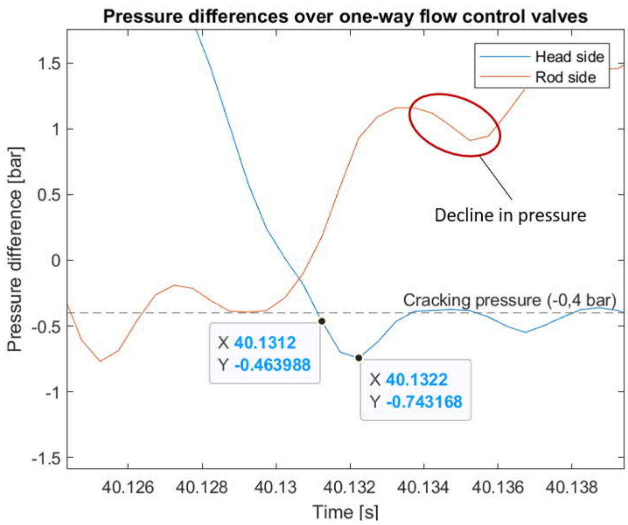

Figure 60 Pressure differences over one-way flow control valves when head side check valve is opening and rod side valve is closing.

However, when the pressure levels are close to the cracking pressure, the sudden additional flow can cause the recently opened check valve to close. The pressure response of the valve closing again might get mixed up with the ambient pressure oscillation, but it might be seen in the pressure difference decline in the opposite side chamber. The decline in pressure difference in the opposite side chamber may also be caused by the pressure reducing valve.

The time interval between reaching the cracking pressure and seeing an increase in the pressure difference is approximately 1 ms. This is an implication of the response of the check valve. However, the sampling time of the data acquisition system was 0,5 ms and the rise time of the pressure sensors from 10 to 90 % full scale value was reported as 1 ms by the manufacturer. Therefore, with the available data it is only possible to state that the response of the check valve is less than or equal to 1 ms.

When the rod side check valve opens, there is no decline in the pressure over the head side valve as seen in Figure 61 (also in Figure 59), which implies that the flow is significant enough to keep the rod side check valve from closing again immediately.

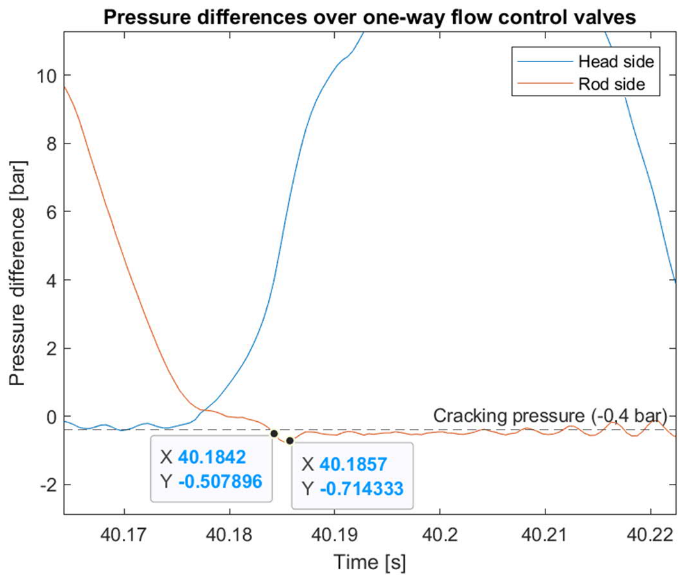

Figure 61 Pressure differences over one-way flow control valve when the rod side check valve is opening.

At 20 Hz, clear stiffness peaks can be seen exceeding the modelled static stiffness by a stretch. As these sorts of peaks were not present in the previous measurements, where the cylinder system was isolated with the needle valves, the cause must be in the system after the hydraulic cylinder. Components and fluid volumes in the fluid lines may cause resonances (or antiresonances).

4.2.3 Dynamic loads with fully throttled one-way flow control

With the valves closed, flow in one direction is entirely blocked. Therefore, the system stiffness was measured in set positions with 10 mm intervals, starting at piston position 5 mm. This resulted in 22 individual stiffness measurements throughout the length of the stroke (5 mm to 215 mm). The stiffness measurements were conducted at three different frequencies, 10, 20 and 30 Hz as shown in Figure 62.

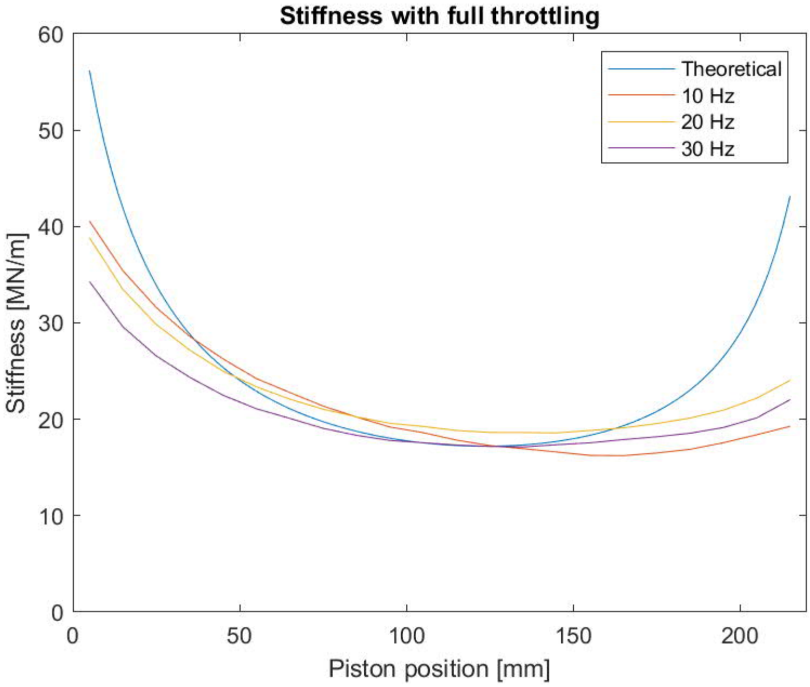

Figure 62 Measured stiffnesses with full throttling of one-way control valves.

The measured stiffnesses agree quite well with the stiffness model. The biggest variances are again in the end positions. Also, at 10 and 20 Hz loading, the measured stiffness is higher than the modeled stiffness in the middle of the stroke.

Measured force amplitudes can be seen from Figure 63. Each curve is a separate test run done with manually opening and closing the one-way flow control valves between loading, therefore the timings do not match.

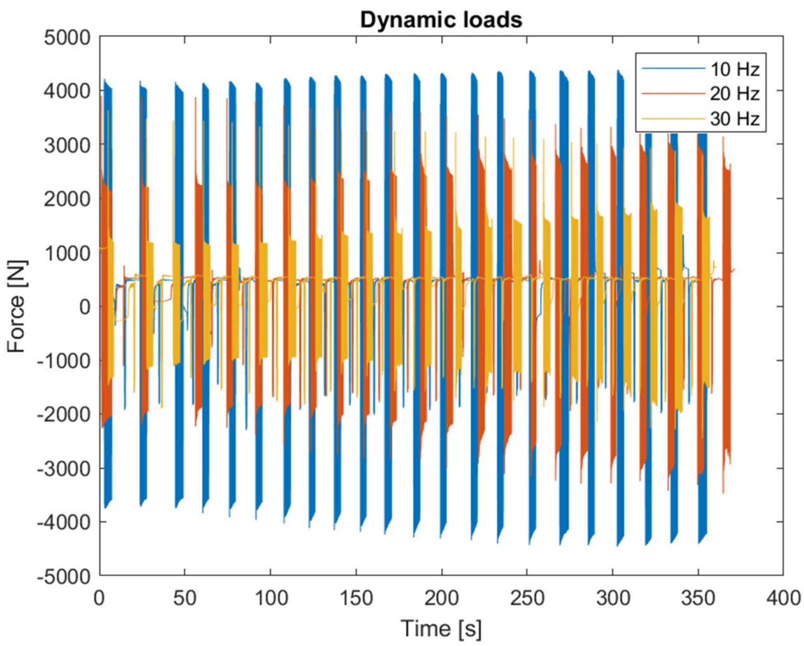

Figure 63 Force data from load cell with different frequencies (test timings not matching).

The higher stiffnesses at 10 and 20 Hz loading is due to the one-way flow control valves allowing fluid only to enter the system. The higher displacement amplitudes of 10 and 20 Hz loading causes higher flow rates through the check valve. As the additional fluid cannot exit the system, the ambient pressure levels rise. The test cylinder rod chamber pressures during the measurements are presented in Figure 64. The increase in pressure level during loading can be seen clearly at 10 Hz loading, the rod chamber pressure oscillates around 70 bar, whereas the set pressure is at 42 bar. As the displacement amplitude decreases when applying higher frequency loads, the amount of new fluid introduced into the test cylinder decreases.

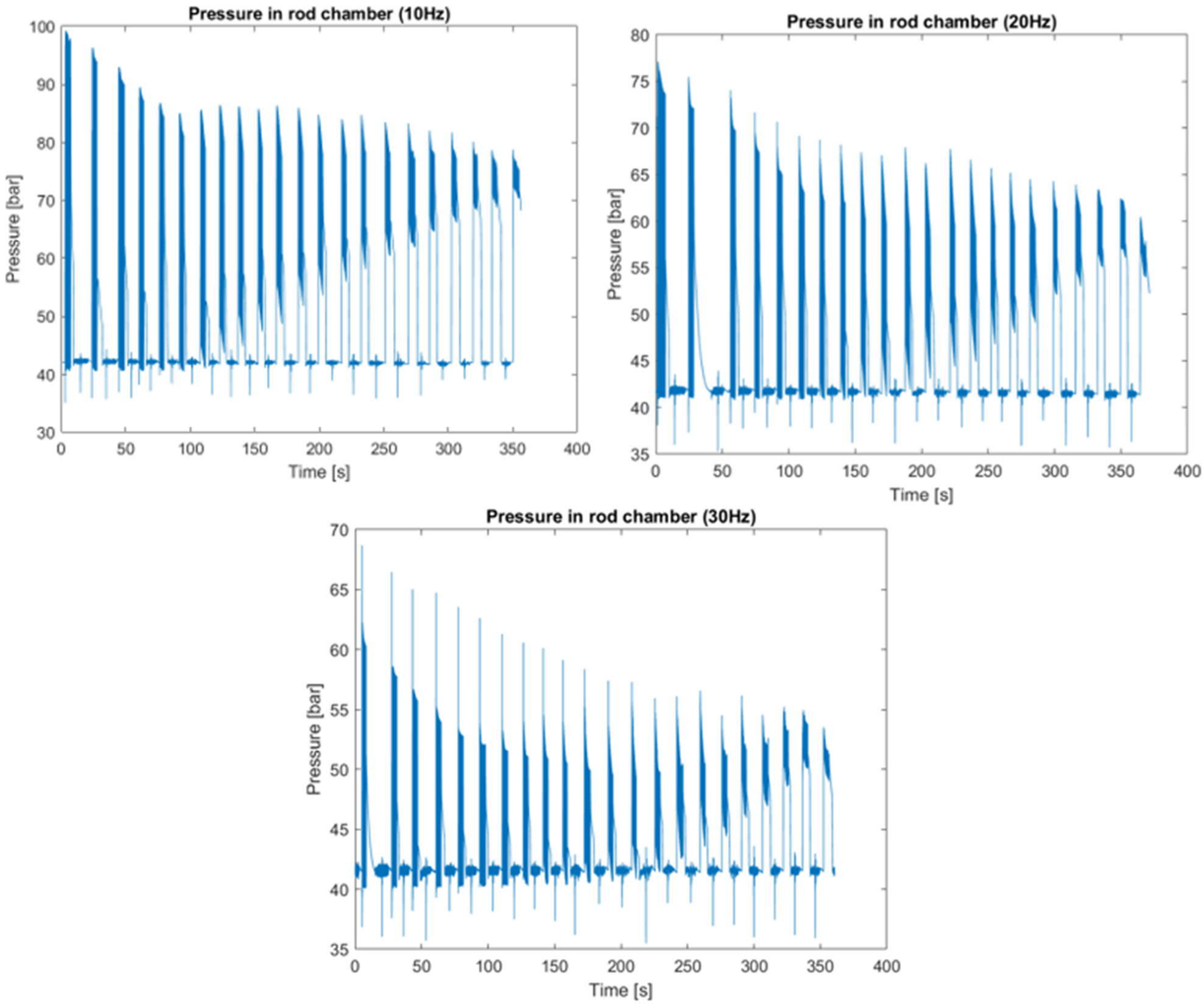

Figure 64 Test cylinder rod chamber pressures during dynamic loading with fully throttled one-way flow control valves.

In the first peak of the dynamic loading, the load deflects the stationary piston to one direction, causing a pressure drop in the opposite side chamber. This forces the check valve of the one-way flow control valve to open, which allows fluid to compensate for the pressure drop. When the load decreases, the check valve is shut and flow through that side is blocked. The new fluid in the system cannot escape from the chamber or fluid line since flow out of the system is blocked entirely. In other words, the dynamic loading increases the pressure levels in the cylinder chambers. The amount of increase in pressure depends on the magnitude of the load, and higher pressure levels lead to higher bulk moduli of the fluid, therefore in this configuration, the stiffness of the hydraulic cylinder system is also highly force-dependent.

The effects of the check valve can be seen from Figure 65, where dynamic loading of 10 Hz frequency with flow control valves fully throttled and needle valves attached are compared. Both datasets are taken at piston position 185 mm. The forces are identical, but the motions inhibit differences. The effects of the one-way flow control valves can be seen as an increase in the magnitude of nonlinearity on the zero-crossing point of force. The check valves cause oscillations when opening and closing and introduce higher degree of nonlinearity to the system.

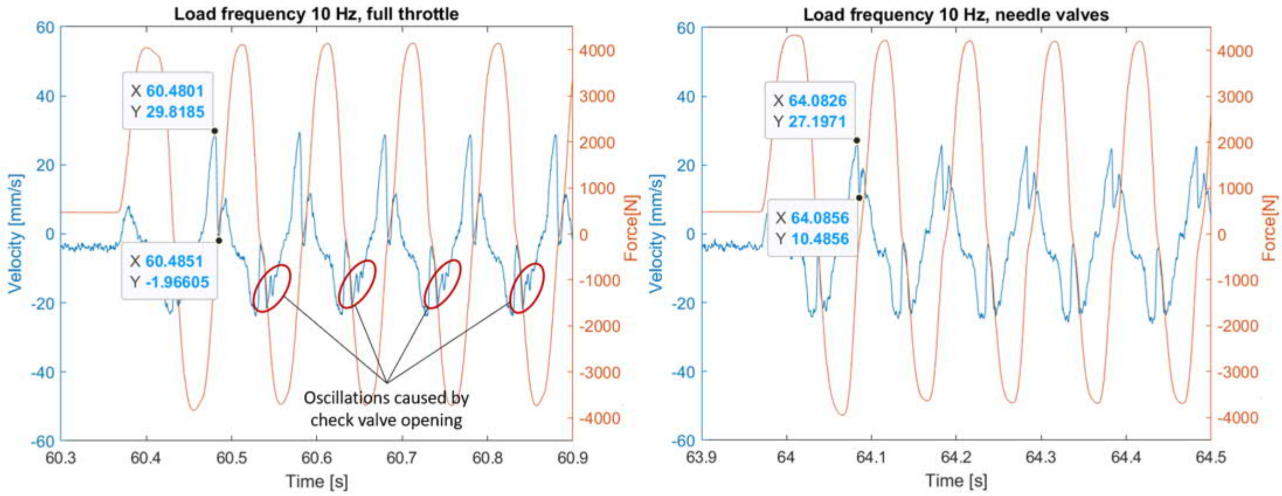

Figure 65 Velocity and force data, piston position 185 mm, fully throttled a) one-way flow control valves, b) needle valves.

5 Discussion

In this chapter, further discussion of the results is presented and suggestions for further research is proposed. The section aims to explain the major anomalies encountered: perceived static stiffness, as well as the stiffness peaks at 20 Hz loading. The validity of the measurements and suggestions for future work are also discoursed.

5.1 Cylinder system static stiffness

The perceived static stiffness of the cylinder system did not depend on the motion direction between the tests. It did, however, vary depend on loading direction; the system stiffness was higher when the loads were upwards, as can be seen in Figure 66.

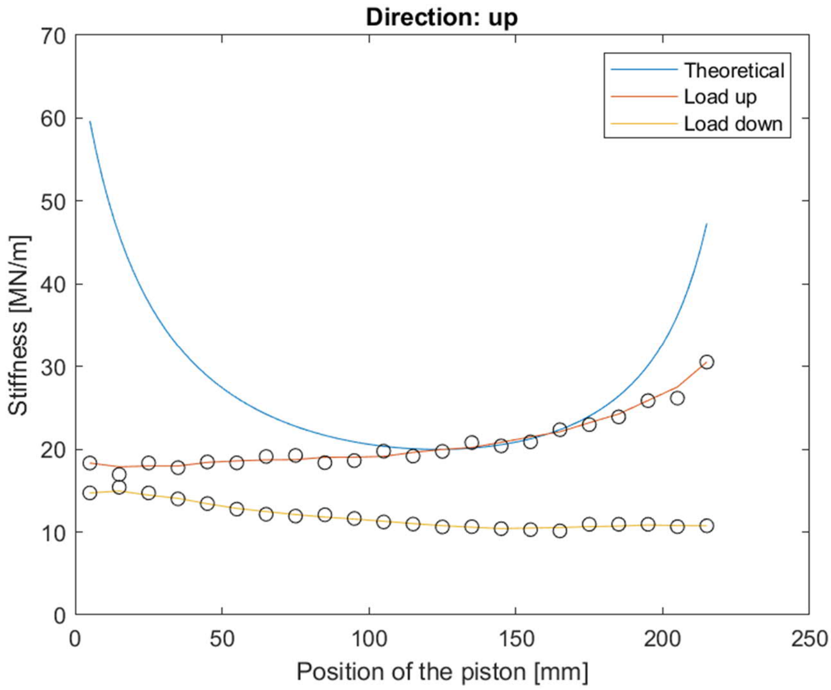

Figure 66 Static stiffness test run, direction up.

The measured stiffnesses are somewhat lower than what is expected. The reason is most likely undissolved air. As the working pressures in the chambers are fairly low, any air contents trapped in the cylinder chambers (at atmospheric pressure) might not get dissolved at all when the working pressures are applied. Uniformly distributed air would only offset the stiffness U-curve to a lower level while maintaining its shape, but an undissolved air volume trapped in the cylinder chambers would start to reduce the stiffness as the piston gets closer to the ends. When the piston is close to the end of the chamber, the relative air content becomes higher, decreasing the effective bulk modulus of the chamber, resulting in a flattened stiffness curve.

A simulation model of the test cylinder system was built based on the literature reviewed in this thesis and the simulation results are shown in Figure 67. In the simulation, a 4 kN force was applied upwards or downwards for a few seconds and the displacement was measured. The simulation model includes the effects of the sealing system. The simulated curves resemble the measured stiffnesses quite well.

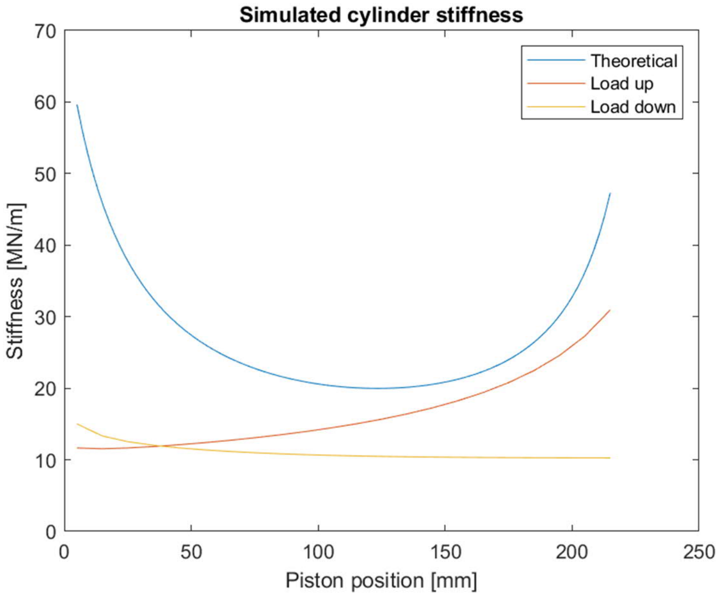

Figure 67 Constant air volume stiffness simulation results. Chamber A air volume: 0,4 ml; chamber B air volume: 0,08 ml.

The results from the dynamic test runs with plugged fluid lines support the constant air volume hypothesis, since the stiffnesses in the ends are lower than expected. The low working pressures and the vertical orientation of the test cylinder make the system more prone to trapped air contents. With higher working pressures, small air contents at atmospheric pressure would not affect the stiffness dramatically, since the air bubble would dissolve into the fluid and the remaining total volume of the air bubble would radically decrease (or decrease to zero) due to the compression of the added pressure.

5.2 Cylinder dynamic stiffness

The stiffness characteristics of the hydraulic cylinder system were measured under dynamic loads with frequencies of 10, 15, 20, 25 and 30 Hz. Unexpected stiffness peaks were discovered at 20 Hz loading frequency, as can be seen in Figure 68. The stiffnesses were also slightly higher than expected at 25 Hz loading. As perceived peaks were not encountered with full throttling (section 4.2.1), the proposed cause was the combined effects of the cylinder with the one-way flow control valves and the pressure reducing valves. Therefore, the cause is a strongly frequency-dependent phenomenon in the system.

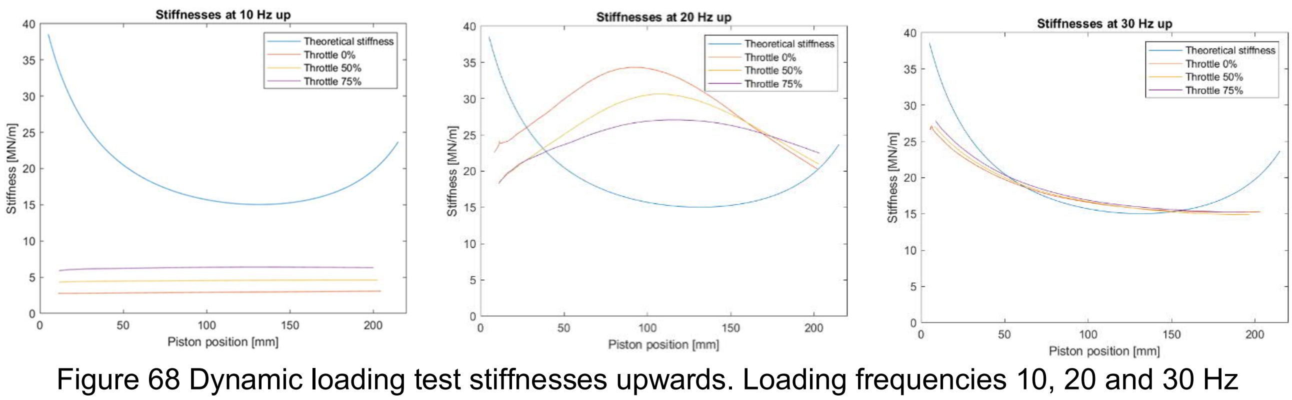

Figure 68 Dynamic loading test stiffnesses upwards. Loading frequencies 10, 20 and 30 Hz

For resonances to occur from fluid lines, the hoses of the system should have been significantly longer, as discoursed in section 2.1.3, so pipe resonance can be ruled out as the cause. The pressure reducing valves used in the test bench were pilot operated valves, which react to pressure variation. It is likely that the valve still reacts to the pressure changes successfully at frequencies of 15 Hz and below and reaches resonance at 20 Hz. At higher frequencies, the valve acts as a passive resistance, restricting flow almost entirely, as the stiffness curves follow the theoretical static stiffness quite well.

One method for increasing the damping could be amplifying the damping in the system. In hydraulic cylinders this can be done by either increasing mechanical friction or internal hydraulic leakage [44]. Increasing mechanical friction means increasing the sealing friction or with mechanical brake systems. The stick-slip phenomenon seen in reciprocating seals is amplified when the sealing friction is increased, causing unpredictability in the system. The dynamic responses of a mechanical brake would also increase the complexity of the system and would require experimental testing to implement. Internal leakage between the cylinder chambers could be introduced to hydraulic cylinders operating in the vicinity of natural frequencies of the system, bringing added damping. Introducing internal leakage also makes the system more complex and more difficult to control. The additional drawback of increasing damping, mechanical or hydraulic, is that the efficiency of the system reduces.

The one-way flow control valves are used as dampers in the system. They resist the flow out of the cylinder chambers. However, their low cracking pressure causes the internal check valve to open when its corresponding chamber is expanding. This results in the loss of the expanding chamber stiffness achieved with the throttling. The damping on the expanding chamber side also decreases. The cracking pressure is as low as 0,4 bar, meaning that the damping and stiffness effects disappear from the expanding chamber even with small pressure differences over the one-way flow control valve. By increasing the cracking pressure, the stiffness effects of the expanding chamber could be utilized at a bigger pressure difference. Dynamics of the check valves should not be significant in this application, since the F600 one-way flow control valve showed to have a response of 1 ms or so. Therefore, it should be safe to state that the dynamics of a check valve with a slightly higher cracking pressure would not cause resonances or interference in the system.

5.3 Measurement accuracy

Fourier analysis enables examining force, velocity, and displacement amplitudes at the desired frequencies. This resulted in calculating the stiffnesses by dividing the force amplitudes by the displacement amplitudes at the loading frequencies. The amplitudes, however, yield no data of the direction. As the tested hydraulic cylinder has different effective piston areas in each chamber and the pressure levels are different (and do not result in a net force of zero), the displacements ought to be different in each direction. The difference is actually seen in the static stiffness test results.

The fluid temperature was controlled with a heat exchanger. The temperatures were between 25 and 30 °C. The thermal effects of 5 °C variance causes the pump pressure levels change slightly, but the test cylinder chamber pressures were kept at constant pressure with the pressure reducing valves.

The extracted force data of the load cell had a slight lag since the pressure data of the test cylinder was ahead in phase. The Kyowa amplifier should be able to record force data at up to a frequency of 10 kHz. Therefore, the cause for the slight phase shift ought to be due the dynamics of the HBM load cell.

The GYSE-A position sensor noise is shown in Figure 69. Without any filtering, the peak-to-peak noise was 0,085 mm. These position measurements are used to calculate the stiffnesses under static loading. The smallest displacements were 0,11 mm. However, the displacements were reliably extracted by averaging the data with the MATLAB smooth function. And since the displacements were static, a longer averaging window could be used to reduce noise of the signal. The noise of the post-processed data was reduced to a peak-to-peak value of 0,011 mm. The resolution of the position measurements was limited by the 16-bit data acquisition system and the sensor scale of 500 mm, to be 0,008 mm.

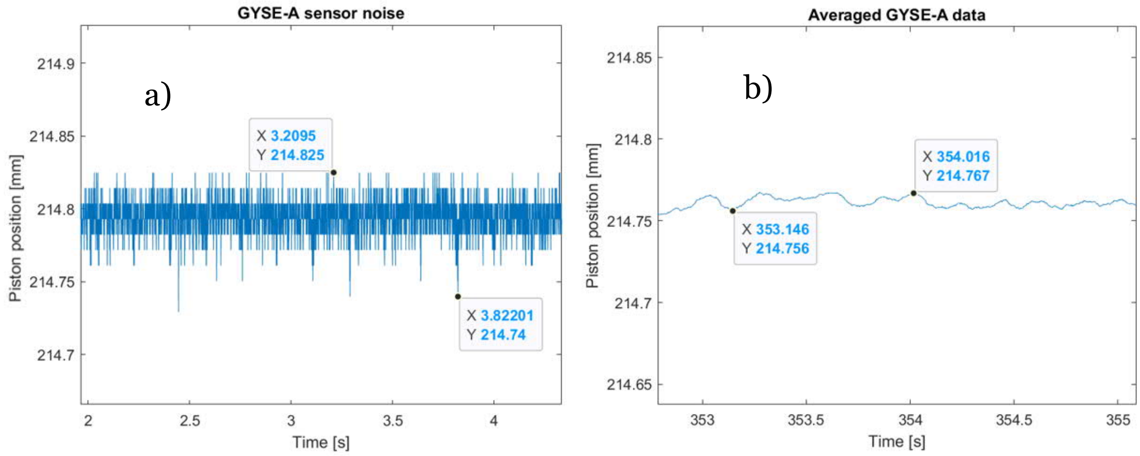

Figure 69 Position sensor data a) unfiltered, b) filtered.

The accelerometers, used to determine the velocity, are piezoelectric charge sensors which measure the rate of change of acceleration. Therefore, the displacement, which is used to calculate the stiffness, is extracted from a measurement integrated three-folds. Each integration introduces an additional margin of error [45]. Integrating a measured signal can be implemented via hardware or software, and in this setup, the integration is done twice in hardware, and once in software. The Nexus charge amplifier, paired with the accelerometers, utilizes internal integral circuits to obtain the velocity. The software integral method used to obtain the displacement was frequency domain integral. There are numerous different software integration methods and the accuracies of each vary [46], [47].

The GYSE-A position sensor is also capable of recording the velocity of the piston. In Figure 70, the velocity data of both the accelerometers and GYSE-A are shown. The measurements are in phase and the magnitudes agree quite well, showing that the velocity could have been extracted from the GYSE-A as well. Concerns of the GYSE-A dynamic response was the main reason, why accelerometers were used. Since the measured velocity amplitude with the GYSE-A sensor is slightly higher at 30 Hz, the resulting stiffness would have in fact been a bit lower if the GYSE-A velocity data would have been used.

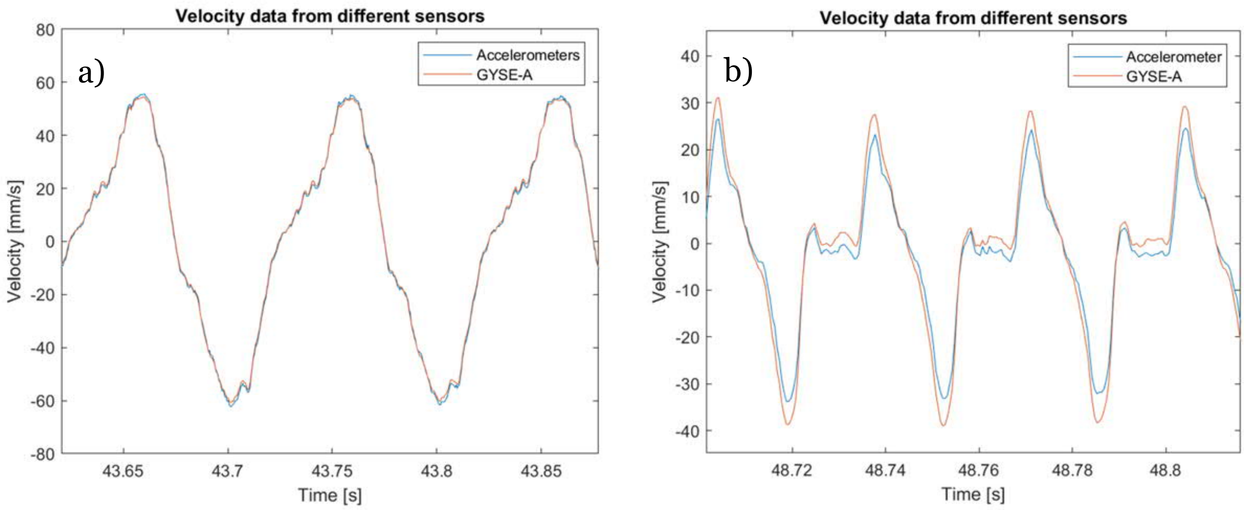

Figure 70 Comparison of velocity data extracted from GYSE-A and accelerometers at load frequency of a) 10 Hz and b) 30 Hz.

The position data of the GYSE-A sensor could have been used directly if the resolution of the setup would have been better. The displacements with 30 Hz loading were below 0,01 mm, which is rather close to the resolution of the measurement (0,008 mm).

5.4 Improvements in the test bench

Active PID feedback control was attempted in the system but proved to be difficult. Position feedback with a velocity feedforward was attempted but as the displacements were small, the signal-to-noise ratio of the position measurements was not satisfactory. Force feedback was also experimented on, but the nonlinearity of the system and the variance of loading frequencies led to difficulties in tuning the control parameters. Also, the proportional valve opening amplitudes were aliased, which means that the load cylinder dynamics were not sufficient for closed loop control in the higher frequencies.

To even reach the passive ±8% openings for the proportional valve, the control amplitudes needed to be amplified for the higher loading frequencies. The control value amplitudes were determined by manually testing different outputs for each loading frequency. The test setup still did not provide optimal test parameters, as the loading force amplitude decreased when the loading frequency increased.

The tested outputs were validated by monitoring the spool position data from the proportional valve with an oscilloscope in addition to the Beckhoff's own measurement of the command signal. Generating constant force amplitudes with the load cylinder proved to be a challenge. Even though the manufacturer provides documentation of having very little to no lag between spool position and command signal at 40 Hz frequency with ±90% command signal, lag was already seen at 20 Hz with 8% command signal amplitude. The same lag was seen in another tested DFPlus proportional valve unit, which could imply that the viscosity of the fluid affects the spool motion significantly. This would require further investigation.

In addition, the proportional valve is not entirely linear, especially close to the zero-crossing point, where the spool operates in the dynamic loading tests. Therefore, uniform loading is difficult to implement without active control, and active control is very difficult to achieve if the command signal and spool position begin to have a lag.

The load cylinder pressure data was measured in both cylinder chambers to capture the dynamics of the loading cylinder as well, but this pressure data did not match the loading force or the test cylinder hydraulic force in the dynamic tests. This may be due to a significant undissolved air content in load cylinder fluid lines. Undissolved air would hinder the dynamics of the pressure sensors significantly since the pressure rise time would increase. Also, the horizontal orientation of the pressure sensors left them prone to entrap air.

The test cylinder chambers were not isolated from each other entirely. Only one pressure supply line was introduced to the pressure reducing valves, and at lower loading frequencies, the pressure oscillation reached the supply line. Isolating the chambers from each other could simplify the behavior of the system and make it easier to interpret. The most reliable way of isolating the chambers would be to have individual pumps for each chamber supply, but in this thesis, the configuration was done according to the paper machine application.

5.5 Future work

The response of the pilot operated pressure reducing valve could be a beneficial subject for further studies. The fact that the perceived stiffness is more than doubled compared to the expected stiffness contains potential for development of a compact, semi-active, low-frequency resonator.

In 5.2, damping is proposed as a solution to increase the dynamic stiffness of the hydraulic cylinder system. Two methods were mentioned: mechanical damping and hydraulic damping. Different sealing system damping characteristics could be studied to see if stiffer seals made a difference. Also, the feasibility of the proposed bypass flow is yet to be validated. The bypass flow would in fact lower the static stiffness of the system but increase the damping. The pressure difference of the chambers and the need for a slow, constant velocity piston motion in its application might hinder the applicability of an added flow channel.

The difficulties of utilizing a hydraulic servo cylinder controlled by a proportional valve was discussed in the previous section. The Parker DFPlus allegedly has the fastest proportional valve response on the market. A functional hydraulic servo cylinder is an attractive method for generating the loads due to the ease of having active control and being able to change loading parameters without modifying the test bench. But since active control was proven difficult possible, another type of loading might have to be considered as well. The loading could be carried out for example by having a rotating mass on the end of the cylinder.

Since undissolved air was seen in the test cylinder system, analysis of the air solubility rate might be beneficial too. When the loads compress the undissolved air, its relative volume slightly decreases and the rate in which that happens could affect the dynamics of the whole cylinder system.

6 Conclusion

In this thesis, the stiffness characteristics of hydraulic cylinders were discoursed. Relevant research was reviewed and utilized to estimate the axial stiffnesses of hydraulic cylinders. Dynamic responses and resonances introduced by hydraulic and mechanical properties were also examined.

The thesis involved an experimental part, in which the stiffness characteristic of a hydraulic cylinder system was tested in a test bench. The tested cylinder system was a subsystem of a paper machine, which is subjected to oscillatory loads in its application. The test cylinder system consisted of the differential hydraulic cylinder and one-way flow control valves connected to its ports. Loads for the test cylinder system were generated with a hydraulic servo.

The cylinder system was examined under static and dynamic loads with varying loading frequencies. The properties of the test cylinder were first examined separately by isolating the cylinder from the rest of the system. To achieve this, the one-way flow control valves were replaced with needle valves. Static and dynamic loads were applied when the needle valves were shut, isolating the test cylinder from the rest of the test cylinder hydraulic circuit. These tests were conducted throughout the cylinder stroke at 10 mm intervals. The results of the static loading tests varied from the predicted stiffness due to trapped air contents in the cylinder chambers, and partially due to the difficulties of estimating the sealing system stiffness. The static loading scenario was also simulated, and the results pointed towards the chambers having constant air contents trapped in the chambers.

Dynamic loads with frequencies of 10, 20 and 30 Hz were applied with the cylinder isolated from the test cylinder hydraulic circuit. The measured stiffnesses from these test runs had better correspondence to the presented literature, but the measured stiffness values still varied significantly in the cylinder ends, confirming the constant air assumption.

The configuration of the hydraulic cylinder system was then modified to its actual use: the needle valves were replaced with one-way flow control valves. Then the dynamic loading tests were run with 10, 15, 20, 25, and 30 Hz while varying the direction and the level of throttling in the one-way flow control valves. These tests indicated heavy influences of the tested hydraulic cylinder from the rest of the system. At 10 and 15 Hz frequency loading, the stiffnesses were significantly smaller than what the literature suggested. At these loading frequencies it was the pilot operated pressure reducing valves which reduced the pressure build-up caused by the dynamic load, resulting in lower stiffnesses. At 20 Hz, the pressure reducing valves reached resonance, causing the stiffness to peak significantly higher than expected. As the frequency was increased, the contribution of the pressure reducing valves decreased and the measured stiffnesses corresponded better to the calculated static stiffness values, though still showing lower stiffnesses in the piston end positions than expected.

The contribution of the one-way flow control valves was studied. The throttling levels did indeed increase the perceived stiffness at lower frequencies, but at loading frequency of over 25 Hz the level of throttle was inconsequential. As the force amplitude was attempted to keep at a constant level, increasing the frequency reduced the resulting velocity and displacement amplitudes. Reduced velocity and displacement amplitudes resulted in smaller volumetric flow as well. The throttling of the valves only contributes to the system if there is flow. With minimal flow, orifices and restrictors do not take part in the dynamics of the system, which was seen in the results in this thesis as well.

The accuracy of the measurements was discoursed and suggestions for improvements and further work included: generating the loading differently (for example a rotating mass in the end of the rod instead of the hydraulic servo), investigating further the resonance of the pressure reducing valve, and isolating the test cylinder chambers from each other entirely by providing pressure supplies to both chambers. The proportional valve control proved to be difficult to implement at higher frequencies. The force amplitude did not remain entirely constant throughout the loading frequency spectra; at higher frequencies, the amplitude decreased due to the proportional valve and load cylinder dynamics.

The aim of the thesis was to study the stiffness characteristics of the proposed hydraulic cylinder system through relevant literature and experimental testing and based on that, propose how to make the stiffness more deterministic and possibly improve it. The most obvious, but significant proposals were reduction of air content in the cylinder chambers, increasing working pressures and increasing the cracking pressure of the one-way flow control valves.

References

[1] M. Jelali and A. Kroll, *Hydraulic Servo-systems: Modelling, Identification and Control*, 1st ed. London: Springer-Verlag London Limited, 2003.

[2] C. M. Harris and A. G. Piersol, *Harris' Shock and Vibration Handbook*, 5th ed. McGraw-Hill, 2002.

[3] E. I. Rivin, *Handbook on Stiffness & Damping in Mechanical Design*. 2010.

[4] H. Feng, Q. Du, Y. Huang, and Y. Chi, "Modelling study on stiffness characteristics of hydraulic cylinder under multi-factors," *Stroj. Vestnik/Journal Mech. Eng.*, vol. 63, no. 7–8, pp. 447–456, 2017, doi: 10.5545/sv-jme.2017.4313.

[5] B. G. Kinker, "Fluid viscosity and viscosity classification," in *Handbook of Hydraulic Fluid Technology*, 2nd ed., 2011, pp. 181–218.

[6] S. Kim and H. Murrenhoff, "Measurement of effective bulk modulus for hydraulic oil at low pressure," *J. Fluids Eng. Trans. ASME*, vol. 134, no. 2, 2012, doi: 10.1115/1.4005672.

[7] H. Gholizadeh, R. Burton, and G. Schoenau, "Fluid bulk modulus: A literature survey," *Int. J. Fluid Power*, vol. 12, no. 3, pp. 5–15, 2011, doi: 10.1080/14399776.2011.10781033.

[8] D. Knezevic and Z. Milovanovic, "Analysis of Changes of Bulk Modulus of Mineral Oil – Effects on the Dynamic Behavior of Hydraulic Actuators," *Int. Conf. Tribol. – Serbiatrib*, no. April 2011, pp. 4–5, 2015.

[9] X. Yuan, X. Zhu, C. Wang, and L. Zhang, "Research on Theoretical Model of Dynamic Bulk Modulus of Gas-Containing Hydraulic Oil," *IEEE Access*, vol. 7. pp. 178413–178422, 2019, doi: 10.1109/ACCESS.2019.2959058.

[10] A. Bureček, L. Hružík, and M. Vašina, "Determination of Undissolved Air Content in Oil by Means of a Compression Method," vol. 61, no. 7–8, pp. 477–485, 2015, doi: 10.5545/sv-jme.2015.2471.

[11] H. Kauranne, J. Kajaste, and M. Vilenius, *Hydrauliteknikka*, 1st ed. WSOY Oppimateriaalit Oy, 2008.

[12] J. Watton, *Fundamentals of Fluid Power Control*. Cambridge University Press, 2009.

[13] H. Ortwig, "Experimental and analytical vibration analysis in fluid power systems," *Int. J. Solids Struct.*, vol. 42, no. 21–22, pp. 5821–5830, 2005, doi: 10.1016/j.ijsolstr.2005.03.028.

[14] J. Mikota, "Contributions to the development of compact and tunable vibration compensators for hydraulic systems," Johannes Kepler University of Linz, 2002.

[15] M. I. Yuce and A. F. Omer, "Hydraulic transients in pipelines due to various valve closure schemes," *SN Appl. Sci.*, vol. 1, no. 9, pp. 1–11, 2019, doi: 10.1007/s42452-019-1146-4.

[16] B. E. Bosserman, W. A. Hunt, R. C. Glover, J. R. Kroon, M. S. Merrill, and G. Z. Watters, "Fundamentals of Hydraulic Transients," *Pump. Stn. Des.*, pp. 6.1-6.13, Jan. 2008, doi: 10.1016/B978-185617513-5.50013-5.

[17] A. B. Muhammad, A. Nasir, S. . Ayo, and B. Ige, "Hydraulic Transient Analysis in Fluid Pipeline : A Review," *J. Sci. Technol. Educ.*, vol. 7, no. 4, pp. 291–299, 2019.

[18] K. Sirvole, "Transient analysis in pipe networks," 2007.

[19] M. S. Ghidaoui, M. Zhao, D. A. McInnis, and D. H. Axworthy, "A review of water hammer theory and practice," *Appl. Mech. Rev.*, vol. 58, no. 1–6, pp. 49–75, 2005, doi: 10.1115/1.1828050.

[20] T. Hayase, P. Cheng, and S. Hayashi, "Numerical analysis of transient flow through a pipe orifice (Time constant for settling flow)," *JSME Int. Journal, Ser. B Fluids Therm. Eng.*, vol. 38, no. 2, pp. 157–163, 1995, doi: 10.1299/jsmeb.38.157.

[21] J. E. Funk, D. J. Wood, and S. P. Chao, "The transient response of orifices and very short lines," *J. Fluids Eng. Trans. ASME*, vol. 94, no. 2, pp. 483–489, 1972, doi: 10.1115/1.3425456.
[22] A. Abdul-Ameer, "Modelling of fluid power transmission systems," *INISTA 2011 - 2011 Int. Symp. Innov. Intell. Syst. Appl.*, pp. 205–211, 2011, doi: 10.1109/INISTA.2011.5946066.
[23] S. Helduser and W. Michael, *O+P technical glossary "Fluid technology from A to Z."* HAWE Hydraulik SE, 2015.
[24] L. Kela and P. Vähäoja, "Measuring Pressure Wave Velocity in a Hydraulic System," *Int. J. Mech. Aerospace, Ind. Mechatron. Manuf. Eng.*, vol. 3, pp. 67–73, 2009.
[25] R. K. Mobley, *Fluid Power Dynamics*. Elsevier, 2000.
[26] "Understand Flow Control Valves (Fluid Power Journal)," 2020. https://fluidpowerjournal.com/understand-flow-control-valves/.
[27] A. Kruisbrink, "The dynamic behaviour of check valves in pipeline systems," City University of London, 1996.
[28] H. Olsson, K. J. Åström, C. Canudas de Wit, M. Gäfvert, and P. Lischinsky, "Friction Models and Friction Compensation," *Eur. J. Control*, vol. 4, no. 3, pp. 176–195, 1998, doi: 10.1016/S0947-3580(98)70113-X.
[29] J. Na, Q. Chen, and X. Ren, "Friction Dynamics and Modeling," in *Adaptive Identification and Control of Uncertain Systems with Non-Smooth Dynamics*, Q. M. Zhu, Ed. Elsevier Science & Technology, 2018, pp. 11–18.
[30] N. B. Do, A. A. Ferri, and O. A. Bauchau, "Efficient simulation of a dynamic system with LuGre friction," *J. Comput. Nonlinear Dyn.*, vol. 2, no. 4, pp. 281–289, 2007, doi: 10.1115/1.2754304.
[31] J. Wu, H. Luo, H. Li, B. Su, Y. Wang, and Z. Li, "The influence of hydrothermal aging on the dynamic friction model of rubber seals," *Polymers (Basel).*, vol. 12, no. 1, p. 102, 2020, doi: 10.3390/POLYM12010102.
[32] J. N. Fuhg and A. Fau, "Surrogate model approach for investigating the stability of a friction-induced oscillator of Duffing's type," *arXiv*, no. September, 2019.
[33] K. J. Åström and C. Canudas-De-Wit, "Revisiting the LuGre Friction Model," *IEEE Control Syst.*, vol. 28, no. 6, pp. 101–114, 2008, doi: 10.1109/MCS.2008.929425.
[34] N. K. Agarwal and C. P. Lawson, "A practical method to account for seal friction in aircraft hydraulic actuator preliminary design," *Proc. Inst. Mech. Eng. Part G J. Aerosp. Eng.*, vol. 231, no. 5, pp. 941–950, 2017, doi: 10.1177/0954410016645371.
[35] S. Balku, "Tribology of Elastomeric and Composite," *Period. Pol Ytechnica Ser. Mech. Eng.*, vol. 43, no. 1, pp. 63–80, 1999.
[36] SKF, "Hydraulic seals and guides." https://www.skf.com/group/products/industrial-seals/hydraulic-seals/general-technical-information/introduction-to-fluid-power/hydraulic-seals-guides.
[37] Parker Hannifin, "Friction Estimation," *Friction Estimation*, 2019. https://www.parker.com/literature/O-Ring Division Literature/Static Files/frictionestimation.pdf.
[38] Parker, "In-line Flow Control Valve." https://ph.parker.com/fi/fi/in-line-flow-control-valve-f-series.
[39] Parker Hannifin, "Parker Catalogue HY11-3500/UK," 2017. https://www.parker.com/Literature/Industrial-Systems-Division-Europe/Catalogues/Industrial Valves UK/04/VMY UK.pdf.
[40] Beckhoff, "C6920 | Control cabinet Industrial PC." https://www.beckhoff.com/fi-fi/products/ipc/pcs/c69xx-compact-industrial-pcs/c6920.html.
[41] Regal, "Cylinder sensor GYSE." https://regal.se/products/position-sensors/cylinder-sensors-regasense/cylinder-sensor-gyse/.

[42] B&K, "Low-Frequency / Low-Level Piezoelectric Charge Accelerometer (Type 4381)." https://www.bksv.com/en/transducers/vibration/accelerometers/charge/4381.
[43] HBM, "HBM U2B tension/compression force sensor." https://www.hbm.com/en/2407/u2b-highly-versatile-load-cell-for-tensile-and-compressive-forces/.
[44] J. Johnson, "Myth #4: High efficiency is always good," *Hydraulics & Pneumatics*, 2008.
[45] A. Brandt, *Noise and Vibration Analysis: Signal Analysis and Experimental Procedures*. John Wiley & Sons, Incorporated, 2011.
[46] Y. Zhu, W. Jiang, X. Kong, Z. Zheng, and H. Hu, "An accurate integral method for vibration signal based on feature information extraction," *Shock Vib.*, vol. 2015, 2015, doi: 10.1155/2015/962793.
[47] A. Brandt and R. Brincker, "Integrating time signals in frequency domain - Comparison with time domain integration," *Meas. J. Int. Meas. Confed.*, vol. 58, pp. 511–519, 2014, doi: 10.1016/j.measurement.2014.09.004.